

2007

Self-pumped Gaussian beam-coupling and stimulated backscatter due to reflection gratings in a photorefractive material

Mohammad Abu Saleh
University of Dayton

Follow this and additional works at: https://ecommons.udayton.edu/graduate_theses

Recommended Citation

Saleh, Mohammad Abu, "Self-pumped Gaussian beam-coupling and stimulated backscatter due to reflection gratings in a photorefractive material" (2007). *Graduate Theses and Dissertations*. 5340.
https://ecommons.udayton.edu/graduate_theses/5340

This Dissertation is brought to you for free and open access by the Theses and Dissertations at eCommons. It has been accepted for inclusion in Graduate Theses and Dissertations by an authorized administrator of eCommons. For more information, please contact mschlange1@udayton.edu, ecommons@udayton.edu.

**Self-pumped Gaussian Beam-coupling and Stimulated
Backscatter due to Reflection Gratings in a
Photorefractive Material**

Dissertation

Submitted to

The School of Engineering of the

UNIVERSITY OF DAYTON

In Partial Fulfillment of the Requirements for

The Degree

Doctor of Philosophy in Electro-Optics

by

Mohammad Abu Saleh

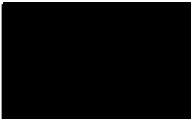
UNIVERSITY OF DAYTON

Dayton, Ohio


August 2007

SELF-PUMPED GAUSSIAN BEAM-COUPPLING AND STIMULATED BACKSCATTER
DUE TO REFLECTION GRATINGS IN A PHOTOREFRACTIVE MATERIAL


APPROVED BY:



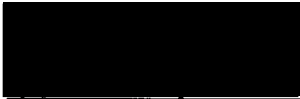
Partha P. Banerjee, Ph.D.
Advisory Committee Chairman
Professor, Electrical and
Computer Engineering Department




Joseph W. Haus, Ph.D.
Committee Member
Professor, Electro-Optics
Graduate Program




Leno M. Pedrotti, Ph.D.
Committee Member
Professor, Physics Department



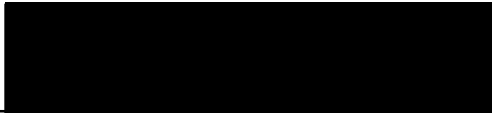
Shekhar Guha, Ph.D.
Committee Member
Principal Material Research Physicist
Air Force Research Laboratory



Dean R. Evans, Ph.D.
Committee Member
Senior Material Research Physicist
Air Force Research Laboratory



Malcolm W. Daniels, Ph.D.
Associate Dean
School of Engineering



Joseph E. Saliba, Ph.D., P.E.
Dean, School of Engineering

ABSTRACT

When overlapping monochromatic light beams interfere in a photorefractive material, the resulting intensity fringes create a spatially modulated charge distribution. The resulting refractive index grating may cause power transfer from one beam (the pump) to the other beam (the signal). In a special case of the reflection grating geometry, the Fresnel reflection of the pump beam from the rear surface of the crystal is used as the signal beam. It has been noted that for this self-pumped, contra-directional two-beam coupling (SPCD-TBC) geometry, the coupling efficiency seems to be strongly dependent on the focal position and spot size, which is attributed to diffraction and the resulting change in the spatial overlaps between the pump and signal. In this work a full diffraction based simulation of SPCD-TBC for a Gaussian beam is developed with a novel algorithm.

In a related context involving reflection gratings, a particular phenomenon named six-wave mixing has received some interest in the photorefractive research. The generation of multiple waves during near-oblique incidence of a 532 nm weakly focused laser light on photorefractive iron doped lithium niobate in a typical reflection geometry configuration is studied. It is shown that these waves are produced through two-wave coupling (self-diffraction) and four-wave mixing (parametric diffraction). One of these waves, the stimulated photorefractive backscatter produced from parametric diffraction, contains the self-phase conjugate. The dynamics of six-wave mixing, and their dependence on crystal parameters, angle of incidence, and pump power are analyzed. A novel order analysis of the interaction equations provides further insight into experimental observations in the steady state. The quality of the backscatter is evaluated through image restoration, interference experiments, and visibility measurement. Reduction of two-wave coupling may significantly improve the quality of the self-phase conjugate.

ACKNOWLEDGEMENTS

My special thanks are in order to Dr. Partha Banerjee, my advisor, for providing the time and guidance necessary for the work contained herein, and for directing this thesis and bringing it to a conclusion with patience and expertise.

I would also like to express my appreciation to everyone who has helped with the work. This includes Dr. Gary Cook, who provided valuable suggestions for some of the experiments and enriched me with countless discussions on photorefractive optics and relevant physics; Dr. Dean Evans who initiated the investigation on the phenomenon of six-wave mixing, served as a committee member, and provided countless suggestions that improved this thesis and my writing in general; Dr. Shekhar Guha, who guided me toward the simulation work and served in my committee; Jennifer Carns, who did some preliminary experimental work on the six-wave mixing; and my committee members Dr. Joseph Haus and Dr. Leno Pedrotti who carefully reviewed the proposal and this thesis.

I would also like to acknowledge the Materials Laboratory at the Air Force Research Laboratory for facilitating all of the experimental work presented in this dissertation and the Dayton Area Graduate Studies Institute for the tuition scholarship for attending the University of Dayton.

Finally, I deeply appreciate the support provided by my wife, Sanjida, for her understanding and sacrifice while this work was being done. I would like to thank my son Oniruddho and daughter Aditi, for their love and affection and for patiently missing many hours of play time with me. Above all, I would like to thank my parents for teaching me the value of rational thinking.

TABLE OF CONTENTS

Abstract.....	iii
Acknowledgements.....	iv
List of symbols.....	viii
List of abbreviations.....	xi
List of figures	xii
List of tables.....	xviii

CHAPTERS	Page
I INTRODUCTION	
1.1 Brief Background of Photorefractive Effect.....	1
1.2 Self-Pumped Contra-directional Two-beam Coupling, Six-wave Mixing and Phase Conjugation.....	2
1.3 Executive Summary of Work in this Dissertation.....	3
1.4 Roadmap of the Dissertation.....	5
1.5 Novelty of the Research.....	7
1.6 Related Publications from the Research.....	7
II THE PHOTOREFRACTIVE EFFECT	
2.1 Introduction.....	9
2.2 The Band Transport Model and Steady State Solutions.....	11
2.3 Two-wave Coupling.....	17
2.4 Two-beam Coupling.....	21
2.5 Conclusions.....	23

III	PREVIOUS RESEARCH ON SPCD-TBC AND SIX-WAVE MIXING	
	3.1 Introduction.....	25
	3.2 Contra-directional Two-beam Coupling.....	26
	3.3 Six-wave Mixing.....	30
	3.4 Conclusions.....	33
IV	EXPERIMENTAL SETUP FOR SIX-WAVE MIXING AND SPBS	
	4.1 Introduction.....	34
	4.2 Photorefractive Samples Used.....	35
	4.3 Six-wave Mixing.....	36
	4.4 The Nature of SPBS.....	39
	4.5 Conclusions.....	40
V	SIMPLIFIED THEORY OF SIX-WAVE MIXING AND SPBS	
	5.1 Introduction.....	42
	5.2 Interaction Equations and their Reduction.....	43
	5.3 Conclusions.....	47
VI	ANALYSIS OF EXPERIMENTAL RESULTS ON SIX-WAVE MIXING AND SPBS	
	6.1 Introduction.....	49
	6.2 Six-wave Mixing at Steady State.....	49
	6.3 The Nature of SPBS.....	55
	6.4 Conclusions.....	58
VII	BEAM PROPAGATION METHOD	
	7.1 Introduction.....	63
	7.2 Beam Diffraction.....	64
	7.3 Discrete Fourier Transform.....	68
	7.4 Conclusions.....	70

VIII	NOVEL ALGORITHM FOR SPCD-TBC WITH GAUSSIAN BEAMS	
	8.1 Introduction.....	71
	8.2 Algorithm.....	71
	8.3 Conclusions.....	78
IX	SIMULATION RESULTS FOR SPCD-TBC WITH GAUSSIAN BEAMS	
	9.1 Introduction.....	80
	9.2 Two-beam Coupling Test.....	81
	9.3 Photovoltaic Field Assisted Beam Coupling.....	82
	9.4 Diffraction Effect in Beam Coupling.....	83
	9.5 Conclusions.....	84
X	CONCLUSIONS	
	10.1 Summary of Work in this Dissertation.....	93
	10.2 Future Work.....	95
	APPENDICES	Page
A	SPCD-TBC SIMULATION CODE	
	A.1 MATLAB® Code.....	97
B	ANALYSIS OF GAUSSIAN BEAMS AND FABRY-PEROT CAVITY SIMULATION	
	B.1 Gaussian Beam in Free Space	131
	B.2 The Fabry-Perot Cavity	137
C	GAUSSIAN BEAM PROPAGATION CODE	
	C.1 MATLAB® Code.....	149
D	FABRY-PEROT CAVITY SIMULATION CODE	
	D.1 MATLAB® Code.....	153
	BIBLIOGRAPHY	172

LIST OF SYMBOLS

α	Linear absorption coefficient
β	Rate of thermal generation of electrons
c	The speed of light
C_i	Complex amplitude of plane wave i
D	Diffusion constant
D_s	Electrostatic displacement
$\overset{=}{\varepsilon}$	Dielectric tensor
$\langle \varepsilon \rangle$	Effective dielectric constant
E	Real Optical Field
E_d	Diffusion field
E_q	Saturation field
E_{pv}	Photovoltaic field
E_s	Space charge field
ϕ	Phase of the grating
γ	Gain coefficient
γ_R	Carrier recombination rate
I	Intensity
J	Current density

k	Wave vector
k_i	Wave vector of the i -th plane wave
k_{iz}	z-component of the wave vector of the i -th plane wave
k_B	Boltzmann constant
k_D	Debye wave number
κ	Photovoltaic constant
K	Grating vector
λ_0	Free space wave length
λ	Wave length inside material
m	Modulation index
μ	Carrier mobility
n	Refractive index
n_o	Index of refraction before any index modulation occurs
N	The electron density
N_A	Density of the acceptor impurities
N_D	Density of donor impurities
N_D^i	Density of ionized donor impurities
q	Electron charge
\bar{r}	Position vector
r_{eff}	Effective electro-optic coefficient
ρ	Charge distribution
s	Cross section for photo-excitation

ζ	Phase coupling coefficient
T	Temperature
ψ	Phase of the wave
ω	Angular frequency

LIST OF ABBREVIATIONS

Abbreviation	Stands for	Defined on page
AR	Anti-reflection	1
BPM	Beam Propagation Method	63
FWM	Four-wave mixing	3
ITO	Indium tin oxide	29
PR	Photorefractive	1
SPBS	Stimulated photorefractive backscatter	3
SPCD	Self-pumped contra-directional	2
TBC	Two-beam coupling	2
TWC	Two-wave mixing	3

LIST OF FIGURES

FIGURE	Page
2.1	The origin of the PR effect due to diffusion..... 10
2.2	Band transport model of the PR effect..... 13
2.3	Two-beam coupling in photorefractive material..... 18
3.1	Change in TBC due to diffraction..... 27
3.2	The photovoltaic noise and its elimination with conductive coating..... 29
3.3	Schematic representation of the experimental arrangement. C_1 denotes the forward propagating pump through the crystal. C_2 represents the result of six-wave mixing in the direction of the Fresnel reflection of the pump from the surface. C_3 and C_4 denote the waves generated in the crystal that are perpendicular to the interface, and consequently along the c -axis. C_5 and C_6 (the SPBS) make up the other two participating waves in the six-wave mixing scheme 31
4.1	Schematic representation of the experimental arrangement. L1-L3: lenses; M1, M2: mirrors; BS1, BS2: beam splitters. The pump is collimated 532 nm light from a Verdi laser. Six-wave mixing is observed on screens S1 and S2. Lens L1 is used to focus the pump onto the PR sample which is placed at its back focus for six-wave mixing experiments. SPBS (C_6) power is measured with the detector shown. Powers in $C_1 - C_5$ are also recorded with similar detectors placed directly in the path of the beams after exit from the crystal in their respective directions. Lens L3 and screen S3 are used during interference experiments for determination of the quality of SPBS. The PR sample is first placed at an arbitrary distance from lens L1 and the SPBS interfered with a portion of the collimated pump reflected by the mirror M1 with lens L2 removed. Thereafter, the sample is reinserted at the back focal plane of L1 and the interference of the SPBS with a portion of the pump focused by L2 and reflected by the mirror M1 is monitored..... 38

5.1	Calculation of contributions to SPBS (C_6) using scattering diagrams, following Eq. (5.1f). The thin lines on the right hand side refer to k-vectors of waves participating in the grating, while the dark lines represent the k-vector of the wave reading the grating.....	45
6.1	(a) Backscattered beam C_6 and linearly reflected light in the direction of C_2 . While the latter is instantaneously generated, C_6 forms between 100 ms-10 s after the pump beam is turned on. The pump beam, in the direction of C_1 passes through a hole on screen S1. (b) Subsequent generation of C_2 and C_3 is seen on screen S1.....	59
6.2	Time dynamics of six-wave mixing for crystal A at an angle of incidence of 4 degrees (in air) for the pump. Screens S1 and S2 in Fig. 2 are replaced by detectors and C_1 - C_5 are focused onto the detectors. The beams are recorded in pairs, with C_1 being common in all cases. The lighter traces correspond to 6 independent traces each for $C_2 - C_6$ and 30 traces for C_1 . The average in each case is shown in dark. Note that the <i>total</i> optical power in the direction of C_2 is plotted. The horizontal dashed line in this graph indicates the component of light in the direction of C_2 due to Fresnel reflection from the crystal surfaces.....	60
6.3	Interference with the reference (pump) when the crystal (or the mirror) is placed at a distance approximately $f/2$ from lens L1. (a) Interference pattern between the reference and the phase conjugate from BaTiO ₃ :Ce. Note the absence of circular fringes due to phase correction from phase conjugation. Inset shows linear fringes when the mirror M1 which reflects the reference is tilted. (b) Interference between the reference and reflection from a plane mirror placed at the location of the crystal). (c) Interference pattern between the reference and the SPBS from LiNbO ₃ :Fe.....	61
6.4	Quantification of the coherence of the SPBS through visibility measurement from interference patterns. (a) Interference pattern between the reference and the SPBS from LiNbO ₃ :Fe. (b) Interference pattern between the reference and a reflection from a plane mirror placed at the location of the crystal). (c) Intensity patterns along a vertical cut through both interference patterns recorded in (a) and (b), which is used for visibility calculations.....	62
7.1	The optical path is broken into a sequence of finite steps.....	63
7.2	A spatial amplitude distribution $E_e(y)$ can be expressed as superposition of plane waves $\mathcal{E}_e(k_y)$. The arrow with i corresponds to the amplitude of	

	the plane wave that has k_{y_i} as its transverse component of the wave vector.....	65
7.3	(a) Geometric depiction of the path the plane wave along the i^{th} wavevector follows to move a distance L along the z -axis. (b) Schematic of longitudinal and transverse components of the i^{th} wavevector	66
7.4	(a) An arbitrary continuous waveform $f(y)$ (b) Discrete sampled waveform $g(y)$ for $f(y)$ shown in Fig. 7.4(a).....	68
8.1	A schematic representation of the origin and path of the pump and signal beams. The signal beam (E_s) is generated by the Fresnel reflection of the pump beam (E_p) at the rear surface of the crystal. Both beams are nominally perpendicular to the boundaries. The paths are shown with angles to help distinguish the beams.....	72
8.2	Interference pattern in the longitudinal direction for a LiNbO ₃ crystal. Crystal length is equal to two wavelengths (532 nm) of light (inside). The number of longitudinal steps (n) per wavelength is 100. Spot size 5 micron.....	73
8.3	Interference pattern in the longitudinal direction for a LiNbO ₃ crystal. The crystal length is equal to ~ 40 microns.....	74
8.4	Flowchart showing the novel algorithm for simulation of SPCD-TBC for a Gaussian beam.....	76
9.1	The transverse Gaussian profile of a $1 \text{ } \mu\text{m}$ pump beam at the front (entrance) face of the crystal (solid line), and the diffracted signal beam coming out through the same crystal boundary (dashed, cross hairs). The crystal is $40 \text{ } \mu\text{m}$ long	85
9.2	Interference pattern (top) and resulting 90° phase shifted index modulation (bottom) for pure diffusion alone. Crystal length is 2 wavelengths inside. Change in index is 0.027.....	86
9.2	Energy exchange between the pump and the signal beam due to the modulated index in Fig. 9.1 due to pure diffusion. Pump power is reduced by about 4% and signal power gains equally. Oscillation in power is artifact.....	86
9.3	Interference pattern (top) and resulting in phase index modulation (bottom). Crystal length is 2 wave lengths inside. Change in index is 0.027, same as Fig. 9.1 for comparison.....	87

9.4	No energy exchange between the pump and the signal beam due to the in phase modulated index in Fig. 9.3. Plot is drawn to the same scale as Fig. 9.2. Oscillation is here is artifact.....	87
9.5	Results in LiNbO ₃ :Fe showing that the negative effect of the grating phase deviation from the optimum 90° is compensated by the positive effect of the larger Δn due to the photovoltaic field that exists in LiNbO ₃ ..	88
9.6	The change in refractive index (top), the phase difference between interference and index modulation (middle), and the change in pump power (bottom) as the photovoltaic field is varied and the diffusion field is held constant. Result shows that the negative effect of the grating phase deviation from the optimum 90° is compensated by the positive effect of the larger Δn	88
9.7	Interference pattern (top) and resulting index modulation (middle), and beam waist size for a 10 μm beam propagating in a 40 μm crystal. Beam waist does not change significantly.	89
9.8	Interference pattern (top) and resulting index modulation (middle), and beam waist size for a 1 μm beam propagating in a 40 μm crystal. Beam waist changes significantly. Interference magnitude is smaller, so is the resulting index modulation.	
9.9	Beam coupling as a function of pump spot size for a 40 μm and a 4 μm long crystal. The percent of power loss is normalized (to maximum power loss in percentage) for both graphs. The Rayleigh range for a 1 μm beam in side LiNbO ₃ is 27 μm	90
9.10	Interference pattern (top) and resulting phase index modulation (middle), and beam waist size for a 1 μm beam propagating in a 40 μm crystal and focused at the front. Interference magnitude is smaller compared to beam focus in the middle (Fig. 9.12) or at the end (Fig. 9.11). Same scale is used for Figs. 9.10 – 9.12.....	91
9.11	Interference pattern (top) and resulting phase index modulation (middle), and beam waist size for a 1 μm beam propagating in a 40 μm crystal and focused at the end. Interference, and index modulation magnitude is larger compared to beam focused at front (Fig. 9.10) or in the middle (Fig. 9.12). Same scale is used for Figs. 9.10 – 9.12.....	91
9.12	Interference pattern (top) and resulting phase index modulation (middle), and beam waist size for a 1 μm beam propagating in a 40 μm crystal and focused in the middle. Interference, and index modulation magnitude is larger compared to beam focused at front (Fig. 9.10) but smaller compared to the beam focused at the end (Fig. 9.11). Same scale is used for Figs. 9.10 – 9.12.....	92

9.13	Beam coupling as a function of pump focus position inside a 40 μm crystal. $x=0$, focused at the entrance, $x=1$, focused at the end. The percent of power loss is normalized (to maximum power loss).....	92
A.1	Schematic representation participating beams and their symbols as used in the code. Beams are normal to crystal surfaces, but shown at an angle for convenience.....	97
B.1	Beam of 5 μm (e^{-1}) focal waist at $z = 0$, using 200 μm <i>x-window</i>	132
B.2	The frequency spectrum using 200 μm <i>x-window</i>	132
B.3	The field shown in Fig. B.1 at $z = 1$ mm, with 200 μm <i>x-window</i>	133
B.4	Beam of 5 μm (e^{-1}) focal waist at $z = 0$, using 2 mm <i>x-window</i>	134
B.5	The frequency spectrum using 2 mm <i>x-window</i>	134
B.6	The field shown in Fig. B.1 at $z = 10$ mm, with 2 mm <i>x-window</i>	135
B.7	5 μm focal waist beam propagating 10 mm through air.....	136
B.8	Energy is conserved (normalized with respect to initial beam energy).....	136
B.9	Schematic representation participating beams and their symbols as used in the code. Beams are normal to crystal surfaces, but shown at an angle for convenience.....	137
B.10	The angles are defined as shown in this diagram.....	138
B.11	Sum of the transmitted fields for the original beam of 5 μm waist.....	141
B.12	Sum of the reflected fields for the original beam of 5 μm waist.....	141
B.13	Sum of the absolute reflected field for the beam of 5 μm waist.....	142
B.14	FFT of sum of the transmitted fields for the original beam of 5 μm waist..	142
B.15	FFT of sum of the reflected fields for the original beam of 5 μm waist.....	143
B.16	FFT of sum of the transmitted fields for a beam of 10 μm waist.....	143
B.17	FFT of sum of the reflected fields for a beam of 10 μm waist.....	144
B.18	FFT of sum of the transmitted fields for a beam of 30 μm waist.....	144

B.19	FFT of sum of the reflected fields for a beam of 30 μm waist.....	145
D.1	Schematic representation participating beams and their symbols as used in the code. (Same as Fig. B.9).	153

LIST OF TABLES

TABLE	Page
4.1 Relevant parameters for all the $\text{LiNbO}_3\text{:Fe}$ crystals used for the study of six-wave mixing and SPBS. ITO: conducting coating of indium tin oxide. AR: Anti-reflection coating.....	33
6.1 Relevant parameters for all the $\text{LiNbO}_3\text{:Fe}$ crystals used for the study of six-wave mixing and SPBS. Reproduced here from Chapter 4 for reader's convenience with the addition of last column, which compares steady-state SPBS powers for the various crystals.....	49

CHAPTER I

INTRODUCTION

1.1 Brief Background of Photorefractive Effect

Photorefractive (PR) materials, as the name suggests, change their refractive index when they are exposed to light. More specifically, when overlapping monochromatic light beams interfere in a PR material, the resulting gradients in the interference pattern cause charge migration, which in turn produces change in the refractive index [1]. This effect is usually described by a band-transport model [2,3] which assumes that the material has a pool of charges that are located in shallow traps. An interference pattern of two laser beams creates an array of bright and dark fringes. When incident light excites the charges into the conduction band, they are free to diffuse away from the bright region to the dark region of the crystal. This produces a periodic charge distribution throughout the illuminated region, which in turn produces a periodic electrostatic field. This field then changes the refractive index of the material through the linear electro-optic effect.

The refractive index grating formed this way is phase shifted 90 degrees with respect to the interference pattern which causes energy from one beam (pump) to be transferred or coupled into another (signal) [1]. This is the diffusion model of photorefraction. In addition to the diffusion process, some anisotropic crystals (e.g., LiNbO_3) exhibit strong

photovoltaic effect, which refers to the tendency of the photo-ionization process (under uniform illumination) to eject the electron in a preferred direction due to the asymmetric potential in the anisotropic crystal. It turns out that the refractive index grating formed from the photovoltaic field alone is in phase with respect to the interference pattern [1], and cannot transfer energy from one beam to another. However, in the presence of a diffusion field, the photovoltaic field can enhance the beam-coupling where the positive effect of the increased index modulation overcomes the negative effect of the non-optimum (less than 90 degree) phase shift. This PR two-beam coupling (TBC) can be achieved by two different geometries: i) co-directional, where both beams (of the same frequency) are traveling nominally perpendicular to the direction of the polar (c) axis, or ii) contra-directional, where the pump beam is along the positive c-axis and the signal beam is along the negative c-axis. Gratings resulting from these two geometries are also referred to as transmission and reflection grating.

1.2 Self-Pumped Contra-directional Two-beam Coupling, Six-wave Mixing and Phase Conjugation

Yeh [4] is one of the first to suggest another variation of the contra-directional geometry where the Fresnel reflection from the rear surface is used as the signal beam and hence it is referred to as self-pumped contra-directional (SPCD) TBC. The resulting reflection grating reduces the transmitted pump energy as the reflected beam gets stronger. MacDonald [5] *et al.* has, thereafter, shown this experimentally. Since then there has been an increasing interest in understanding the grating writing dynamics and various characteristics of these reflection gratings [6].

Cook *et al.* [6] have observed that the contra-directional TBC efficiency is very strongly dependent on the spot size of the pump beam with the optimum being at around a few microns (e^{-1} radius). In addition they have also observed that the TBC efficiency varies significantly depending on the position of the focal spot with respect to the crystal faces along the c-axis. An approximate theory has been developed by Cook *et al.* [6] to show the spot size dependence of the TBC efficiency. A complete theoretical model that accounts for the diffraction of the beam in a PR medium and would consequently demonstrate the spot size and focal position dependence has not been formulated yet.

It has been known that for the contra-directional beam-coupling oblique incidence of a pump on PR crystals (e.g., LiNbO₃, or KNbO₃), nominally propagating opposite the gain direction (along +c axis) gives rise to six waves which interact through two-wave coupling (self-diffraction) and four-wave mixing (parametric diffraction) [7, 8]. Theory for reflection grating suggests that one of the six waves, propagating in the reverse direction of the pump and hence called the stimulated PR backscatter (SPBS), contains the phase conjugate of the pump [9]. Theory also suggests that two of the other participating waves propagate along the $\pm c$ axes. Randomly scattered light in some of these six directions may get amplified by self-diffraction, commonly called PR two-wave coupling (TWC), or by coupling with light in other directions through parametric diffraction, commonly called four-wave mixing (FWM) [9].

1.3 Executive Summary of Work in this Dissertation

We have focused on two aspects of the photorefractive effects, the self-pumped contra-directional (SPCD) two-beam coupling (TBC) and stimulated PR back-scatter (SPBS)

leading to six-wave mixing. We have extended the knowledge on stimulated back scatter and six-wave mixing by detailed experimental work on various $\text{LiNbO}_3\text{:Fe}$ crystals and a novel order analysis of the six interactive waves. In addition, we have simulated the SPCD-TBC for a Gaussian beam in a PR media.

Specifically, in this work, six-wave mixing in $\text{LiNbO}_3\text{:Fe}$, resulting from a 532 nm pump obliquely incident on the crystal which leads to SPBS, as well as beams traveling normal to the interface along the $\pm c$ axes, are investigated. The time dynamics of the six waves are investigated for various $\text{LiNbO}_3\text{:Fe}$ crystals (with different coatings, absorption coefficients and thicknesses) to advance the understanding of the six-wave mixing.

Expanding on the work by Kukhtarev *et al.* [9], a novel order analysis for the steady-state of the six waves is also presented and used to explain some of the experimental results. In the process, we have shown that a reduced set of steady-state equations resulting from the order analysis could be used to model six wave interactions in the future. The reduced equations also show that the SPBS contains contributions from self-diffraction and parametric diffraction. Since the latter contribution is proportional to the phase conjugate of the incident wave, the SPBS is subjected to the classic image restoration test for phase conjugates. Finally, the quality of the SPBS is investigated using interferometric methods, including measurement of the fringe visibility. We conclude that the phase conjugation may be contaminated by the self-diffraction. It is postulated that reduction of self diffraction may significantly improve the phase conjugate in SPBS.

Furthermore, in this work a novel algorithm using the split step beam-propagation technique that accounts for the diffraction of the Gaussian beam in the PR medium and simulates self-pumped contra-directional beam-coupling has been developed. This would enable us to have a better understanding of the effect of focal position and spot size dependence of TBC efficiency, and grating strength distribution inside the crystal. To the best of our knowledge, the self-pumped contra-directional TBC has not been simulated before for a focused beam using any beam-propagation method.

Our simulation agrees with some key elements of PR beam-coupling. We have simulated two gratings, one of which is in-phase with the interference pattern (photovoltaic field dominated) and the other one being 90 degrees out of phase with the interference pattern (diffusion field dominated), and have observed that only the out-of-phase grating results in beam-coupling, in agreement with standard theory [1]. It is also observed through our simulation that the overall effect of the photovoltaic field on two-beam coupling depends on the trade-off between the negative effect of the phase deviation from the optimum 90 degree and the positive effect of the larger Δn , which is in agreement with experimental observations by Cook *et al.* [10]. Our simulation also shows the change in beam-coupling with change in pump spot size, or the location of the focus of the pump inside the crystal.

1.4 Roadmap of the Dissertation

Chapter 1: Introduction of the PR effect, contra-directional beam coupling and six-wave mixing related to the dissertation, uniqueness of work and publications.

- Chapter 2: More details discussion on the theory of the PR effect; the band transport model and steady-state solution; and the theory of the two-wave and the two-beam coupling in PR media.
- Chapter 3: Summary of previous research in contra-directional beam-coupling and six-wave mixing.
- Chapter 4: Experimental investigation of six-wave mixing in $\text{LiNbO}_3\text{:Fe}$ crystals and the phase-conjugate nature of the SPBS.
- Chapter 5: Theory of the six-wave mixing; coupled wave and material equations, and a novel order analysis that results in reduced sets of equations.
- Chapter 6: Experimental results and discussions on six-wave mixing and nature of SPBS.
- Chapter 7: Theory of the beam propagation method.
- Chapter 8: A novel BPM algorithm for self-pumped contra-directional Gaussian beam-coupling in PR media.
- Chapter 9: Simulation results for contra-directional self-pumped beam-coupling and discussions.
- Chapter 10: Conclusions and future work.
- Appendix A: The MATLAB[®] code for SPCD-TBC algorithm in Chapter 8.
- Appendix B: Simulation of Gaussian beam in air and simulation of Fabry-Perot cavity with BPM in linear media.
- Appendix C: The MATLAB[®] code for the simulation of Gaussian beam in air.
- Appendix D: The MATLAB[®] code for the simulation of a Fabry-Perot.
- References.

1.5 Novelty of the Research

In this work, a novel algorithm that accounts for the diffraction of the Gaussian beam in the PR medium and simulation of self-pumped (where the signal is the Fresnel reflection from the second crystal surface) contra-directional TBC has been developed. To the best of our knowledge, the self-pumped contra-directional TBC has not been simulated before for a focused beam using any beam-propagation method. Six-wave mixing in LiNbO_3 has been investigated for the first time. The partial presense of phase-conjugate in the steady state of the SPBS has been demonstrated. The detailed dynamics of six-wave mixing and their dependence on various parameters are presented here for the first time to the best of our knowledge. Using a novel order analysis for the steady-state of the six waves we has shown that the resulting reduced set of steady-state equations agrees with experimental observations.

1.6 Related Publications from the Research

1. Work on the six-wave mixing and nature of SPBS is going to be published in Applied Optics:

M. A. Saleh, P. P. Banerjee, J. Carns, G. Cook, and D. R. Evans, "Stimulated photorefractive backscatter leading to six-wave mixing and phase conjugation in iron doped lithium niobate," Applied Optics, vol. 46, 2007. (8/10/07)
2. Dynamics of six-wave has been presented at CLEO 2005:

M. A. Saleh, J. Gibson, G. Cook, D. R. Evans, and P. P. Banerjee, "Self-pumped stimulated backscattering and six-wave mixing in Fe:LiNbO_3 ," CLEO, Baltimore, MD, May 2005.
3. Work on the algorithm of the self-pumped contra-directional Gaussian beam-coupling has been published in the Proceedings of SPIE:

M. A. Saleh, G. Cook, S. Guha, P. P. Banerjee and D. R. Evans, "Self-pumped contra-directional two-beam coupling in a photorefractive material using beam propagation simulation," *Proc. SPIE*, 5560, pp. 26-33, 2004.

4. Simulation of the photovoltaic and diffusion dominated PR beam-coupling has been presented in the SPIE Great Lake Symposium:

M. A. Saleh, P. P. Banerjee, and D. R. Evans, "Diffusion and photovoltaic-assisted grating formation in photorefractive counter-propagating two-beam coupling," *Great Lakes Photonics Symposium*, Dayton, OH, June 2006.

CHAPTER II

THE PHOTOREFRACTIVE EFFECT

2.1 Introduction

The PR effect is a phenomenon in which the local refractive index of a medium is changed by the illumination of a beam of light with spatial variation of the intensity. This is schematically illustrated in Fig. 2.1. When two plane waves of the same frequency interfere inside the crystal they produce a spatially modulated intensity distribution $I(x)$, shown in Figure 2.1(a). Free charge carriers (assumed to be electrons only for simplicity) are generated through photoionization at a rate that is proportional to the local value of the optical intensity. These carriers can diffuse through the crystal, or can drift in response to a static electric field. Both processes can be observed experimentally [1]. For convenience, only diffusion is considered in Fig. 2.1. As shown in Figure 2.1(b), the electron density is smallest in the regions of maximum optical intensity, because electrons have preferentially diffused away from these regions. The spatially varying charge distribution $\rho(x)$ gives rise to a spatially varying electrostatic field distribution, shown in Figure 2.1(c). The maxima of the field $E_s(x)$ are shifted by 90 degrees with respect to those of the charge density distribution $\rho(x)$. This is a

consequence of Gauss' law $\vec{\nabla} \cdot \vec{D}_s = \rho$, where D_s is the electrostatic displacement. This implies that $dE_s/dx = 4\pi\rho/\epsilon$, which causes E_s to be phase shifted from ρ and I . Figure 2.1(d) shows the refractive index variation $\Delta n(x)$ that is produced through the linear electro-optic (Pockels) effect by the field $E(x)$. Assuming a positive electro-optic coefficient, Δn has the opposite sign of $E_s(x)$ since $\Delta n = -\frac{1}{2}n^3r_{eff}E_s$. Most significantly, Δn is also 90 degree phase shifted with respect to the intensity distribution, a condition conducive to the transfer of energy between the two incident waves [1].

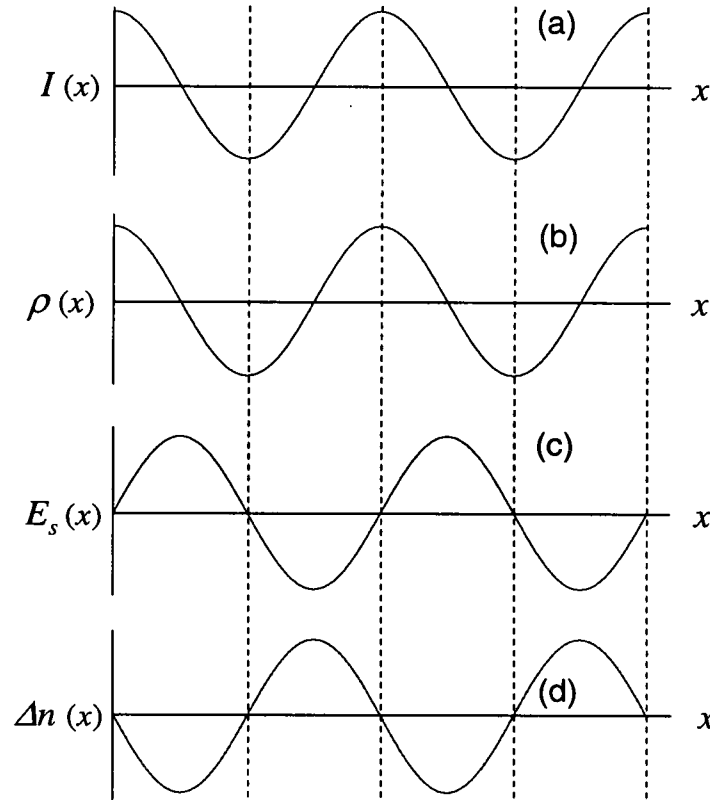


Figure 2.1: The origin of the PR effect due to diffusion [1]. (a) Two plane waves interfere to produce modulated intensity. (b) Free charge carriers are generated and diffuse to give charge distribution. (c) Charge distribution gives rise to electric field distribution. (d) Linear electro-optic effect produces refractive index variation.

The theoretical analysis of this process is described by the band transport model, to be discussed in Section 2.2. Following that we describe how the PR process can facilitate energy exchange between two plane waves (Section 2.3) and two Gaussian beams (Section 2.3).

2.2 The Band Transport Model and Steady State Solutions

The band transport model of photorefraction is commonly credited to Kukhtarev and coworkers [2,3]. This model presupposes that the PR effect is due solely to one type of charge carrier, which we will assume to be electrons in what follows. Figure 2.2 shows an energy level diagram depicting the process of photoexcitation, drift, diffusion and trapping. The band transport model can be quantified on the basis of the following four equations, called the Kukhtarev equations [11].

(1) Let the density of donor impurities be N_D , of which N_D^i are ionized. The rate of electron generation is $(sI + \beta)(N_D - N_D^i)$, whereas the rate of trap capture is $\gamma_R N N_D^i$, where N is the electron density, s is the cross section for photo-excitation, β is the rate of thermal generation of electrons, I is the light intensity and γ_R is the electron-ionized trap recombination rate. Thus the rate equation for N_D^i , neglecting the thermal generation (i.e. $\beta \ll sI$), can be written as:

$$\frac{\partial N_D^i}{\partial t} = sI(N_D - N_D^i) - \gamma_R N N_D^i. \quad (2.1)$$

(2) The rate of generation of electrons is the same as that of ionized impurities except that the electrons are mobile whereas the impurities are stationary. The transport of electrons, which gives rise to current, may affect the electron density. Thus, the rate equation for the electron density due to the ionization and transport can be written as:

$$\frac{\partial N}{\partial t} = \frac{\partial N_D^i}{\partial t} + \frac{1}{q} \bar{\nabla} \cdot \bar{J}, \quad (2.2)$$

where \bar{J} is the current density and $-q$ is the electron charge.

(3) The current density has contributions from the drift of charge carriers due to the electrostatic field and the diffusion due to the gradient of carrier density and thus can be written by Eq. 2.3, where μ is the carrier mobility, E_s is the electrostatic field, k_B is the Boltzmann constant and T is the temperature:

$$\bar{J} = qN\mu\bar{E}_s + k_B T \mu \bar{\nabla} N. \quad (2.3)$$

Some crystals also have current contribution from the photovoltaic effect, the consequence of that will be discussed later in this Chapter.

(4) Gauss' law for the electrostatic space charge field can be written as:

$$\bar{\nabla} \cdot (\bar{\epsilon} \bar{E}_s) = -q(N + N_A - N_D^i). \quad (2.4)$$

where $\bar{\epsilon}$ is the dielectric tensor; N_A is the density of the acceptor impurities, assumed to be all ionized by trapped electrons.

Since the change in the refractive index is directly caused by the space charge field, the goal is to determine the space charge field for steady state and as a function of time (transient solution) from the Kukhtarev equations. Analytical solutions only exist for some special cases. We will consider one such case, namely, the two-beam coupling.

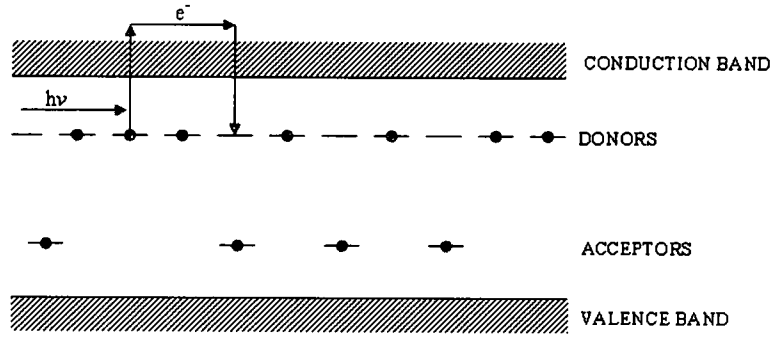


Figure 2.2: Band transport model of the photorefractive effect.

Consider the incidence of two plane waves of the same frequency onto a PR medium. Let the total optical field be written as

$$E = \text{Re}[C_1 \exp(j\omega t - j\vec{k}_1 \cdot \vec{r}) + C_2 \exp(j\omega t - j\vec{k}_2 \cdot \vec{r})] \quad (2.5)$$

where C_1 , C_2 are the (complex) wave amplitudes, ω is the angular frequency, and \vec{k}_1 , \vec{k}_2 are the wave vectors. If the polarization states of these two waves are the same, they will form an interference pattern with an intensity given by

$$I = I_0 + \text{Re}[I_1 \exp(-j\vec{K} \cdot \vec{r})], \quad (2.6)$$

where

$$I_0 = |A_1|^2 + |A_2|^2, \quad I_1 = 2A_2 \cdot A_1^* \quad (2.7a)$$

and \vec{K} is the grating wave vector defined as

$$\vec{K} = \vec{k}_2 - \vec{k}_1. \quad (2.7b)$$

The magnitude of the grating vector is related to the period (Λ) of the interference pattern. The ratio $2I_1 / I_0$ is known as the modulation index (m) [1]. It is also commonly referred to as modulation depth [11].

For simplicity, let us examine the steady state solutions. By setting the time derivatives to zero for Eqs. (2.1) through (2.4), we get

$$\begin{aligned}
sI(N_D - N_D^i) - \gamma_R NN_D^i &= 0, \\
\bar{\nabla} \cdot \bar{J} &= 0, \\
\bar{J} &= qN\mu\bar{E}_s + k_B T \mu \bar{\nabla} N, \\
\bar{\nabla} \cdot \bar{\epsilon} \bar{E}_s &= -q(N + N_A - N_D^i).
\end{aligned} \tag{2.8}$$

Now, since Eq. (2.8) is a nonlinear coupled set of equations, they cannot be solved exactly. However, if it is assumed that the depth of modulation m is small ($m \ll 1$), an approximate closed form solution exists. Under such an assumption, the higher spatial harmonic terms can be ignored and we can write the space charge field as

$$\bar{E}_s(\bar{r}) = \bar{E}_{s0} + [\bar{E}_{s1}(\bar{r}) \exp(-j\bar{K} \cdot \bar{r}) + c.c.]. \tag{2.8}$$

After writing similar expressions for N, N_D^i, \bar{J} and then substituting them in Eq. (2.8), we equate terms with common \bar{r} dependences. Assuming that the dc field \bar{E}_{s0} is parallel to the grating vector \bar{K} , one obtains the following expression for E_{s1} [11]:

$$E_{s1} = \frac{jK \frac{k_B T}{q} - \frac{\bar{K} \cdot \bar{E}_{s0}}{K}}{1 + \frac{K^2}{k_D^2} + j \frac{q\bar{K} \cdot \bar{E}_{s0}}{k_B T k_D^2}} \frac{I_1}{I_0}, \tag{2.9}$$

where \bar{E}_{s0} is the dc field, k_D is known as the Debye wave number, expressible as

$$k_D^2 = \frac{q^2}{\langle \epsilon \rangle k_B T} \frac{N_A}{N_D} (N_D - N_A) \tag{2.10}$$

where $\langle \varepsilon \rangle$ is the effective dielectric constant. The expression (2.9) can be further reduced for the case when $E_{s0} = 0$, known as the case of pure diffusion. The space charge field is

then given by

$$E_{s1} = \frac{jK \frac{k_B T}{q} \frac{I_1}{I_0}}{1 + \frac{K^2}{k_D^2}}. \quad (2.11)$$

Equation (2.11) could be then expressed as [11],

$$E_{s1} = \frac{jE_d \frac{I_1}{I_0}}{1 + \frac{E_d}{E_q}}. \quad (2.12)$$

by defining two parameters $E_d (= Kk_B T / q)$ and $E_q (= qN_A / \langle \varepsilon \rangle K)$ as diffusion field and saturation field, respectively. Diffusion field is a measure of the field strength required to inhibit the separation of charge due to thermal agitation and saturation field is the maximum achievable electric field for a given charge density. We should note that Eq. (2.12) is for the case when the dc field $E_{s0} = 0$. Similarly, using these two parameters Eq. 2.9 (which is for the case when the dc field $E_{s0} \neq 0$) can be rewritten as [11]

$$E_{s1} = \frac{jE_d - E_0 \frac{I_1}{I_0}}{1 + \frac{E_d}{E_q} + j \frac{E_0}{E_q}}. \quad (2.13)$$

The two equations Eq. (2.12) and Eq. (2.13) for the amplitude of the space charge field are key results of the band transport model for the steady state. Equation (2.11) also reveals the important fact that when there is no applied field ($E_{s0} = 0$), the space-charge field has a 90-degree phase shift with respect to the intensity interference pattern. However, when there is an applied field, this field not only changes the magnitude of the

space charge field, but also alters its spatial phase. This becomes especially important when we consider the photovoltaic effect. In addition to diffusion, some anisotropic crystals (i.e., LiNbO_3) exhibit strong photovoltaic effect which refers to the tendency of the photo-ionization process (under uniform illumination) to eject an electron in a preferred direction due to the asymmetric potential in that anisotropic crystal [11]. If the crystal is illuminated and open circuited, there will be a constant electrostatic photovoltaic field (E_{pv}) in the crystal at steady state. The drift current due to this field will build an opposing bulk electrostatic field, which may cancel the photovoltaic field ($E_0 = -E_{pv}$) [11]. It has been shown that for a relatively low power CW laser (mW), only a minute amount of charge leakage into the surrounding air (through the crystal surface or within the bulk of the crystal) would be sufficient to prevent the buildup of the opposing bulk field ($E_0 \neq -E_{pv}$) [10]. The sum of bulk field and the photovoltaic field can be substituted in Eq. (2.13) in place of E_0 to derive the following equation for the space-charge field.

$$E_{s1} = \frac{jE_d - (E_0 + E_{pv})}{1 + \frac{E_d}{E_q} + j \frac{(E_0 + E_{pv})}{E_q}} \frac{I_1}{I_0}. \quad (2.14)$$

To fully appreciate the effect of the applied field, the space-charge field (Eq. 2.14) can be written as [11]

$$E_1 = \frac{jE_d}{1 + \frac{E_d}{E_q}} \left[\frac{1 + j \frac{(E_0 + E_{pv})}{\bar{E}_d}}{1 + j \left(\frac{(E_0 + E_{pv})}{E_d + E_q} \right)} \right] \frac{I_1}{I_0}. \quad (2.15)$$

The first term on the right-hand side of the equation is simply the space-charge field in the absence of any applied dc or photovoltaic field. The term inside the square brackets represents a scaling factor due to the presence of a dc electric field (applied or photovoltaic or combination of both). This scaling factor is a complex number and thus the presence of a dc or photovoltaic field not only changes the magnitude of the space-charge field, but also alters its spatial phase. This affects the beam-coupling characteristics of the grating in a complex way and will be discussed more in detail in the simulation results in Chapter 9.

2.3 Two-wave Coupling

When two coherent waves intersect inside a PR material, the generated refractive index grating will affect the propagation of these two waves. Since Bragg scattering is perfectly phase matched [11], when wave 1 is scattered by the index grating, the diffracted light propagates along the direction of wave 2, and vice versa, as shown in Figure 2.3. This may lead to energy coupling between the two waves. This can occur for both co-directional and contra-directional geometries. In order to calculate the amount of energy transfer we need the coupled equations for both waves as a function of propagation distance in the material.

Let the total optical field of the two waves be written as

$$E = \text{Re}[C_1 \exp(j\omega t - j\vec{k}_1 \cdot \vec{r}) + C_2 \exp(j\omega t - j\vec{k}_2 \cdot \vec{r})] \quad (2.16)$$

where C_1 , C_2 are the (complex) wave amplitudes, ω is the angular frequency, and \vec{k}_1 , \vec{k}_2 are the wave vectors.

The index of refraction including the fundamental component of the intensity-induced gratings can be written as [11]

$$n = n_0 + \text{Re} \left[\frac{n_1}{2} \exp(j\phi) \frac{C_1^* C_2}{I_0} \exp(-j\bar{K} \cdot \bar{r}) \right], \quad (2.17)$$

where $\bar{K} = \bar{k}_2 - \bar{k}_1$ is the grating vector, and $I_0 = |C_1|^2 + |C_2|^2$, n_0 is the index of refraction when no light is present, n_1 is the amplitude of the change of index (a positive number), ϕ is the phase, indicating the degree to which the index grating is shifted spatially with respect to the light interference pattern. For a material with known material parameters, expressions for $n_1 e^{j\phi}$ can be derived using the space-charge field solutions that were shown earlier in this Chapter, and the electro-optic coefficient.

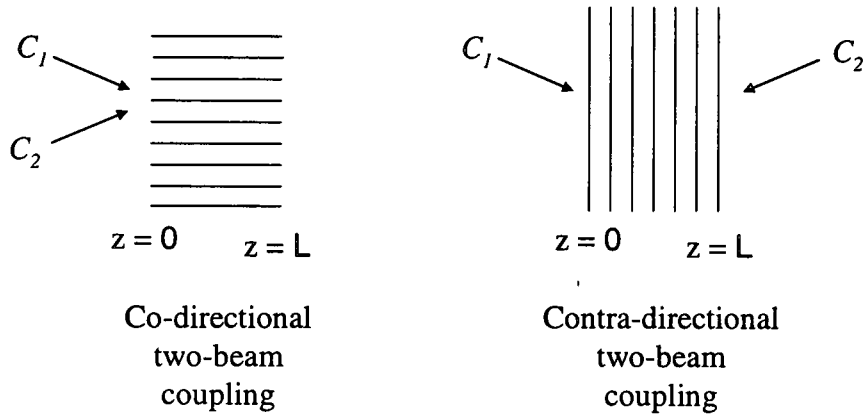


Figure 2.3: Two-beam coupling in photorefractive material [11].

To investigate wave coupling, we substitute Eq. (2.26) into the Helmholtz equation

$$\nabla^2 E + \frac{\omega^2}{c^2} n^2 E = 0 \quad (2.18)$$

and assume, for the sake of simplicity, that wave amplitudes C_1 and C_2 are functions of z only. Here we only solve for the steady state, so C_1 and C_2 are also taken to be time independent. Using the slowly varying amplitude approximation, that is,

$$\left| \frac{d^2}{dz^2} C_i \right| \ll \left| \beta_i \frac{d}{dz} C_i \right|, \quad i = 1, 2 \quad (2.19)$$

we obtain

$$2j\beta_1 \frac{d}{dz} C_1 = \frac{\omega^2 n_0 n_1}{c^2 I_0} e^{-j\phi} C_2^* C_1, \quad (2.20)$$

$$2j\beta_2 \frac{d}{dz} C_2 = \frac{\omega^2 n_0 n_1}{c^2 I_0} e^{-j\phi} C_1^* C_2, \quad (2.21)$$

where k_{1z} and k_{2z} are the z -component of the wave vectors \bar{k}_1 and \bar{k}_2 inside the medium, respectively. Now, two-wave mixing can be classified as co-directional and contra-directional, as discussed below.

2.3.1 Co-directional Wave Coupling ($k_{1z}k_{2z} > 0$)

Referring to Figure 2.3(a), we consider the case when the two optical waves enter the medium from the same side at $z = 0$. For convenience we only consider the symmetric case

$$k_{1z} = k_{2z} = k \cos \theta = \frac{2\pi}{\lambda} n_0 \cos \theta, \quad k = |\bar{k}_1| = |\bar{k}_2|, \quad (2.22)$$

where 2θ is the angle between the waves inside the medium, and n_0 is the index of refraction of the medium. Now if we redefine the optical fields as $C_1 = \sqrt{I_1} \exp(-j\psi_1)$

and $C_2 = \sqrt{I_2} \exp(-j\psi_2)$, and substitute Eq. (2.22) in Eqs. (2.20) and (2.21), it can be shown [11] that

$$\frac{d}{dz} I_1 = -\gamma \frac{I_1 I_2}{I_1 + I_2} - \alpha I_1, \quad (2.23)$$

$$\frac{d}{dz} I_2 = \gamma \frac{I_1 I_2}{I_1 + I_2} - \alpha I_2 \quad (2.24)$$

and

$$\frac{d}{dz} \psi_1 = \zeta \frac{I_2}{I_1 + I_2}, \quad (2.25)$$

$$\frac{d}{dz} \psi_2 = \zeta \frac{I_1}{I_1 + I_2} \quad (2.26)$$

where γ and ζ are related to n_1 by [11]

$$\gamma = \frac{2\pi n_1}{\lambda \cos \theta} \sin \phi, \quad \zeta = \frac{\pi n_1}{\lambda \cos \theta} \cos \phi. \quad (2.27)$$

In Eqs. (2.23) and (2.24), the last term has been added to account for attenuation, with α denoting the bulk absorption coefficient. By examining the coupled equations, we can observe that in the absence of material absorption ($\alpha = 0$), I_2 is an increasing function of z provided γ is positive. This indicates that the energy is flowing from wave 1 to wave 2. The direction of energy flow is determined by the sign of γ which depends on the orientation of the crystal axis.

2.3.2 Contra-directional Wave Coupling ($k_{1z} k_{2z} < 0$)

We now consider the case when the two waves enter the medium from opposite faces, as shown in Figure 2.3(b). Again for convenience we only consider the symmetric case

$$k_{1z} = -k_{2z} = k \cos \theta = \frac{2\pi}{\lambda} n_0 \cos \theta, \quad (2.28)$$

where θ is the angle between each of the waves and the z -axis inside the medium.

Again, substituting Eq. (2.36) in Eqs. (2.20) and (2.21), it can be shown [11] that

$$\frac{d}{dz} I_1 = -\gamma \frac{I_1 I_2}{I_1 + I_2} - \alpha I_1, \quad (2.29)$$

$$\frac{d}{dz} I_2 = -\gamma \frac{I_1 I_2}{I_1 + I_2} + \alpha I_2 \quad (2.30)$$

and

$$\frac{d}{dz} \psi_1 = \zeta \frac{I_1 I_2}{I_1 + I_2}, \quad (2.31)$$

$$\frac{d}{dz} \psi_2 = -\zeta \frac{I_1 I_2}{I_1 + I_2}, \quad (2.32)$$

where γ and ζ are related to n_1 as before.

Comparing Eqs. (2.29) and (2.30) with Eqs. (2.23) and (2.34), we note that there is a sign difference for wave 2. This is due to the fact that wave 2 is now propagating along the negative z -axis. According to Eqs. (2.36) and (2.37), for a positive γ , energy flows from wave 1 to wave 2, as was the case for co-directional.

Closed form solutions of these coupled equations exist for co-directional and contra-directional geometries for non-absorbing material ($\alpha = 0$). For all other cases numerical solutions are used.

2.4 Two-beam Coupling

The formulation above in Section 2.3 is for two-wave coupling. For a slowly focusing beam, it is assumed that the coupled-wave theory is acceptable for beam-coupling as

well. This approximation may not be valid for a tightly focused beam. In the section below, we look at an alternate formulation of the steady state solution that permits a beam-coupling theory. The wave-coupling theory presented in Section 2.3 makes use of Eq. (2.17) in conjunction with the space-charge field solutions that are presented earlier in Section 2.2, which is for plane waves. For beam-coupling we need a solution for the space-charge field for a beam, which could then be used to calculate the index modulation using the linear electro-optic effect.

The coupled set of simplified Kukhtarev equations, including diffusive and photovoltaic effects, can be decoupled in the steady state and can be approximately solved to yield the following relation for the space-charge field $E_s(x, y, z)$ [12]

$$E \approx \frac{D}{\mu N_D (sI + \beta)} (sN_D \nabla I + \frac{\kappa \alpha \gamma_R N_A}{qD} I) = E_{DIFF} + E_{PV}, \quad (2.33)$$

where γ_R is the carrier recombination rate; μ is the carrier mobility; α is the absorption coefficient; κ is the photovoltaic constant; β is the thermal generation rate; N_A is the acceptor concentration; N_D is the donor concentration; q is the electric charge; s , the ionization cross section per quantum of light; and D the diffusion constant that is given by the Einstein relationship [$D = (k_B T / e) \mu$, where k_B is the Boltzmann constant and T is the temperature]. Also, $I(x, y, z)$ denotes the intensity distribution along the transverse coordinates x , and y at position z in the PR material. In Eq. (2.33), the first term on the right-hand side is the contribution from the effect of diffusion, whereas the second term describes the photovoltaic effect.

Ignoring any thermal or elasto-optic contribution, the over all induced refractive index $\Delta n(x, y, z)$ may be expressed as [12]

$$\begin{aligned}
\Delta n &= (\Delta n)_{DIFF} + (\Delta n)_{PV} \\
&= -\frac{1}{2} n^3 r_{eff} ((E)_{DIFF} + (E)_{PV})
\end{aligned} \tag{2.34}$$

where, n is the refractive index, r_{eff} is the effective electro-optic coefficient. Using this formulation, the space-charge field and induced index can be calculated for any arbitrary shaped beam. Since closed form expression for beam-coupling is not available, a split-step beam propagation method could be used to compute the space-charge field, index modulation and evolution of the beam in the PR media [12].

2.4 Conclusions

We have described the physics of the PR effect, the band transport model and the theory of beam-coupling for plane waves and Gaussian beams. The theoretical formulation for the space-charge field is different for these two cases. For plane-wave coupling, closed form coupled equations can be formulated. For two-beam coupling such a closed form solution does not exist. Computer simulations, such as BPM have been used to demonstrate beam-coupling in transmission grating geometry [12]. To the best of our knowledge, for the self-pumped contra-directional (SPCD) two-beam coupling (TBC) (where the signal is the Fresnel reflection from the second crystal surface) BPM simulation has not been done.

In what follows in Chapter 3, we review some earlier work on self-pumped contra-directional (SPCD) two-beam coupling (TBC), where a reflection grating formed between a single pump beam and its Fresnel reflection from the rear face of the crystal (signal beam) facilitates energy coupling. In Chapter 3, we also review earlier work on a

phenomenon called six-wave mixing that is closely related to SPCD-TBC. In subsequent chapters we show new experimental work on six-wave mixing (Chapters 4-6) and a novel BPM simulation of SPCD-TBC (Chapters 7-9).

CHAPTER III

PREVIOUS RESEARCH ON SPCD-TBC AND SIX-WAVE MIXING

3.1 Introduction

Photorefractive self-pumped contra-directional (SPCD) two-beam coupling (TBC) in $\text{LiNbO}_3\text{:Fe}$ resulting from the formation of a reflection grating has been a recent subject of investigation [6]. Use of this coupling geometry has the advantage of simplicity in that only one incident beam is used, while the second beam is generated by the reflection from the back of the crystal. The power of the transmitted beam drops (and that of the reflected beam rises) with time as the PR grating inside the medium is built up, providing a measure of the TBC efficiency. Here, we review some of the earlier work on SPCD-TBC in Section 3.2. During the SPCD-TBC, if the pump beam is obliquely incident on the front face of the $\text{LiNbO}_3\text{:Fe}$ crystal, a particular phenomenon of SPBS leading to six-wave mixing has been observed [7,9]. We review earlier work on six-wave mixing in Section 3.3.

3.2 Contra-directional Two-beam Coupling

In order to understand contra-directional two-beam coupling using a single incident pump beam it is essential to have an estimate of the gain coefficient (γ) experimentally. Since this is an intrinsic material property, it would be the same whether a single pump beam, or two separate degenerate beams are used to write the reflection grating. Accurate contra-directional gain measurements in Fe:LiNbO₃ are very difficult since reflections from the surfaces of the crystal act as false signals and compete with the injected signal [13]. To overcome this problem, Cook *et al.* [6] have measured the gain by using a prismatic Fe:LiNbO₃ crystal. The chosen shape of the crystal allows the pump and signal beams to be incident at Brewsters' angle (thus eliminating all reflections), while internally allowing both beams to propagate along the c-axis. The measured [6] gain coefficient with this setup for Fe:LiNbO₃ (100 cm⁻¹) is significantly higher than what was calculated (20 cm⁻¹) for diffusion dominated charge transport [14]. The photovoltaic effect has been identified as the most likely mechanism for generating the observed high optical gain [10]. Prior to this it has been strongly believed that photovoltaic effect does not contribute to the gain coefficient (or two-beam coupling efficiency) since the photovoltaic field is cancelled out by the bulk field that is generated internally in the crystal. By applying external bias voltage, Cook *et al.* [10] have directly shown that in reality the bulk field does not cancel the photovoltaic field E_{pv} and thus E_{pv} plays a significant role in the beam coupling.

An advantage of SPCD-TBC is that the signal beam from the Fresnel reflection at the second surface overlaps with the pump beam, even when focused tightly. However, it has also been observed that the coupling efficiency (quantified by the power transferred

from the pump beam to the signal beam) is significantly dependent on the focusing geometry (spot size) [15, 16, 17], and focal position of the beam. This is shown in Fig. 3.1. It has been theorized [16] that diffraction of the beam and dark conductivity contributes to this. Beams of different spot sizes diffract by different amounts, thus the intensity distribution in the overlapped region of the pump and the Fresnel reflected signal varies significantly with spot size. Since dark conductivity destroys the grating as it forms, the variation in intensity distribution due to diffraction enhances the effect of dark conductivity.

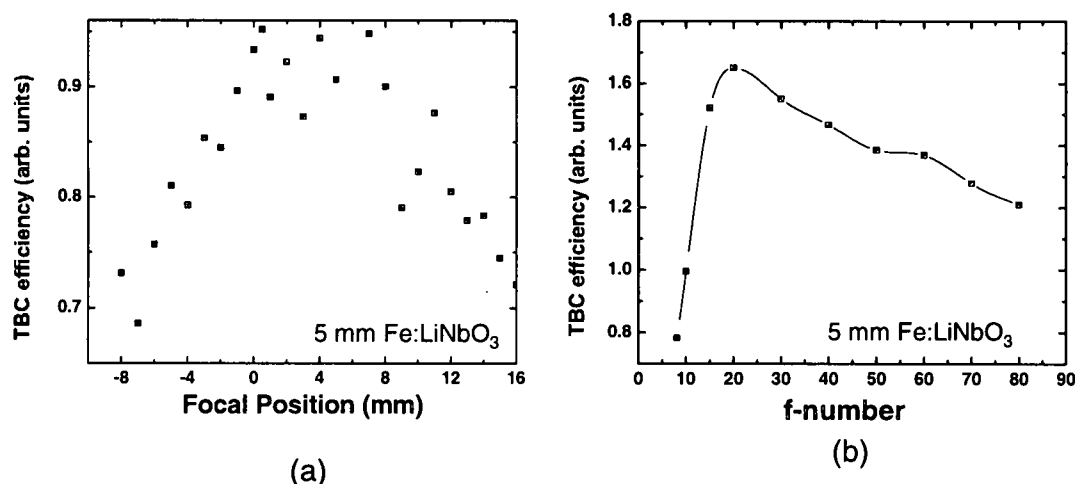


Figure 3.1: Change in TBC due to diffraction. TBC efficiency changes as (a) the pump beam is focused at different planes inside the crystal which is about 10 times larger than the Rayleigh range. (b) the spot size of the pump beam changed [17].

Cook *et al.* [16] have modified the two-wave coupling equations for contra-directional geometry in the steady state (Eqs. 2.29 and 2.30) by including an expression

for $\frac{dI}{dz}$ from the geometric focusing effect. They have shown that, due to beam diffraction alone, intensity changes as:

$$\frac{dI}{dz} = -\frac{2(z-f)I}{z_R^2 + (z-f)^2}, \quad (3.1)$$

where f is the distance from the focusing lens to the focused beam spot. The effects of the dark conductivity are included by using a thermal equivalent intensity [16]. This is an effective light intensity I_{dark} , which can erase the gratings. With these modifications, the contra-directional two-wave coupling equations (2.37) become

$$\frac{dI_{pump}}{dz} = -\alpha I_{pump} - \gamma \frac{I_{pump} I_{signal}}{I_{pump} + I_{signal} + I_{dark}} - \frac{2(z-f)I_{pump}}{z_R^2 + (z-f)^2}, \quad (3.2)$$

$$\frac{dI_{signal}}{dz} = +\alpha I_{signal} - \gamma \frac{I_{pump} I_{signal}}{I_{pump} + I_{signal} + I_{dark}} - \frac{2(z-f)I_{signal}}{z_R^2 + (z-f)^2}. \quad (3.3)$$

By varying the distance from the lens to the focused beam spot (f), one could also calculate the difference in wave-coupling due to focusing at different planes of the crystal (with respect to the c-axis faces). For a fast focusing geometry the theoretical model does not agree very well with the experimental results. This may be due to the fact that the model is based on plane wave coupling theory.

Another significant PR phenomenon that has been of interest recently is the photovoltaic induced noise in the steady state transmitted pump signal [6]. It has long been observed [18,19] that the transmitted and back-scattered light periodically has a sudden change (a jump) during the two-beam coupling. This jump has been attributed to the quasi-breakdown of the uniform component of the photovoltaic field [19,20], due to electric discharge at the crystal surface. Recently, Evans *et al.* [20] have shown that

these jumps can be prevented by coating the crystal with a transparent conducting indium tin oxide (ITO), or an insulating anti-reflection transparent coating (SiO_2) layer. Figure 3.2 shows the transmitted pump light as a function of time. It is observed that the pump transmission (solid line) drops as the reflection grating is formed. After some time (which decreases with increasing pump power) jumps are observed in the transmission. The rise time of these jumps has been measured by Evans *et al.* [20] to be approximately 5 nanoseconds (limited by the detector speed). Figure 3.2 also shows that when the PR sample is coated with indium tin oxide (ITO), the transmitted light does not show the jumps any more. Similar results are obtained [20] with an insulating anti-reflection (AR) coating (SiO_2). It has been theorized [20] that the conducting ITO coating prevents the electric discharge by allowing the accumulated charge to spread over a larger surface area and the anti-reflection coating prevents the electric discharge by insulating the accumulated charge from the surrounding air.

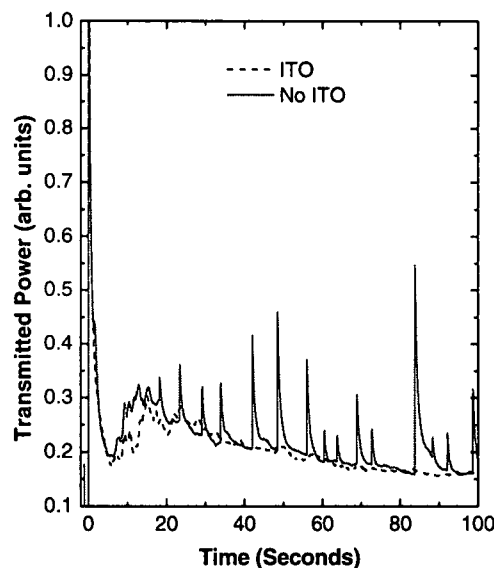


Figure 3.2: The photovoltaic noise and its elimination with conductive coating [20].

Recently, Evans *et al.* [21] have experimentally shown that the grating is always the strongest near the front face of the crystal (facing the laser). This is done by using optical erasure technique, where the grating is erased with a focused beam from the side (perpendicular to the c-axis). The erasure of the grating changes the transmission of a low power probe beam, providing quantitative information about the strength of the grating that was present in that plane prior to erasure [21].

3.3 Six-wave Mixing

In a related context involving reflection gratings, a particular phenomenon of SPBS leading to six-wave mixing has received some interest in the PR research. When a focused beam is obliquely incident on the c-face of the crystal (incident beam propagation is nominally opposite the direction of gain, resulting in reflection grating geometry), a stimulated PR back-scatter (SPBS) is observed along with 5 other waves inside the crystal. Among other non-linear materials, PR KNbO_3 has been observed to exhibit six-wave mixing [7, 9]. Six-wave mixing has also been observed in other PR materials, like LiNbO_3 [22, 23]. The observed six-wave mixing between waves $C_1 - C_6$ within the crystal can be understood using the schematic shown earlier in Fig. 3.3.

SPBS has been of significant interest in the area of PR research. In particular, PR backscatter leading to phase conjugation processes have been theoretically and experimentally studied in various contexts [7,9,22-26]. In this dissertation, we report on

SPBS in PR LiNbO_3 for a specific experimental arrangement that leads to six-wave mixing, and phase-conjugation from four-wave mixing or “parametric diffraction”.

A detailed theoretical and experimental study of stochastic backscatter has been performed by Shamonina *et al.* [27], where it has been shown that a large local response such as in PR LiNbO_3 can stimulate a noisy backscatter. Amplification of the backscattered light in PR materials along the c -axis of the crystal has been reported in Refs. [22 - 26]. References 22 and 23 report transient contra-directional self-phase

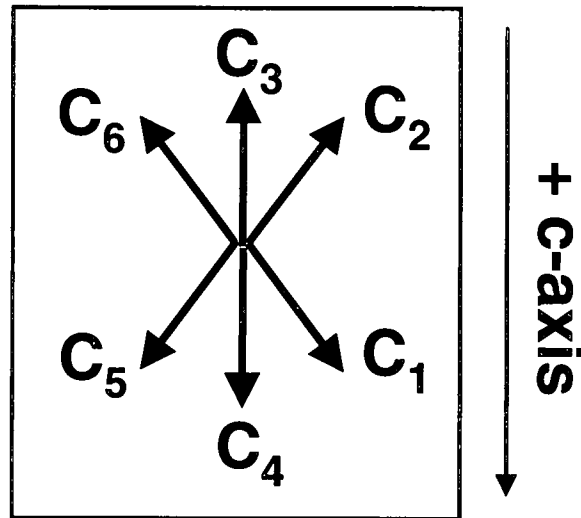


Figure 3.3: Schematic representation of the six waves inside the crystal. C_1 denotes the forward propagating pump through the crystal. C_2 represents the result of six-wave mixing in the direction of the Fresnel reflection of the pump from the surface. C_3 and C_4 denote the waves generated in the crystal that are perpendicular to the interface, and consequently along the c -axis. C_5 and C_6 (the SPBS) make up the other two participating waves in the six-wave mixing scheme [24].

conjugation due to stimulated backscatter in $\text{LiNbO}_3\text{:Fe}$. In this case, a strongly focused incident beam at nominally normal incidence on the crystal with its c -axis oriented

opposite to the direction of propagation of the beam generates back reflection which contains the phase conjugate. A phase distorter which is inserted in the path of the incident beam originally to verify phase conjugation is also shown to optimize its quality (fidelity) by further increasing the divergence of the strongly focused incident beam [22,23]. Recently, strong stimulated backscatter leading to self-pumped phase conjugation has been observed in $\text{LiNbO}_3\text{:Mg}$ at 351 nm where the PR sample exhibits large ultraviolet photorefractivity [26].

For an obliquely incident pump, PR backscatter, and phase conjugation resulting from six-wave mixing have been demonstrated in PR $\text{KNbO}_3\text{:Fe}$ [7, 9]. In that case, the pump light is typically incident on the c-face of the crystal with an angle of about 10 degrees with respect to the c-axis, giving rise to beams traveling forward, backward, and normal to the interface, along with the phase conjugates. A transient contra-directional self-phase conjugation in PR KNbO_3 has also been observed using strongly focused beam at nominally normal incidence and a moving random phase plate [23]. In a separate PR material, such as BaTiO_3 , self-pumped phase conjugation has been observed when the pump is obliquely incident on a crystal face other than the c-face, due to either corner-reflection [28] or generation of SPBS [29].

The observed six-wave mixing has been modeled [9] following the schematic shown Fig. 3.3. Scattered light in these six directions may get amplified by self diffraction or by parametric diffraction. Considering reflection gratings only and starting from Maxwell's equations, a set of six coupled equations can be derived for the complex amplitudes of the interacting optical fields inside the PR material, nominally propagating in the directions 1-6 as shown in Fig. 3.3 [9].

The quality of the phase-conjugate has been studied by various methods. The fidelity of phase conjugation resulting from amplification of Brillouin scattering has been quantitatively assessed through interferometric techniques [30]. In PR materials, the fidelity of a pair of phase conjugate beams has been monitored by measuring the visibility of fringes in interference experiments [31].

3.4 Conclusions

Here, we have reviewed some of the earlier work on SPCD-TBC. In particular we have discussed:

- a) the issues related to the high 'gain' measured in $\text{LiNbO}_3\text{:Fe}$,
- b) the role of photovoltaic field in beam-coupling,
- c) an approximate beam-coupling model that approximates the diffraction effects of a focused beam and combines it with plane-wave coupling theory,
- d) photovoltaic induced noise in beam-coupling and the way of reducing it,
- e) grating strength distribution with the $\text{LiNbO}_3\text{:Fe}$ crystal after SPCD-TBC.

We have also reviewed earlier work on six-wave mixing. In particular we have discussed:

- a) observation of SPBS in various media, and theoretical and experimental study,
- b) observation of self-pumped phase conjugation in various PR media,
- c) observation of six-wave mixing in $\text{KNbO}_3\text{:Fe}$,
- d) a set of coupled equations for the interacting six-waves.

Before discussing the theory of six-wave mixing in detail (Chapter 5) we describe the six-wave mixing experiments that we have conducted on a set of $\text{LiNbO}_3\text{:Fe}$ crystals with different types of dopings and surface coatings.

CHAPTER IV

EXPERIMENTAL SETUP FOR SIX-WAVE MIXING AND SPBS

4.1 Introduction

In this work, six-wave mixing in $\text{LiNbO}_3\text{:Fe}$, resulting from a 532 nm pump obliquely incident on the crystal and traveling nominally along the $+c$ axis and with polarization perpendicular to the plane of incidence, is investigated. Reflection of the pump from the back surface of the crystal generates a counter-propagating signal which then interferes with the pump to give rise to reflection gratings. Furthermore, this geometry also leads to stimulated photorefractive backscatter (SPBS), as well as beams traveling normal to the interface along the $\pm c$ axes. The net result is six interacting waves (beams) traveling through the crystal and interacting with each other via reflection gratings. Six-wave mixing between waves $C_1 - C_6$ within the crystal can be understood using the schematic shown in Fig. 3.1. Scattered light in the six directions have contributions from self diffraction or parametric diffraction, as will be clear from the theory in Chapter 5. Experimental observations, as well as analysis of some results using the theory is presented in Chapter 6.

4.2 Photorefractive Samples Used

Iron doped lithium niobate crystals of various doping concentrations, coatings, and thicknesses are used as PR samples. The crystals and their different parameters are presented in Table 4.1.

Table 4.1. Relevant parameters for all the $\text{LiNbO}_3\text{:Fe}$ crystals used for the study of six-wave mixing and SPBS. AR: Anti-reflection coating. ITO: conducting coating of indium tin oxide.

crystal marked	mol % Fe_2O_3 in the melt	c-axis length (mm)	coatings on z-surfaces	absorption coefficient (cm^{-1})
A	0.03	10	none	0.43
B	0.05	10	none	1.20
C	0.03	10	AR	0.47
D	0.05	10	ITO	1.17
E	0.05	5	none	1.19

All crystals have a cross-sectional area of 10 mm x 10 mm. In general, the experiments have been performed using crystal A; however, several supplementary experiments have been conducted using crystals B, C, D, and E. In particular,

- (i) crystal B has been used to study the effect of higher Fe doping on six-wave mixing and SPBS;

- (ii) crystal C, which is anti-reflection (AR) coated, has been used to study the effect of initial scatter upon reflection of the pump from the back surface of the crystal on six-wave mixing and SPBS;
- (iii) crystal D, which is ITO coated, has been used to study the effect of buildup of photovoltaic charges on six-wave mixing and SPBS; and
- (iv) crystals B and E have been used to compare the effect of interaction length on six-wave mixing and SPBS.

Care is taken to remove gratings that build up in the crystals by subjecting them to a baking cycle, which involves heating them to 250 C and cooling them back to room temperature, between successive sets of measurements. Finally, to compare the SPBS from the $\text{LiNbO}_3\text{:Fe}$ crystals with a standard phase conjugator, a 5 mm x 5 mm x 5 mm $\text{BaTiO}_3\text{:Ce}$ crystal has been used as well.

4.3 Six-wave Mixing

The experimental arrangement to investigate six-wave mixing is shown in Fig. 4.1. The unexpanded 532 nm beam from a Verdi laser is focused with either a 750 mm or a 200 mm focal length lens (placed as L1) to waist sizes¹ of 90 or 25 microns, respectively. The crystal is mounted on a rotation stage in order to study the dependence of the six-wave mixing on the angle of incidence of the pump, which is introduced nominally along the +c-axis and consequently opposite to the direction of the gain. The small angle, in air, between the pump propagation direction and c-axis is recorded. The crystal is placed at the focus and the pump beam is allowed to pass through a hole on screen S1 (see

¹ Waist size is measured at e^{-2} radius of the intensity in the dissertation.

Figure 4.1). Screen S2 is placed behind the crystal to show all transmitted beams. C_1 denotes the forward propagating pump through the crystal. C_2 represents the result of six-wave mixing in the direction of the Fresnel reflection of the pump from the surface. C_3 and C_4 denote the waves generated in the crystal that are perpendicular to the interface, and consequently along the c -axis. C_5 and C_6 (the SPBS) make up the other two participating waves in the six-wave mixing scheme [24].

For a 90 micron waist size beam, an incident power of 65 mW (100 mW before the BS1) is used. We have found experimentally that for incident powers below 60 mW, six-wave mixing does not occur in any reasonable period of time. Using significantly more power causes photovoltaic noise [20, 32], which tends to wash out the SPBS (C_6) with each occurrence of the quasi-periodic photovoltaic breakdown.

The time evolutions of all interacting waves are monitored with a dual channel Newport 2832-C power meter and Newport 818-SL power detectors. Since only two beams can be recorded simultaneously, C_1 is kept common in all cases. Monitoring C_1 is crucial in order to ensure that its initial intensity, which should correspond to the linear transmission through the crystal, is the same for all measurements. Monitoring of C_1 also ensures that we do not have accidental incidence on a crystal defect or on a resident grating. Care is taken to reduce other scatter from being added to the SPBS by placing multiple irises along the path of C_6 (not shown on Fig. 2 for simplicity). The power in C_6 is detected after it is partially reflected off the second beam splitter BS2. All other beams (C_1 - C_5) are detected by focusing them onto a second detector. Six independent

traces for each beam of $C_2 - C_6$ are recorded in order to check reproducibility of the experimental results.

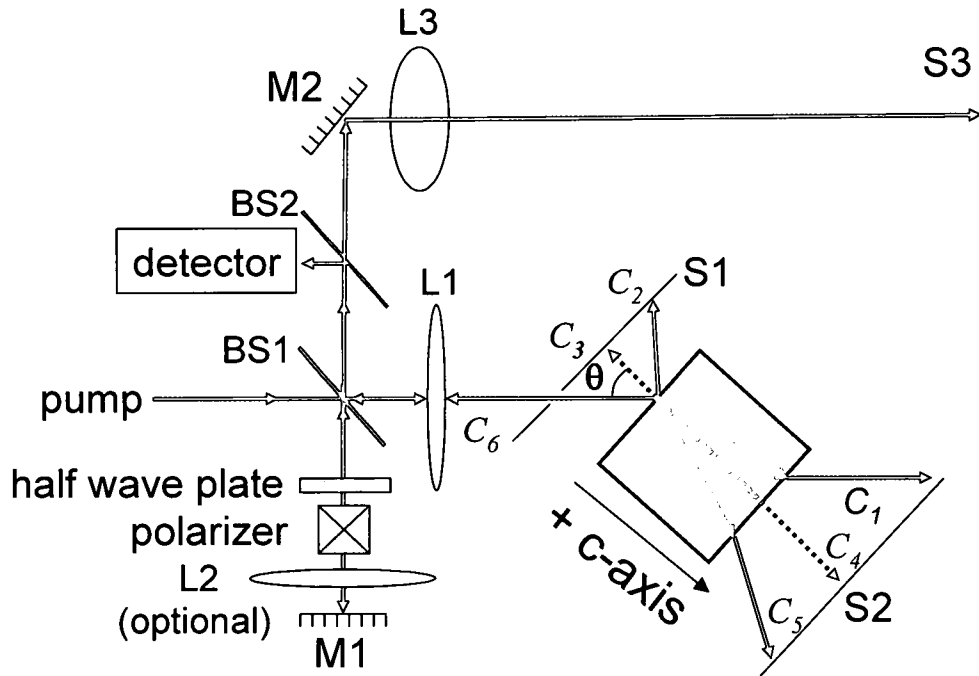


Figure 4.1: Schematic representation of the experimental arrangement. L1-L3: lenses; M1, M2: mirrors; BS1, BS2: beam splitters. The pump is collimated 532 nm light from a Verdi laser. Six-wave mixing is observed on screens S1 and S2. Lens L1 is used to focus the pump onto the PR sample which is placed at its back focus for six-wave mixing experiments. SPBS (C_6) power is measured with the detector shown. Powers in $C_1 - C_5$ are also recorded with similar detectors placed directly in the path of the beams after exit from the crystal in their respective directions. Lens L3 and screen S3 are used during interference experiments for determination of the quality of SPBS. The PR sample is first placed at an arbitrary distance from lens L1 and the SPBS interfered with a portion of the collimated pump reflected by the mirror M1 with lens L2 removed. Thereafter, the sample is reinserted at the back focal plane of L1 and the interference of the SPBS with a portion of the pump focused by L2 and reflected by the mirror M1 is monitored.

4.4 The Nature of SPBS

As explained in Section 1.2 and Chapter 5, the observed SPBS C_6 consists of both self diffraction terms and parametric diffraction terms. Thus, the SPBS is expected to exhibit the nature of a phase conjugate partially. The SPBS from $\text{LiNbO}_3\text{:Fe}$ is therefore subjected to the well-established image restoration test [28], and compared with results from self-pumped phase conjugation from a $\text{BaTiO}_3\text{:Ce}$ sample.

The nature of the SPBS from $\text{LiNbO}_3\text{:Fe}$ is further investigated through the interference setup also shown in Fig. 4.1. A reference beam is derived from the pump beam by using a beam splitter (BS1). The reference beam is passed through an adjustable attenuator (combination of wave plate and polarizer) to make its power similar to that of the SPBS. Equal powers of the reference beam and SPBS are necessary to calculate the fringe visibility and extract information about the coherence of the SPBS. In the reference arm part of the interferometer, the pump beam is reflected with a mirror M1 after passing through the focusing lens L2.

For the first part of the interference experiment, when the crystal is placed at an arbitrary distance from lens L1, lens L2 is omitted. The motivation for this comes from the fact that a beam counter-propagating to the pump will not generate any circular fringes after retracing its path through an arbitrarily placed lens L1 and interfering with the collimated reference beam if and only if it is a perfect phase conjugate. This concept is first tested with a $\text{BaTiO}_3\text{:Ce}$ crystal (a good phase conjugator), a plane mirror (which is not a phase conjugator and therefore expected to produce good fringes), and finally the $\text{LiNbO}_3\text{:Fe}$ samples. In our experiment, the crystal is placed at a distance approximately $f/2$ behind L1 of focal length $f=750$ mm, and the pump power adjusted to maintain the in-

focus intensity. For recording purposes, these fringes are expanded with a strongly focusing lens L3 ($f = 50$ mm) and projected on to screen S3. The fringe pattern on screen S3 is photographed with a 7 mega pixel digital camera (Sony DSC-W7). A variable neutral density filter is used to avoid saturation of the camera. Time evolution of the fringes is also monitored.

In the second part of the interference experiment (coherence test), both the $\text{LiNbO}_3\text{:Fe}$ crystals and the plane mirror described above are placed at the focus of the lens L1. Placing the crystals and the mirror at the focus results in a collimated beam after it propagates back through the lens L1. The second lens L2 ($f = 750$ mm) is now inserted to introduce phase curvature. Circular fringes generated using this interference procedure are recorded with the digital camera. Fringe visibility is calculated for both cases from the interference pictures using MathCAD in order to quantify the quality of the interference fringes, and hence to infer the quality of the phase conjugate generated using $\text{LiNbO}_3\text{:Fe}$.

4.5 Conclusions

In this chapter the experimental setup for SPBS leading to six-wave mixing in iron doped lithium niobate crystals of various doping concentrations, coatings, and thicknesses is discussed. The experimental technique to monitor the time evolutions of all six interacting waves are detailed. Experimental techniques for the well-established image restoration test for a self-pumped phase conjugation, such as using PR $\text{BaTiO}_3\text{:Ce}$ is described. Finally, an interference experiment to further determine the nature of the SPBS from $\text{LiNbO}_3\text{:Fe}$ is proposed.

In the following chapter we discuss a set of coupled wave and material equations that models the observed-six wave mixing [9]. Expanding on the work by Kukhtarev *et al.* in Ref. 9, a novel order analysis for the steady-state of the six waves is also presented in Chapter 5.

CHAPTER V

SIMPLIFIED THEORY OF SIX-WAVE MIXING AND SPBS

5.1 Introduction

The observed six-wave mixing is modeled using a set of coupled wave and material equations. Expanding on the work by Kukhtarev *et al.* in Ref. 9, a novel order analysis for the steady state of the six waves is also presented and used to explain some of the experimental results. For the benefit of readers, the implications of some of the terms used later in this work will be briefly explained here.

First, the term optical *beam* or *field* implies a collection of plane waves, as decomposed into its angular plane wave spectrum. The word *wave*, unless otherwise explicitly stated, implies a (*uniform*) *plane wave*. A *strongly focused* or *scattered beam* is therefore clearly not one plane wave, but a collection of many plane waves. Secondly, in PR wave mixing, two plane waves with complex amplitudes designated by C_i, C_j , whether incident independently or created from reflection from a boundary, scatter, etc., form an induced refractive index proportional to $C_i^* C_j$ (and its complex conjugate). When the grating is simultaneously read out by C_i , the resulting diffracted wave ($\propto C_i C_i^* C_j$) loses the phase information of C_i and hence cannot be called its phase

conjugate. This is called *self diffraction* [7, 9], also commonly called *two-wave coupling* (TWC). On the other hand, if a different wave, call that C_k , reads the grating, the corresponding diffracted wave ($\propto C_k C_i^* C_j$) contains the phase conjugate of C_i [11]. This is called *parametric diffraction* [7, 9], also commonly called *four-wave mixing* (FWM). In this context, the work on phase conjugation in, for instance, $\text{LiNbO}_3\text{:Fe}$, using strongly focused beams and/or random phase plates [22,23] should be referred to as *two-beam coupling* or *multi-wave mixing*, since their strongly focused beam of 200 microns Rayleigh range has a divergence angle of approximately a few degrees, while the strongly focused beam passing through the random phase plate has a divergence angle six times as much [22]. In our case, we have conducted experiments using weakly focused beams with a waist of approximately 100 microns, which corresponds to divergence angles which are at least an order of magnitude smaller and therefore resembles a plane wave more closely.

5.2 Interaction Equations and their Reduction

The observed six-wave mixing can be modeled following the schematic shown earlier in Fig. 3.3 in Chapter 3. Scattered light in these six directions may get amplified by self diffraction or by parametric diffraction. Considering reflection gratings only, from Maxwell's equations the following coupled equations can be derived for the complex amplitudes C_m ($m=1,...,6$) of the interacting optical fields nominally propagating in the directions 1-6 shown in Fig. 3.1 inside the PR material [9]:

$$L_1 C_1 = n_{12} C_2 + n_{13} C_3 + n_{16} C_6 + n_{46} C_3 + n_{56} C_2 \quad (5.1a)$$

$$L_2 C_2 = n_{21} C_1 + n_{24} C_4 + n_{25} C_5 + n_{65} C_1 + n_{35} C_4 \quad (5.1b)$$

$$L_3 C_3 = n_{31} C_1 + n_{34} C_4 + n_{35} C_5 + n_{64} C_1 + n_{24} C_5 \quad (5.1c)$$

$$L_4 C_4 = n_{42} C_2 + n_{43} C_3 + n_{46} C_6 + n_{53} C_2 + n_{13} C_6 \quad (5.1d)$$

$$L_5 C_5 = n_{52} C_2 + n_{53} C_3 + n_{56} C_6 + n_{12} C_6 + n_{42} C_3 \quad (5.1e)$$

$$L_6 C_6 = n_{61} C_1 + n_{64} C_4 + n_{65} C_5 + n_{21} C_5 + n_{31} C_4 \quad (5.1f)$$

where L_m are dimensionless operators defined as $L_m = (\nabla_{T_m}^2 + 2jk_{z_m} \partial / \partial z_m) / k_0^2$; $k_0 = 2\pi / \lambda$ is the wave number in the crystal, λ is the optical wavelength in the crystal, and k_{z_m} is the propagation constant of the m -th field ($m = 1, \dots, 6$) along its nominal propagation direction z_m . Also, $\nabla_{T_m}^2$ is the Laplacian in the plane transverse to the nominal direction of propagation of the m -th field. In our reported experiments, the angles between the various interacting fields are no greater than 3 degrees inside the crystal; furthermore, due to *weak* focusing, all interacting fields can be approximately regarded as quasi-plane waves, implying minimal propagational diffraction within the interaction region. The spatial amplitudes of the dielectric permittivity grating n_{ij} formed from nominally counter-propagating interacting fields C_i, C_j can be found from material equations and a standard PR band-transport model [7] as:

$$\tau_{ij} \partial n_{ij} / \partial t = \gamma_{ij} C_i C_j^* - \beta_{ij} n_{ij}, \quad (5.2)$$

where $n_{ij} = n_{ji}^*$, τ_{ij} denotes the Maxwell relaxation time, and parameters γ_{ij}, β_{ij} depend on crystal symmetry. As stated above, only reflection gratings are considered, since transmission gratings have wavevectors for which the electro-optic coefficients are much smaller. Similar optical and material equations appear in Korolkov et al. [23] and references therein, with the difference that in their paper, propagation of, and interactions between, the *composite* forward and backward traveling optical fields are modeled.

Using (5.2), the first three terms in each equation in (5.1) represent self diffraction terms, while the last two terms represent parametric diffraction. The last equation in (5.1) that signifies the spatial evolution of the SPBS is illustrated in Fig. 5.1, where the scattering diagrams explicitly show grating formation and readout for self diffraction and parametric diffraction.

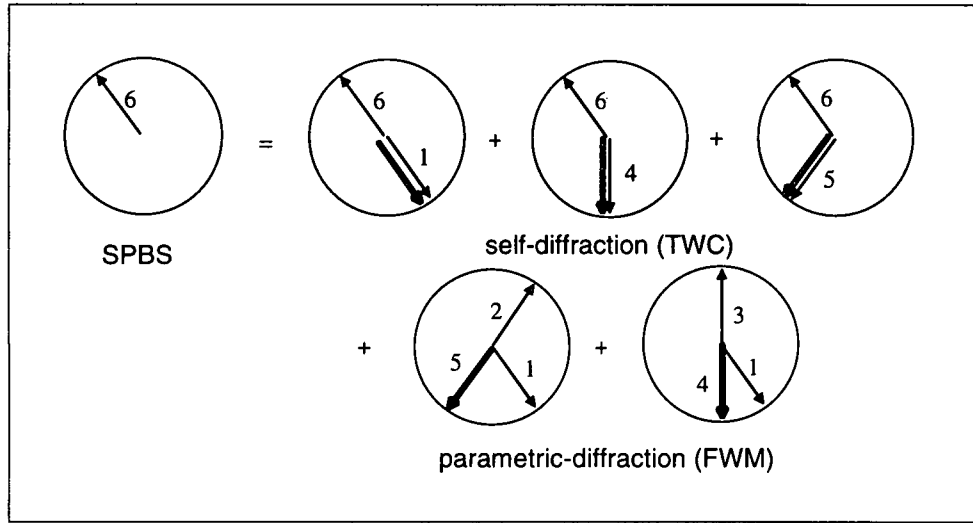


Figure 5.1: Calculation of contributions to SPBS (C_6) using scattering diagrams, following Eq. (5.1f). The thin lines on the right hand side refer to k-vectors of waves participating in the grating, while the dark lines represent the k-vector of the wave reading the grating.

In what follows, it is shown that a heuristic order analysis of Eqs. (5.1a-f) along with (5.2) can give further insight into the nature of various interacting waves and how they are formed. Although heuristic, inferences from this order analysis can explain some of our experimental results for the steady state, as described in the following Section. One can assign book-keeping parameters δ to the reflection coefficient, and ε to the backscattering. If C_1 is assigned the order $\delta^0 \varepsilon^0$, then C_2 , to a first approximation, would be of order $\delta^1 \varepsilon^0$ since it is generated by the reflection of C_1 from the back surface

of the crystal. The wave C_3 , presumably generated by the backscatter of C_1 upon reflection from the back surface, would be of order $\delta^1 \varepsilon^1$, while C_4 formed by the reflection of C_3 from the front surface would have order $\delta^2 \varepsilon^1$. Such order assignments cannot be done for C_5 and C_6 since these are exclusively generated through parametric diffraction and amplified through self diffraction. With the initial assigned orders for the waves $C_1 - C_4$, it can be shown from Eq. (5.1f), along with the steady-state limit of Eq. (5.2): $n_{ij} \propto C_i C_j^*$, that C_6 could have the next higher order $\delta^3 \varepsilon^2$ arising from the order of the last term $n_{31} C_4$ on the RHS which represents parametric diffraction. With this assumption, it is observed that the first term $n_{61} C_1$ in Eq. (5.1f) representing self diffraction also has the same order. A similar order analysis for C_5 based on Eq. (5.1e) shows that its dominant order is $\delta^4 \varepsilon^2$ arising from the terms $n_{12} C_6$ and $n_{42} C_3$. Using this, it is observed that the next higher order, viz. $\delta^5 \varepsilon^2$ in Eq. (5.1f) is the term $n_{21} C_5$. It turns out that this term is non-negligible under certain experimental conditions, to be described later. In a similar way, all the other equations (5.1a)-(5.1f) can be revisited, and terms up to two orders higher in δ and one order higher in ε retained. This results in the reduced set of equations (5.3a)-(5.3f) below:

$$L_1 C_1 = n_{13} C_3 (O : \delta^1 \varepsilon^0) + n_{12} C_2 (O : \delta^1 \varepsilon^1), \quad (5.3a)$$

$$L_2 C_2 = n_{21} C_1 (O : \delta^1 \varepsilon^0), \quad (5.3b)$$

$$L_3 C_3 = n_{31} C_1 (O : \delta^1 \varepsilon^1), \quad (5.3c)$$

$$L_4 C_4 = n_{42} C_2 (O : \delta^4 \varepsilon^1), \quad (5.3d)$$

$$L_5 C_5 = (n_{12} C_6 + n_{42} C_3) (O : \delta^4 \varepsilon^2) + n_{52} C_2 (O : \delta^6 \varepsilon^2), \quad (5.3e)$$

$$L_6 C_6 = (n_{61} C_1 + n_{31} C_4) (O : \delta^3 \varepsilon^2) + n_{21} C_5 (O : \delta^5 \varepsilon^2). \quad (5.3f)$$

One of our objectives in this work is to determine the nature of C_6 . As seen from Eq. (5.3f), C_6 contains contributions from (a) self diffraction ($n_{61}C_1$), and (b) parametric diffraction ($n_{31}C_4$ and $n_{21}C_5$), which contain the phase conjugate of C_1 as stated earlier in the Introduction. This will have relevance in Chapter 6 (Section 6.2) where the nature of SPBS is investigated using interferometric techniques.

Equation (5.3a) suggests that as C_1 self diffracts, it couples its power to C_2 and C_3 , as also evidenced from Eqs. (5.3b) and (5.3c). It should be noted that additional factors, also significantly affecting C_3 , are not included in the above theory. For instance, C_3 points in the direction of the gain, which gives C_3 an advantage over other participating waves when it comes to coupling power into the waves. In addition, C_3 and C_4 may also grow due to Fabry-Perot effect under the right conditions, where the reflected scatter from the pump is amplified along the gain direction. Furthermore, the angle between the pump and the c -axis also affects the growth of all six-waves, since two-beam coupling efficiency diminishes with increasing angle (i.e., decreasing overlap). This is most significant for C_3 since it primarily acquires power from C_1 (Eq. 5.3c) through self diffraction. The same statement is also true for C_2 , as it also gains power mostly from C_1 (Eq. 5.3b) through self diffraction. The relevance of this discussion will be clear in the following chapter when experimental results on six-wave mixing are presented.

5.3 Conclusions

In this chapter we have discussed a set of coupled wave and material equations that models the observed six-wave mixing [9]. It is shown here that the generated SPBS

contains contributions from self diffraction and parametric diffraction, the latter containing the self-phase conjugate of the pump. Expanding on the work by Kukhtarev *et al.* in Ref. 9, a novel order analysis for the steady-state of the six waves is presented here.

In Chapter 6, we discuss the experimental observations from six-wave mixing in iron doped lithium niobate crystals of various doping concentrations, coatings, and thicknesses. We report the time dynamics of the six-waves and conditions for the formation of two beams C_3 and C_4 that are opposite two each other and normal to the crystal faces. We also discuss a careful study of the SPBS, which includes image restoration test, interference with the pump, and visibility measurement.

CHAPTER VI

ANALYSIS OF EXPERIMENTAL RESULTS ON SIX-WAVE MIXING AND SPBS

6.1 Introduction

In this chapter, we report the time dynamics of the six-waves and conditions for the formation of two beams C_3 and C_4 that are opposite two each other and normal to the crystal faces. Six-wave mixing is investigated for iron doped lithium innovate crystals of various doping concentrations, coatings, and thicknesses. We also discuss six-wave mixing in the stead state and compare our experimental result with the reduced set of coupled Eqs. (5.3a-c) that was derived through the novel order analysis. Finally, we discuss the result of a careful study of the SPBS, which includes image restoration test, interference with the pump, and visibility measurement.

6.2 Six-wave Mixing at Steady State

Figure 6.1 shows photographs of the intensity patterns observed on screen S1 before and after C_3 is formed for an incident angle of 4 degrees (in air) using crystal A. The pump power is 65 mW and is focused by L1 of focal length $f=750$ mm to a spot size of 90 microns. Initial brightness in the direction of C_2 comes from the instantaneous Fresnel

reflection from the crystal surfaces. The light around the hole on screen S1 (through which the incident beam is introduced) is only from the stimulated photorefractive SPBS C_6 . It is observed that C_6 generally forms between 100 ms -10 s after the pump beam is turned on, as further discussed below.

Similar photographs of intensity patterns observed on screen S2 have been also recorded, but not shown here for the sake of brevity. It is observed that all participating waves maintain the same polarization (which is vertical, and hence perpendicular to the plane of incidence) as the incident pump. The typical generation times for C_3 and C_4 , propagating along the $\pm c$ - axes, are of the order of a few seconds for the incident angle and the pump power used in the experiment. A careful monitoring of C_3 and C_4 sometimes reveals the presence of a hexagonal structure. This is in agreement with previous observations of hexagon formation for normal and oblique incidence using $\text{KNbO}_3\text{:Fe}$ [7], and for normal incidence using $\text{LiNbO}_3\text{:Fe}$ and a feedback mirror [33]. It has been shown that the hexagonal formation in C_3 and C_4 is from amplification and self-organization of light initially scattered into Fabry-Perot modes [7].

The formation of Fabry-Perot modes is influenced by

- (a) the amount of scatter in the direction of C_3 and C_4 , and
- (b) the interaction length between the participating waves.

Hypothesis (a) is supported by the following observations:

- (i) increasing the angle of incidence of the 65 mW pump above a certain critical angle, viz., 8 degrees (in air) for crystal A, inhibits formation of C_3 and C_4 , for a focused spot size of 90 microns;

- (ii) using crystal C, which is anti-reflection coated, and thus has very low reflection coefficient and accordingly low initial scattering along C_3 , yields intensities of C_3 and C_4 which are an order of magnitude smaller than that observed using crystal A for the same incident power, angle, and pump spot size.

Note that under identical conditions, using crystal B, which has higher dopant concentration, yields intensities of C_3 and C_4 which are comparable to that observed for crystal A. The reason for this is that although crystal B has larger Fe concentration than crystal A and hence has higher gain, the absorption in crystal B is also correspondingly higher (see Table 6.1, reproduced here from Chapter 4 for reader's convenience with the addition of last column).

Table 6.1. Relevant parameters for all the $\text{LiNbO}_3\text{:Fe}$ crystals used for the study of six-wave mixing and SPBS. Reproduced here from Chapter 4 for reader's convenience with the addition of last column, which compares steady-state SPBS powers for the various crystals.

crystal marked	mol % Fe_2O_3 in the melt	c-axis (mm)	coatings on z-surfaces	absorption coefficient (cm^{-1})	SPBS at 4° incidence (μW)
A	0.03	10	None	0.43	60
B	0.05	10	None	1.20	20
C	0.03	10	AR	0.47	4
D	0.05	10	ITO	1.17	20
E	0.05	5	None	1.19	5

Hypothesis (b) is supported by the following observations:

- (i) using a shorter crystal, viz., crystal E, of thickness 5 mm (see Table 4.1), the intensities of C_3 and C_4 , and SPBS C_6 , are typically an order of magnitude smaller than what is observed for crystal B;
- (ii) experimentation with a more tightly focused 25 micron 65 mW beam (using lens L1 of focal length 200 mm) shows that the critical incident angle to generate C_3 and C_4 decreases to 2 degrees for crystal A. This is because with a smaller spot size, there is less effective interaction length between the participating beams to initiate the growth of C_3 and C_4 .

We would like to comment that both hypotheses (a) and (b) are supported by the results in Kukhtarev et al. [9], which show that the threshold condition for observation of light in the directions of C_3 and C_4 is determined by the magnitude of the “seeding scattering parameter” and the effective interaction length. Antireflection coating reduces the seeding scattering, while larger angles and smaller waists, or shorter crystal, reduce the interaction length.

The time dynamics of six-wave mixing using crystal A for a duration of approximately 40 minutes are shown in Figure 6.2 for an incidence angle of 4 degrees (in air), pump power of 65 mW and pump spot size of 90 microns. The observations and pertinent discussion are summarized below:

- (a) **Steady-state powers:** For crystal A, the SPBS (C_6) power is around 60 microwatts averaged over multiple measurements of the powers in C_1 through C_5 (see Figure 6.2), as explained in Section 4.1. For completeness, SPBS powers for all crystals (A-E) have been tabulated in Table 6.1. Also, Figure 6.2 shows that the powers in C_4 , C_5 , and C_6 (in the order of hundred microwatts in the steady state) are an order of magnitude lower compared to C_1 , C_2 and C_3 (milliwatts in the steady state). These observations are in agreement with our steady state theory, since according to Eqs. (5.1a-f), C_1 , C_2 and C_3 have much lower orders of δ, ε compared to that of C_4 , C_5 , and C_6 . In this sense, the order analysis and the experimental steady-state results corroborate each other, and hence it is justifiable to perform numerical simulations on six wave mixing from the reduced set of Eq. (5.3a-f), rather than the full complete set of Eq. (5.1a-f), along with appropriate boundary conditions. This is beyond the scope of the present paper and will be pursued in the future. A consequence of the inferences above regarding the respective powers in the six participating waves is that any temporal fluctuations around the steady state are more noticeable for the lower power waves, viz., C_6 .
- (b) **Temporal behavior:** Once the pump is turned on, it is observed that C_6 starts to form first within a few seconds, followed subsequently by C_3 , C_4 , and C_5 . While the *linear Fresnel-reflected* intensity of the

incident light from the crystal interfaces in the direction of C_2 is instantaneous (as seen from the sharp initial jump), the nonlinearly generated C_2 evolves at a time scale similar to the longer rise time of C_6 . Also, as C_1 and C_3 reach steady state, C_6 attains steady state as well. This is in agreement with our heuristic theory since from Eq. (5.3f), it is observed that the nature of C_6 at or near steady state should be primarily determined from the nature of the first two terms on the right hand side since these are of lower order in δ, ϵ . When Fabry-Perot modes leading to amplification of C_3 , and hence C_4 , are supported, the behavior of C_6 should also depend on the combined behavior of C_1, C_3 and C_4 . As C_1, C_3 and C_4 reach steady state, C_6 is therefore expected to reach steady state as well.

- (c) **Photovoltaic noise:** It has been observed that for crystal A, all the participating waves show quasi-periodic flashes (spikes in power) (see Figure 6.2) simultaneously at about every 7 minutes, in approximately 10% of the experiments. For the darker crystal B, these spikes occur in every experiment (not shown here for the sake of brevity), and their frequency is much higher, occurring simultaneously at approximately every 50 sec. for all of the six participating waves. In contra-directional two-beam coupling these flashes have been attributed to destruction of the grating owing to photovoltaic breakdown [20,32]. It is observed that in crystal B, because of photovoltaic breakdown, C_2 , C_3 , C_6 show a

decrease in power (down spike, not shown) while C_1 , C_4 , and C_5 correspondingly show an increase in power (up spike). During the occasional flashes that occur in Crystal A, the same trend is also observed. Since it has been shown that the photovoltaic noise can be reduced by ITO coating the crystal [20,32], the six-wave mixing experiment has been repeated using the ITO coated crystal D (see Table 1). The time dynamics (not shown here) show that photovoltaic pulsations in all participating waves are, in fact, eliminated in the ITO coated crystal.

- (d) **Dependence on angle of incidence:** The average SPBS power does not change with the angle of incidence up to 30 degrees, when C_3 and C_4 do not form. On average, the power in C_6 is similar to the $\theta = 4$ degrees case shown in Fig. 6.2 and of the order of 60 microwatts.

6.3 The Nature of SPBS

As detailed in Chapter 4, the nature of SPBS is investigated using imaging and interferometric methods. The results and pertinent discussion are summarized below:

- (a) **Image restoration:** It is observed that while $\text{BaTiO}_3\text{:Ce}$ recreates the image of the Air Force Resolution Chart clearly, crystals A and B yield at best fuzzy images of the resolution chart where the images cannot be seen clearly. This is in agreement with our theory which shows that SPBS has contributions from self diffraction and parametric diffraction (Eq. (5.3f)),

with only parametric diffraction contributing to the phase conjugation of the incident wave(s).

- (b) **Interference of SPBS with the collimated pump:** With the BaTiO₃:Ce sample and crystal B deliberately positioned at approximately $f/2$ behind lens L1 to introduce arbitrary phase curvature, the resulting observations are presented in Fig. 6.3. The SPBS from BaTiO₃:Ce after retracing its path emerges collimated and does not produce any concentric rings when it is interfered with the collimated pump (see Fig. 6.3(a)). The absence of circular fringes is not due to lack of coherence, as evident from the linear fringes (shown in the inset) that results when the reference beam is slightly tilted. Figure 6.3(b) shows the stable concentric fringes that result when the pump beam is reflected by a mirror from the same position $f/2$ behind L1. When the crystal B is placed at the same distance behind L1, the circular fringes do appear (Fig. 6.3(c)) and tend to be very unstable. It is observed that fringes appear within a minute after the pump is turned on (when the SPBS first appears). Although the total SPBS power is approximately constant, the fringes appear and disappear aperiodically over a time scale of approximately 5 minutes.

The lack of fringes in the case of BaTiO₃:Ce should be from phase conjugation [24] through parametric diffraction. The circular fringes observed when using a mirror are due to the phase curvature introduced from the lens L1. For the case of LiNbO₃:Fe, the SPBS comprises both self diffraction and parametric diffraction, and there is a continuous

exchange of power between the parametrically diffracted and self diffracted backscatter as observed from the absence and presence of fringes.

- (c) **Coherence test:** As discussed in Section 4.4, the quality of SPBS and the contribution of parametric diffraction in $\text{LiNbO}_3\text{:Fe}$ is assessed by recording the fringes obtained using crystal B (Fig. 6.4a) and a plane mirror (Fig. 6.4b) for comparison. Fringe visibility is then calculated using $V = (I_{\max} - I_{\min}) / (I_{\max} + I_{\min})$ [34]. Since the SPBS fringes from sample B do not have uniform visibility, a vertical cut through the center of the figure has been taken since it shows better contrast than a horizontal cut. For the mirror, $V = 0.65$, while for the SPBS using sample B, $V = 0.30$ upon choosing the second and third peaks on the left of the center peak on the vertical cuts (Fig. 6.4c). It is speculated that the decreased visibility is from the contribution of self diffraction in SPBS. Competition between self-diffracted light and parametrically diffracted light, which is phase-conjugate of C_1 (as shown in Fig. 6.2 in the oscillatory nature of C_6), reduces the overall coherence of the SPBS C_6 , but does not destroy it completely.

It is proposed that reduction of self diffraction, through use of a tightly focused pump [35], or through grating translation by piezoelectrically induced low frequency vibrations in the crystals [36], may significantly improve the phase conjugate in SPBS in the six-wave mixing geometry. In the contra-directional beam coupling geometry, where the pump is normally incident on the crystal and the c-axis is oriented opposite to the

direction of propagation, it has already been shown that only a very tightly focused pump results in transient phase-conjugate reflection [22,23].

6.4 Conclusions

Six-wave mixing in different samples of $\text{LiNbO}_3\text{:Fe}$ with various concentrations, coatings and thicknesses has been investigated for oblique incidence of a 532 nm pump with respect to the c-axis. It is shown that the generated SPBS contains contributions from self diffraction and parametric diffraction, the latter containing the self-phase conjugate of the pump. A consequence of six-wave mixing is the generation of waves (and, sometimes, hexagonal patterns) traveling along the $\pm c$ axes, whose intensities depend on the amount of scatter along the $\pm c$ axes and the interaction length of the six waves in the crystal. The time dynamics and the steady states for all participating waves have been experimentally studied and reconciled with inferences from approximate heuristic steady state theory. In the process, we also show that a reduced set of steady state equations based on a novel order analysis can be used to model six wave interactions in the future. A careful study of the SPBS, which includes image restoration test, interference with the pump, and visibility measurement, suggests that the phase conjugation may be contaminated by the self diffraction. It is postulated that reduction of self diffraction may significantly improve the phase conjugate in SPBS.

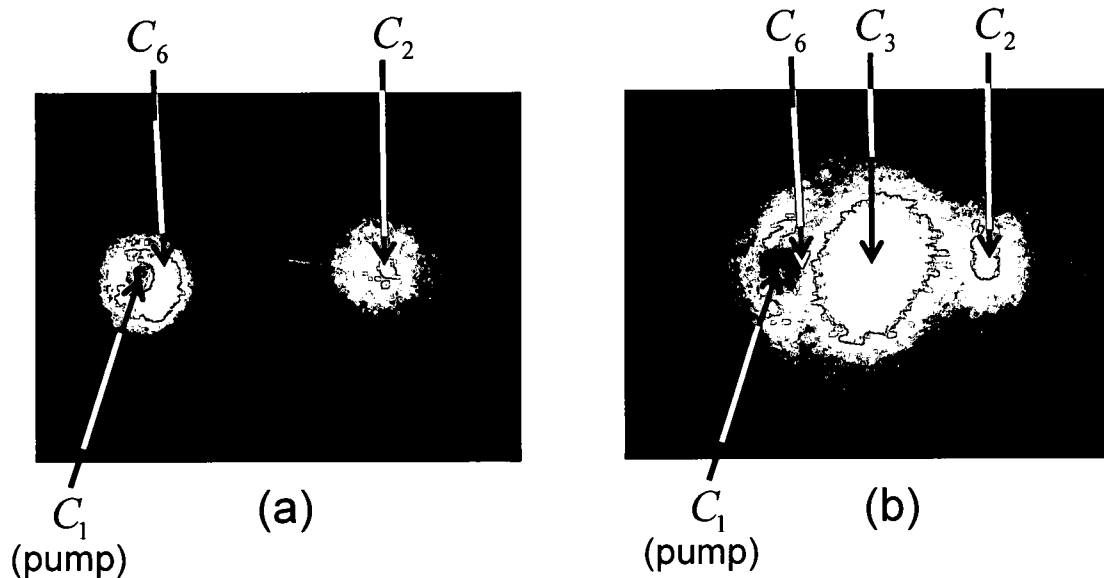


Figure 6.1: (a) Backscattered beam C_6 and linearly reflected light in the direction of C_2 . While the latter is instantaneously generated, C_6 forms between 100 ms-10 s after the pump beam is turned on. The pump beam, in the direction of C_1 passes through a hole on screen S1. (b) Subsequent generation of C_2 and C_3 is seen on screen S1. The bright spot along C_2 also includes the instantaneously generated Fresnel reflected light.

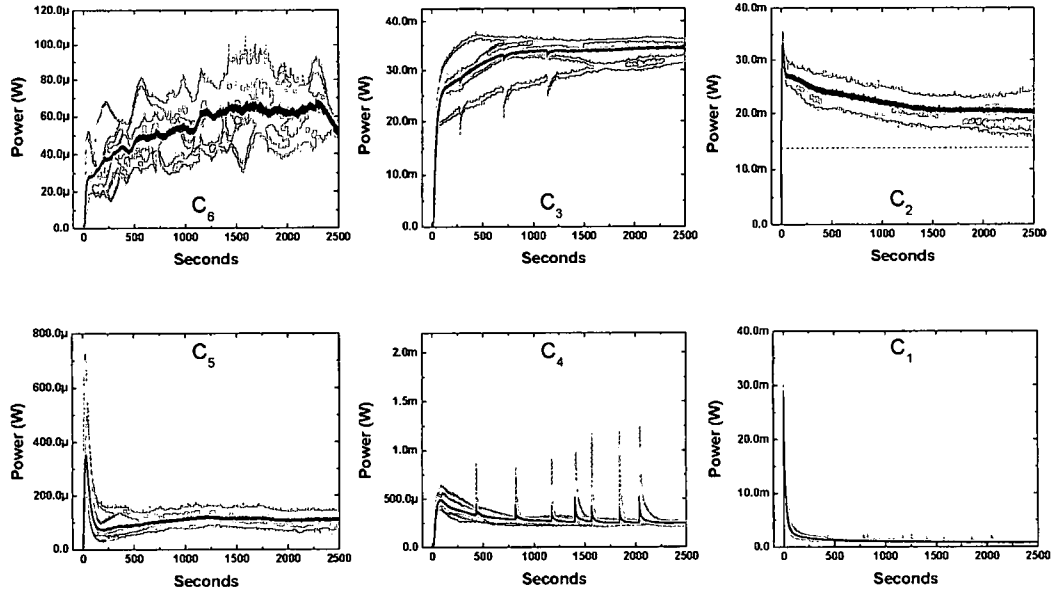


Figure 6.2: Time dynamics of six-wave mixing for crystal A at an angle of incidence of 4 degrees (in air) for the pump. Screens S1 and S2 in Fig. 2 are replaced by detectors and C_1 - C_3 are focused onto the detectors. The beams are recorded in pairs, with C_1 being common in all cases. The lighter traces correspond to 6 independent traces each for $C_2 - C_6$ and 30 traces for C_1 . The average in each case is shown in dark. Note that the *total* optical power in the direction of C_2 is plotted. The horizontal dashed line in this graph indicates the component of light in the direction of C_2 due to Fresnel reflection from the crystal surfaces.

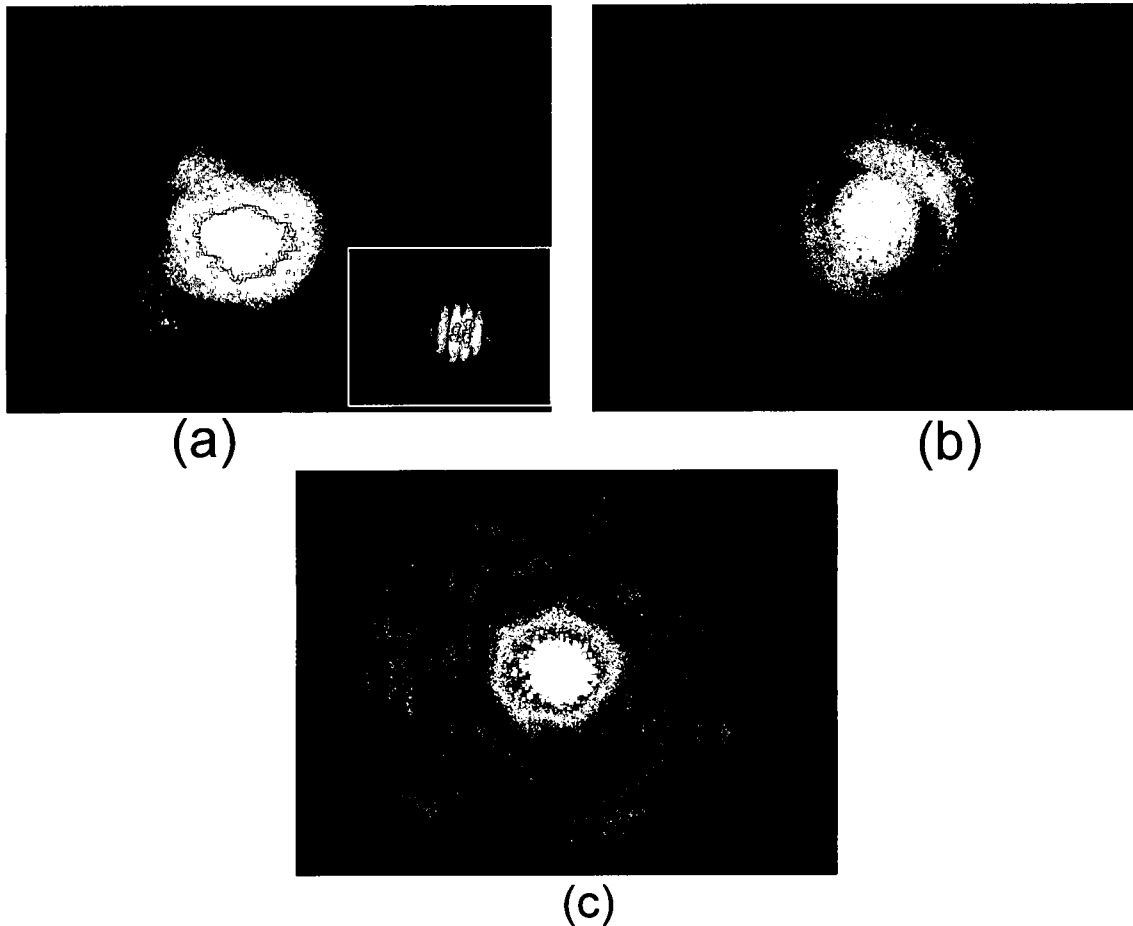


Figure 6.3: Interference with the reference (pump) when the crystal (or the mirror) is placed at a distance approximately $f/2$ from lens L1. (a) Interference pattern between the reference and the phase conjugate from BaTiO₃:Ce. Note the absence of circular fringes due to phase correction from phase conjugation. Inset shows linear fringes when the mirror M1 which reflects the reference is tilted. (b) Interference between the reference and reflection from a plane mirror placed at the location of the crystal). (c) Interference pattern between the reference and the SPBS from LiNbO₃:Fe.

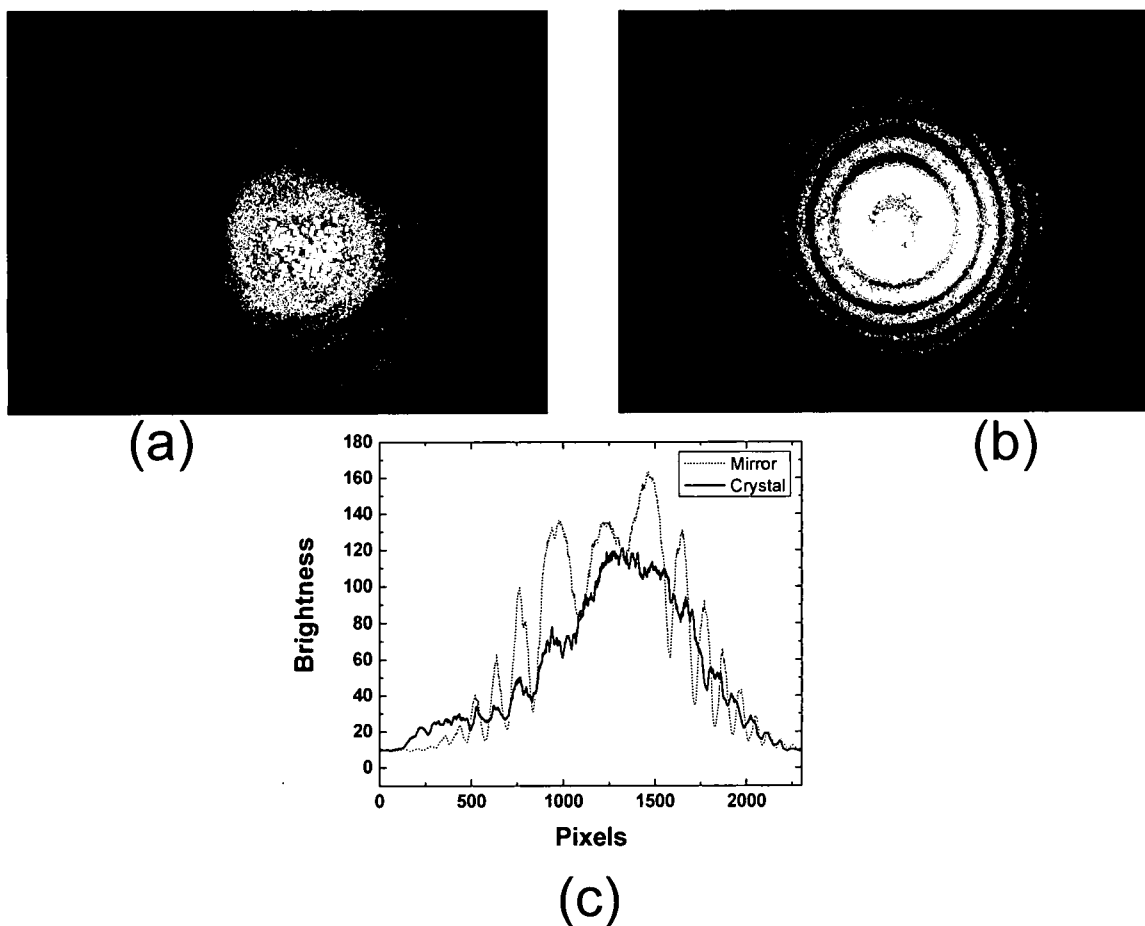


Figure 6.4: Quantification of the coherence of the SPBS through visibility measurement from interference patterns. (a) Interference pattern between the reference and the SPBS from $\text{LiNbO}_3\text{:Fe}$. (b) Interference pattern between the reference and a reflection from a plane mirror placed at the location of the crystal). (c) Intensity patterns along a vertical cut through both interference patterns recorded in (a) and (b), which is used for visibility calculations.

CHAPTER VII

BEAM PROPAGATION METHOD

7.1 Introduction

Before describing the novel algorithm (Chapter 8) that has been developed to simulate self-pumped contra-directional (SPCD) two-beam coupling (TBC), a review of the basics of beam propagation method is presented here. The beam propagation method (BPM) is a numerical technique for simulating the propagation of optical fields. BPM is a powerful technique that can simulate optical propagation through any arbitrary refractive index profile.

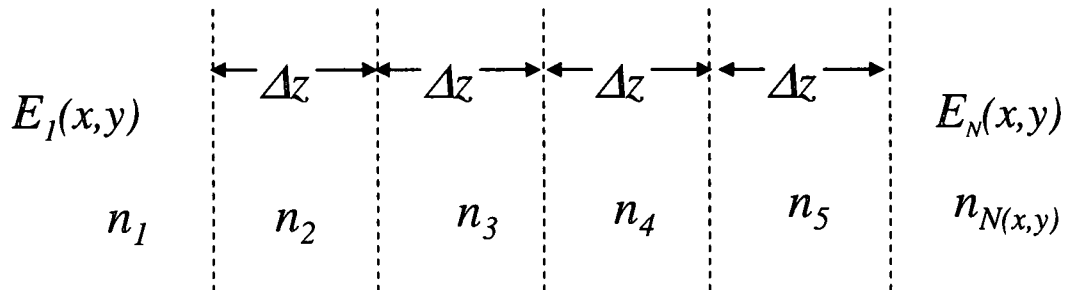


Figure 7.1: The optical path is broken into a sequence of finite steps [37].

In particular, starting from an initial optical field distribution E_1 (1 stands for the field being at step 1) the BPM technique can calculate how it is modified during propagation through N longitudinal sections of the medium, in order to obtain the optical field distribution E_N at a distance $z = N\Delta z$ [37] as shown in Fig. 7.1. Each section of the beam path can have any arbitrary index of refraction. For propagation through one medium only $n_1 = n_2 = \dots = n_N = n_0$.

The optical field² E is resolved into its different (angular) plane wave components and the propagation of each component is considered separately before superposing them to find the resultant field after propagation in each short uniform section. The justification for why BPM works is that each plane wave component E automatically satisfies the wave equation.

BPM is used for the calculation of the optical field profiles in the design of such practical optical components as tapered lasers, tapered amplifiers, tapered waveguides, waveguide directional couplers, optical filters and modulators [37].

7.2 Beam Diffraction

BPM simulates optical diffraction by resolving the optical field into separate plane wave components, i , each of which has its own wavevector $\vec{k}_i = \sqrt{k_{i_x}^2 + k_{i_y}^2 + k_{i_z}^2}$. The phase change due to propagation of each plane wave component, taking into account the different directions of each wavevector, is calculated and the resultant field is obtained by superposing the different plane waves. The Fourier transform relates the spatial domain

² Note, E represents the total optical field of an arbitrary beam, and hence the notation for complex amplitude C is not used here.

(x, y) to the spatial frequency (k_x, k_y) domain at every propagation distance z . For the case of one transverse dimension along y :

$$E(y) = \frac{1}{2\pi} \int_{-\infty}^{\infty} \mathcal{E}(k_y) \exp(jk_y y) dk_y, \quad (7.1)$$

where

$$\mathcal{E}(k_y) = \int_{-\infty}^{\infty} E(y) \exp(-jk_y y) dy. \quad (7.2)$$

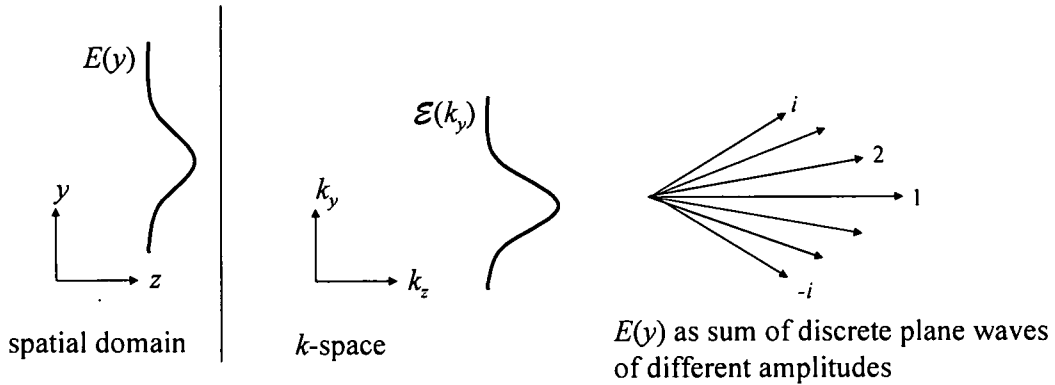


Figure 7.2: A spatial amplitude distribution $E(y)$ can be expressed as superposition of plane waves $\mathcal{E}(k_y)$. The arrow with i corresponds to the amplitude of the plane wave that has k_{i_y} as its transverse component of the wave vector [37].

The decomposition of $E(y)$ into its spectrum and eventual discretization of the spectrum is shown in Fig. 7.2. To determine the phase change of each plane wave component as it propagates, consider Fig. 7.3(a) for the i^{th} plane wave component of $E(y)$. In order to reproduce the spatial amplitude of the beam after a distance L is traveled we need to determine the phase accumulated by each component plane wave. To get to the plane at $z = L$, the wave will have to travel a slightly longer distance,

$L' = L / \cos \theta_i$, than would a wave traveling parallel to the z -axis. Following the Fig.

7.3(b) we can write,

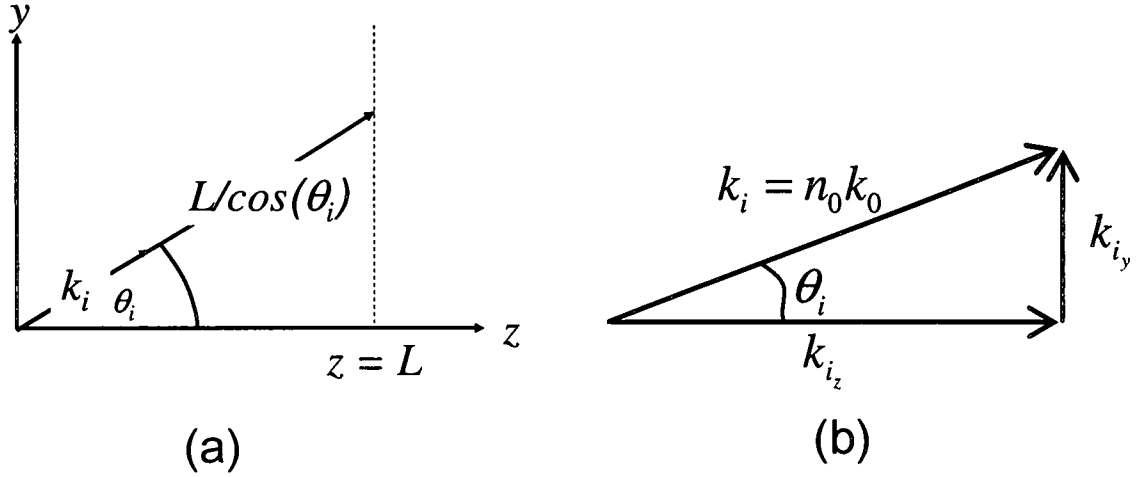


Figure 7.3: (a) Geometric depiction of the path the plane wave along the i^{th} wavevector follows to move a distance L along the z -axis. (b) Schematic of longitudinal and transverse components of the i^{th} wavevector

$$\cos \theta_i = \frac{\sqrt{n_0^2 k_0^2 - k_{i_y}^2}}{n_0 k_0} \quad (7.3)$$

Using the small angle approximation we can rewrite Eq. 7.3 as

$$\cos \theta_i = 1 - \frac{1}{2} \frac{k_{i_y}^2}{n_0^2 k_0^2} \quad (7.4)$$

Thus,

$$\frac{L}{\cos \theta_i} \approx \frac{L}{1 - \frac{1}{2} \frac{k_{i_y}^2}{n_0^2 k_0^2}} \cong L \left(1 + \frac{1}{2} \frac{k_{i_y}^2}{n_0^2 k_0^2} \right) \quad (7.5)$$

and the phase change ψ_i experienced by the plane wave going from $z = 0$ to $z = L$ is

$$\psi_i = n_0 k_0 \frac{L}{\cos \theta_i} \approx n_0 k_0 L \left(1 + \frac{k_{iy}^2}{2n_0^2 k_0^2} \right). \quad (7.6)$$

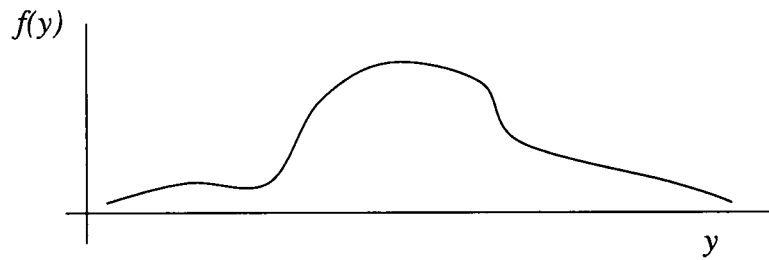
This formulation is considered the paraxial approximation. When the small angle approximation is not valid (e.g. spot size smaller than 3 μm [38,39]) the paraxial approximate is not valid. According to Guha [40] for an optical system with f-number below 2.5 paraxial approximation also breaks down for light propagation from the lens to the focal region. When paraxial approximation is not valid the phase change can be expressed exactly as

$$\psi_i = n_0 k_0 \frac{L}{\cos \theta_i} = n_0 k_0 \frac{L}{\sqrt{1 - \frac{k_{iy}^2}{n_0^2 k_0^2}}}. \quad (7.7)$$

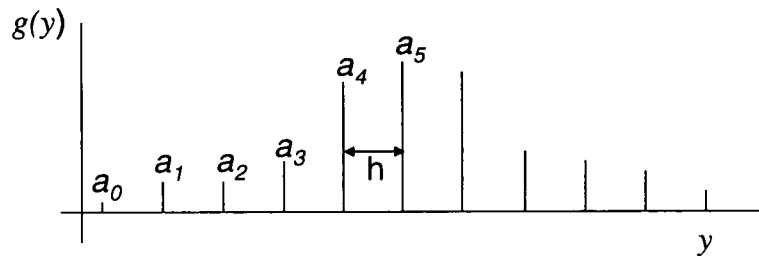
In BPM, the discrete Fourier transform (DFT) algorithm is commonly used to decompose a spatial field into a superposition of plane waves [37]. The amplitude of each plane wave component (obtained from DFT) does not change but their phases are modified according to Eq. (7.6). The spatial distribution of the optical field after propagating to $z = L$ is found by taking the inverse DFT of the phase-modulated plane waves. The resultant optical field distribution thus obtained will automatically incorporate the effects of diffraction. The discrete Fourier transform (DFT) is explained more thoroughly in the next section.

7.3 Discrete Fourier Transform

Consider sampling an arbitrary continuous waveform $f(y)$ shown in Figure 7.4(a) at regular intervals h in y to obtain a discrete sampled waveform $g(y)$ as shown in Figure 7.4(b).



(a)



(b)

Figure 7.4: (a) An arbitrary continuous waveform $f(y)$ (b) Discrete sampled waveform $g(y)$ for $f(y)$ shown in Fig. 7.4(a).

The sampled waveform may be approximated by a train of Dirac pulses weighted by the amplitude coefficients a_i

$$g(y) = a_0\delta(y) + a_1\delta(y-h) + a_2\delta(y-2h) + \dots + a_m\delta(y-mh). \quad (7.8)$$

The spatial Fourier transform of the sampled waveform is then:

$$g(k_y) = a_0 + a_1e^{-jk_yh} + a_2e^{-jk_y2h} + \dots + a_me^{-jk_ymh}, \quad (7.9)$$

where k_y is the spatial frequency corresponding to y . This Fourier transform of the sampled waveform is called the discrete Fourier transform (DFT). The terms

$e^{-jk_yh}, e^{-jk_y2h}, \dots, e^{-jk_ymh}$ are repetitive in the spatial frequency domain, with a period of $\frac{2\pi}{h}$.

Hence the spectrum from the DFT must be repetitive with a period of $\frac{2\pi}{h}$. From Eq.

(7.11) we can see that negative frequencies (values of $k < 0$) are merely complex conjugates of the corresponding positive frequency component. From the same equation we also see that the DFT of an array of N discrete real samples produces an array of N complex elements.

Each complex number stored in the array produced by DFT represents the amplitude and phase of a particular spatial frequency component. For example the i^{th} number from a sampled waveform containing an odd number, $(m+1)$, of elements ($i = 0, 1, 2, 3, \dots, m/2$) gives the amplitude and phase of the plane wave with spatial frequency:

$$k_{y_i} = \frac{i \cdot 2\pi}{mh} \quad \text{for } i = 0, 1, 2, 3, \dots, m/2 \quad (7.10)$$

The amplitude of the plane wave component is the magnitude of the complex number and the phase is the argument of the complex number.

The fast Fourier transform (FFT) is an efficient algorithm to perform DFT, and is provided as a standard function in MATLAB[®]. As outlined in the beginning of this chapter, upon taking the FFT of a discrete spatial beam profile, incorporating the accumulated phase (7.6) to each plane wave spectrum after a small distance of propagation (Δz), and upon finally taking the inverse FFT, we can calculate the spatial beam profile at a small distance Δz .

7.4 Conclusions

In this chapter we have reviewed the basics of the beam propagation theory and how the discrete Fourier transform could be used to implement the theory into a simulation code. In the following Chapter 8, we discuss the novel algorithm that we have developed to simulate the SPCD-TBC.

CHAPTER VIII

NOVEL ALGORITHM FOR SPCD-TBC WITH GAUSSIAN BEAMS

8.1 Introduction

A split-step Fourier transform-inverse Fourier transform beam propagation method [37] (FFT-BPM) using MATLAB[®] is used to simulate the self-pumped contra-directional (SPCD) two beam coupling (TBC) for a Gaussian beam. We have chosen to simulate this particular aspect of beam-coupling with reflection grating since SPCD-TBC has not been simulated before for a Gaussian beam. This simulation would help us model the spot size dependence and focusing position dependence of SPCD-TBC. Furthermore, a variation of the SPCD-TBC is also the origin of the six-wave mixing phenomenon, which has been studied experimentally in this work.

8.2 Algorithm

The bi-directionality of the simulation (opposing directions of the pump and signal beams) is handled by treating the two counter-propagating directions in sequence and then using an iterative shooting method to find the converged solution. The schematic of

the beam propagation algorithm is shown in Fig. 8.1. The dark lines on the left and right sides of Fig. 8.1 represent the front and rear surfaces of the photorefractive crystal respectively and the crystal c-axis is perpendicular to these faces. In this work we are only considering the case of a uniaxial crystal, LiNbO₃. For uniaxial crystals with light propagation along the polar axis, only one transverse polarization vector is required to be defined. The crystal longitudinal propagation direction is split into n steps (shown by the dashed lines). The incident pump beam is presently defined with a Gaussian amplitude profile and the e^{-1} radius spot size³ characterizes the focusing condition. Other transverse beam profiles may be substituted for the Gaussian, to suit specific experimental parameters.

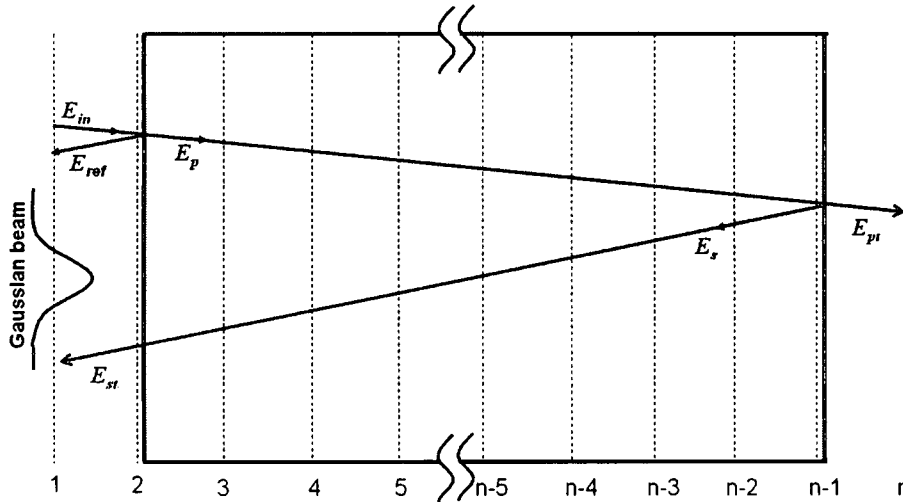


Figure 8.1. A schematic representation of the origin and path of the pump and signal beams. The signal beam (E_s) is generated by the Fresnel reflection of the pump beam (E_p) at the rear surface of the crystal. Both beams are nominally perpendicular to the boundaries. The paths are shown with angles to help distinguish the beams.

8.2.1 Linear Simulation

The pump beam is usually chosen to be focused at the front surface of the crystal. Focus at any point inside the crystal is accomplished by doing a beam propagation through a

³ Spot size is measured at e^{-1} radius of the field, which is the same as e^{-2} radius of the intensity.

crystal of desired length, taking the complex conjugate of the field and using that as the initial field. This gives a starting field that has already diffracted and has the reversed phase. The amplitude of the incident optical field E_{in} is adjusted to use any desired power for the pump beam. During simulation the field retains both amplitude and phase information at every propagation step. To minimize computational error, we have used the exact phase factor given by Eq. (7.7). However, we noticed that down to 1 μm spot size there was no difference in simulation result whether we used the paraxial approximation of Eq. (7.6) or exact phase term of Eq. (7.7).

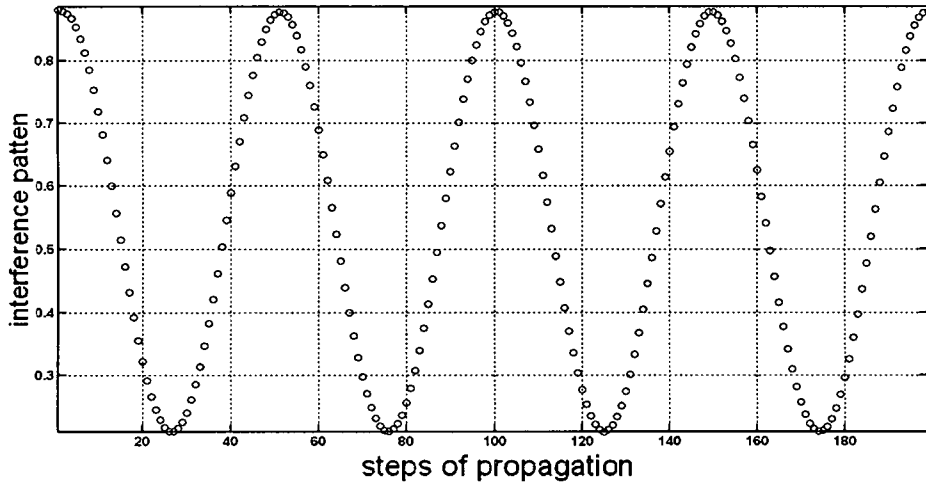


Figure 8.2. Interference pattern in the longitudinal direction for a LiNbO₃ crystal. Crystal length is equal to two wavelengths (532 nm) of light (inside). The number of longitudinal steps (n) per wavelength is 100. Spot size 5 micron.

As the beam enters the crystal (at step 2), part of it is reflected (E_{ref}). The transmitted beam (E_p) is propagated to the rear boundary, where part of this beam is transmitted (E_{pt}) and remainder is reflected (E_s) (at step $n-1$). At each propagation step the local value of the pump field ($E_p(i)$) is saved in a buffer. The signal beam, E_s is then propagated in the opposite direction to the pump beam, until it travels through the front face of the crystal

(E_{st}). At each step the signal beam field $E_s(i)$ is also saved in a buffer. The $E_s(i)$ buffer is then added to the previously buffered pump beam field $E_p(i)$ to produce the interference array. At the i^{th} longitudinal step the intensity of the interference pattern is then given by $|E_p(i) + E_s(i)|^2$. Since the fields are defined as transverse arrays, the interference at every i^{th} longitudinal step also has a transverse profile. This transverse profile of the interference however is computationally very costly, since for each step this has to be saved in the buffer. Moreover, since we are simulating an interference pattern the step size along the longitudinal direction must be substantially smaller than the wavelength.

It is determined that for a crystal of thickness λ , n has to be at least 40 to produce a smooth interference pattern. For the contra-directional TBC it is the intensity modulation in the longitudinal direction that is of greatest importance, since the electro-optic coefficient is weak perpendicular to the c-axis. Hence, we employed an alternate approximate method of simulating the interference with less computational load. We saved only the peak of the field (instead of the whole transverse array) in the buffer. This results in an interference pattern without a transverse profile. This approximation did not result in any significance difference in our simulation but improved the required CPU time by two orders of magnitude.

Figure 8.2 shows the peak of the interference at every step in the longitudinal direction (each point of the plot represent the peak of the transverse profile at that step) for a thin LiNbO₃ crystal. The length of the simulated crystal equals two wavelengths ($\lambda = \lambda_0/n_0$) inside the crystal, where λ_0 is taken to be 532 nm, and the ordinary refractive index (n_0) of LiNbO₃ is used. Because there is no absorption loss and no beam diffraction in this short distance, the interference has constant amplitude.

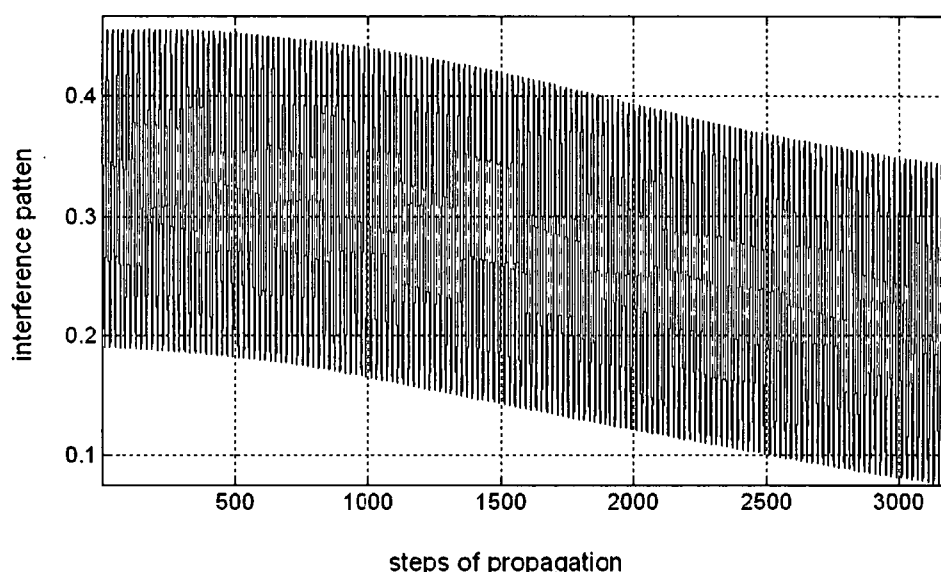


Figure 8.3. Interference pattern in the longitudinal direction for a LiNbO_3 crystal. The crystal length is equal to ~ 40 microns.

Figure 8.3 shows another example of a interference pattern for a much larger (40 micron) lithium niobate crystal and for a beam with spot size 1 micron, focused at the entrance of the crystal. Because of the divergence, the beam amplitude changes with propagation and consequently results in a gradually decaying interference pattern. Producing this interference pattern through the crystal completes the linear cycle (when both pump and beam has traversed the crystal) of the simulation.

8.2.2 Nonlinear Simulation

Following the linear cycle, the photorefractive effect is simulated through a nonlinear cycle of beam propagation. In this cycle the buffered modulated intensity can be used to determine the space-charge field by using the formalism in Chapter 2, Eq. (2.33). The change in index then can then be determined by considering the electro-optic effect

through Eq. 2.34. The computational load of the simulation restricted our simulation within 40 micron thin layer of lithium niobate crystal. If the material parameters for lithium niobate is used to calculate the space-charge field and index modulation the resulting non-linearity causes minimal beam-coupling in such a thin crystal. Therefore, for qualitative simulation we have used the following simplified versions of Eqs. (2.33) and (2.34):

$$n = n_0 + \Delta n \quad (8.1a)$$

$$\Delta n \propto E_{sc} \quad (8.1b)$$

$$E_{sc}(\text{diffusion}) = C_{df} \cdot \nabla I(x, y, z) \quad (8.1c)$$

$$E_{sc}(\text{photovoltaic}) = C_{pv} \cdot I(x, y, z) \quad (8.1d)$$

where n_0 is the bulk index of refraction of the crystal and Δn is the change in index due to the space-charge field. For an index modulation (grating) generated by diffusion alone, Eq. (8.1c) relates the space-charge field to the gradient of the modulated intensity through the constant C_{df} . This essentially makes space-charge field (and the grating) 90° out-of-phase with respect to the interference pattern. For a grating arising from the photovoltaic field alone, the space-charge field can be directly related to the interference pattern through the constant C_{pv} . For this case, the resulting grating is in phase with the interference pattern.

The non-linear cycle proceeds in a similar manner to the linear cycle. The buffered interference pattern intensity profile from the linear cycle is used to estimate the modified local refractive index variations through (Eqs. 8.1b-d). The values of the coefficients C_{df} and C_{pv} are chosen such that significant beam coupling is observed. This is discussed

more in detail in Section 9.1. The refractive index change at each space-step in the calculations is treated as a dielectric boundary. As the pump beam E_p propagates through the index modulated crystal, the power of the beam is diminished at every step due to reflection losses at the dielectric boundaries, and the local values of E_p are stored in a buffer. Each grating reflected beam from the pump (pumpscatter) is propagated all the way out of the crystal. This grating scattered light is added to the buffered signal array. Each grating reflected beam from the signal (going toward the back surface of the crystal) is propagated all the way out of the crystal and added to the buffered pump array. As a first order approximation it is assumed that scattered light from the pump and signal beams do not go through additional scattering during the propagation through the grating.

At the end of this first non-linear cycle, the interference pattern is slightly modified. Subsequent iterations of this non-linear cycle continue to modify the interference pattern (and the modulated index). When the difference between two successive interference patterns is within a chosen tolerance value (we have used 5%), convergence is assumed and the TBC efficiency is determined. All of the scattered beams that exit through the front and rear faces of the crystal are summed ($E_{p(sc)}$ and $E_{s(sc)}$ respectively). Through out the crystal, the value of the pump buffer and signal buffer reflects the converged value of the pump and signal after loss or gain. In the case of pure charge diffusion, for the c-axis oriented along the direction of pump propagation, constructive interference occurs for the back scattered light while the transmitted light suffers destructive interference. This interference occurs due to the phase difference between the interference and grating patterns, and the phase change in the scattered beams due to the reflections from the grating. The constructive and destructive interference directions are

reversed when the crystal c-axis is reversed. Because of the destructive and constructive interference the pump beam and the signal beam losses and gains power in the direction of respective propagation.

This algorithm for SPCD-TBC is summarized below in the flow chart of Fig. 8.4.

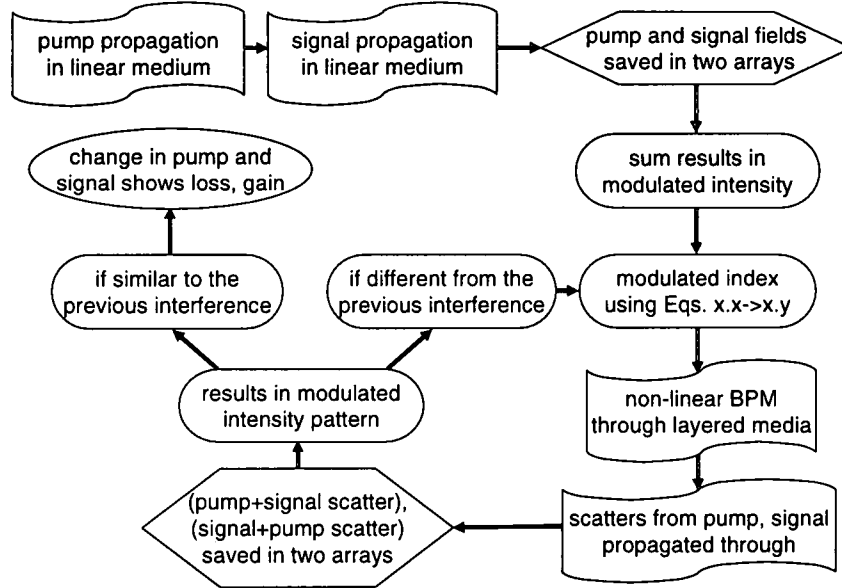


Figure 8.4: Flowchart showing the novel algorithm for simulation of SPCD-TBC for Gaussian beams.

8.3 Conclusions

In this chapter we present the novel algorithm for simulating the self-pumped contra-directional two beam coupling for a Gaussian beam. A split-step Fourier transform-inverse Fourier transform beam propagation method [37] (FFT-BPM) using MATLAB[®] is used. The simulation is broken down to two parts,

- (a) linear simulation, where the Gaussian pump and Fresnel reflected signal are propagated through the linear PR media to establish the interference pattern,

(b) nonlinear simulation, where the space-charge field and subsequently the index modulation is calculated from the interference distribution and the pump and signal goes through beam-propagation through this modulated index. Each step is treated as a dielectric boundary and light scattered at each of these boundaries are propagated out of the crystal as well. As a first order approximation, we do not consider secondary reflections for these scattered beams. The pump and signal beams are combined with scattered beams that are traveling in the same direction, to produce the beam-coupling.

The nonlinear round is repeated until a converged interference pattern is established. Finally, the TBC efficiency is calculated by taking the difference of the linear transmission of the pump and the transmission of the pump (with added signal scatter) after the nonlinear propagation.

The code of simulation of SPCD-TBC is presented in Appendix A. Before simulation the PR beam-coupling we have verified the validity of the linear propagation code by simulating a Fabry-Perot cavity. The Fabry-Perot simulation code is presented in Appendix B and comparison of simulation result with theory is presented in Appendix C.

In the next Chapter 9 we present the simulation result in a PR media. We show two proof-of-concept simulations that show well established characteristics of the PR self-pumped beam coupling. Following that we show beam coupling as a function of spot size and focal position to show that the simulation correctly accounts for beam diffraction.

CHAPTER IX

SIMULATION RESULTS FOR SPCD-TBC WITH GAUSSIAN BEAMS

9.1 Introduction

The goal of this work is to provide a complete simulation of self-pumped two-beam coupling (TBC) using exact diffraction of an arbitrarily shaped pump beam. This would enable us to simulate the dependence of the TBC efficiency on focal spot size and position. The simulation could additionally help us to investigate other intriguing aspects of self-pumped TBC, such as the amount of beam coupling in the presence of both diffusion and photovoltaic effect, the relative phase shift between the intensity grating and the induced refractive index grating, etc. The computational load however became overwhelming due to the fact that exact Gaussian beams were used in the simulation, which needed to be decomposed into its angular plane wave components, and sampling step size in the photorefractive material needs to be a small fraction of the period of the interference pattern for a reflection grating. Even with our improved algorithm that uses a 1D transverse array (instead of 2D) to buffer the interference pattern, it still takes about 12 hours to simulate in a 40 μm long crystal. The transverse profile of the Gaussian For such a thin crystal, if we use the material parameters for LiNbO_3 , the change in refractive

index is not sufficient to cause computationally detectable beam coupling. Therefore, we have used artificial nonlinearity, using the simplified Eqs. (8.1a) through (8.1d) and have chosen the two parameters C_{pv} and C_{df} to within a range of values that can produce index modulation in the order of 0.03. This is sufficient to achieve 1-2% of beam coupling in a photorefractive material that is 2 wavelengths in length. Similar index modulation would produce ~15% power coupling in a crystal that is 40 μm long. We present two proof-of-concept simulations that show well established characteristics of the PR self-pumped beam coupling. Following that we show beam coupling as a function of spot size and focal position to show that the simulation correctly accounts for beam diffraction. The Gaussian transverse profile of the pump beam and the contra-directional signal beam is shown in Fig. 9.1. A pump beam with a 1 μm spot⁴ travels through a 40 μm long crystal and the Fresnel reflected signal beam travels back 40 μm again. Consequently there is noticeable diffraction observed in Fig. 9.1.

9.2 Two-beam Coupling Test

It is well known [1] that a grating can only cause power coupling between two counter-propagating plane waves if the grating is 90° phase shifted with respect to the interference produced by the two waves. For a grating that is in phase with the interference pattern, there can be no beam coupling. Extending on this established fact, we assume that for a weakly focusing beam, similar beam coupling behavior should be observed. We simulate a beam-coupling where the grating is 90° phase shifted with the interference (Fig. 9.2), and in a crystal that is 2 wavelengths long. Following Eq. (8.1c),

⁴ Spot size is measured at e^{-1} radius of the field, which is the same as e^{-2} radius of the intensity.

we have chosen C_{df} such that the change in index is 0.027. Figure 9.3 shows the energy exchange between the pump and the signal beam due to the out-of-phase induced refractive index. Scattered light from the signal beam destructively interferes with the pump beam to diminish the pump power. Conversely, scattered light from the pump beam constructively interferes with the signal beam to increase the signal power. This is a distinctive feature of energy exchange due to beam coupling. In this case of simulation, pump power is reduced by about 4% and signal power gains equally. The observed oscillation in the power in Fig. 9.3 is an artifact⁵.

Figure 9.4 shows the interference pattern (top) and resulting induced refractive index modulation (bottom) that is in phase with the interference. Following Eq. (8.1d), we have chosen C_{pv} such that the change in index is 0.027, same as in Fig. 9.2, for purposes of comparison. We observe from Fig. 9.5 that there is no energy exchange between the pump and the signal beam.

9.3 Photovoltaic Field Assisted Beam Coupling

Cook *et al.* in Ref. 10 have shown that in $\text{LiNbO}_3\text{:Fe}$, the negative effect of the grating phase deviation from the optimum 90° is compensated by the positive effect of the larger Δn due to the photovoltaic field that exists in LiNbO_3 . Figure 9.6 shows that the beam coupling is at its minimum when 15 kV dc field is externally applied on to the crystal. The beam coupling is minimal at this point when the dc field cancels out⁶ the photovoltaic field [10]. As it is shown by Eq. (2.14) in Section 2.2, the presence of

⁵ The oscillation comes from the difficulty of calculating the power of (pump + signal scatters) or (signal + pump scatter) at any given point inside the nonlinear media. The actual coupling is calculated by accounting for the amplified signal or diminished pumps outside the crystal, where the index is constant.

⁶ This experiment is discussed more in detail in Chapter 3.

photovoltaic field has a negative effect on the phase of the index modulation. However, the photovoltaic field may change the magnitude of Δn to overcome this negative effect. Figure 9.6 also shows that larger photovoltaic field may actually enhance the beam coupling.

We do a similar simulation by keeping the C_{df} constant (equivalent of a fixed diffusion effect) and by increasing the value of C_{pv} . The result is shown in Fig. 9.7. We observe that upon increasing C_{pv} from zero, the phase shift is reduced from 90° (for the diffusion alone case) and Δn increases as well. The TBC efficiency (represented by ΔP_{pump}) also continues to get bigger with increasing C_{pv} values, and is significantly stronger for larger values. This proves that the negative effect of the grating phase deviation from the optimum 90° is compensated by the positive effect of the larger Δn .

9.4 Diffraction Effect in Beam Coupling

We now study the effect of the diffraction of a Gaussian beam on TBC in a contrapropagating geometry. Figures 9.8 and 9.9 show the intensity interference and refractive index modulation due to $10\ \mu\text{m}$ and $1\ \mu\text{m}$ focal spot size beams, respectively, and focused on the entry face of the crystal, propagating through a crystal of length $40\ \mu\text{m}$. The Rayleigh range for 1 micron beam inside LiNbO_3 is $27\ \mu\text{m}$. We notice from Fig. 9.8 that inside the $40\ \mu\text{m}$ crystal, the width of the $10\ \mu\text{m}$ spot beam does not change significantly. However the spot size of the $1\ \mu\text{m}$ beam does have a noticeable change, as shown in Fig. 9.9. Consequently the magnitudes of the interference, and correspondingly the refractive index modulation, are diminished for the $1\ \mu\text{m}$ spot size beam. This results in reduced beam coupling. We repeat this simulation for a range of spot sizes and for

shorter crystal lengths, viz., 4 μm . Figure 9.10 shows the beam coupling as a function of pump spot size for a 40 μm and a 4 μm long crystal. The percent of power loss is normalized (to the maximum power loss in percentage) for both graphs. We observe that for the 4 μm sample simulation, there is no difference in the beam coupling, since that is significantly smaller than the Rayleigh range of the smallest spot size. It is thus clear that diffraction causes a decrease in beam coupling.

We have also simulated the dependence of beam coupling on position of the focus inside the crystal. Figure 9.11 shows the interference pattern (top) and resulting phase index modulation (middle), and beam waist size for a 1 μm beam propagating in a 40 μm crystal and focused at the front face of the crystal. Figure 9.12 shows the interference pattern (top) and resulting phase index modulation (middle), and beam waist size for a 1 μm beam propagating in the 40 μm crystal, but now focused at the end face of the crystal. Finally, Fig. 9.13 shows the interference pattern (top) and resulting phase index modulation (middle), and beam waist size for a 1 μm beam propagating in a 40 μm crystal and focused in the middle of the crystal. Identical scales have been used for Figs. 9.11 – 9.13. We observe that the interference and refractive index modulation magnitudes are the largest when the beam focused at the back (Fig. 9.12), and smallest when the beam is focused at the front (Fig. 9.11). The trend is the same for the TBC efficiency, as seen from Fig. 9.14. Thus, diffraction of the beam affects beam-coupling.

9.5 Conclusions

In this Chapter we have simulated SPCD-TBC using exact diffraction of a Gaussian pump beam. Because of the intense computational load involved, we have considered a

crystal that is 40 μm long. For this crystal, we have used amplified change in the magnitude of modulated index in order to produce significant beam coupling. We present two proof-of-concept simulations that show well established characteristics of the PR self-pumped beam coupling. Following that we show beam coupling as a function of spot size and focal position to show that the simulation correctly accounts for beam diffraction. For our simulation in the 40 μm long crystal beam coupling starts to drop off below 4 μm spot size. We also observe that coupling is optimum when the beam is focused at the rear surface.

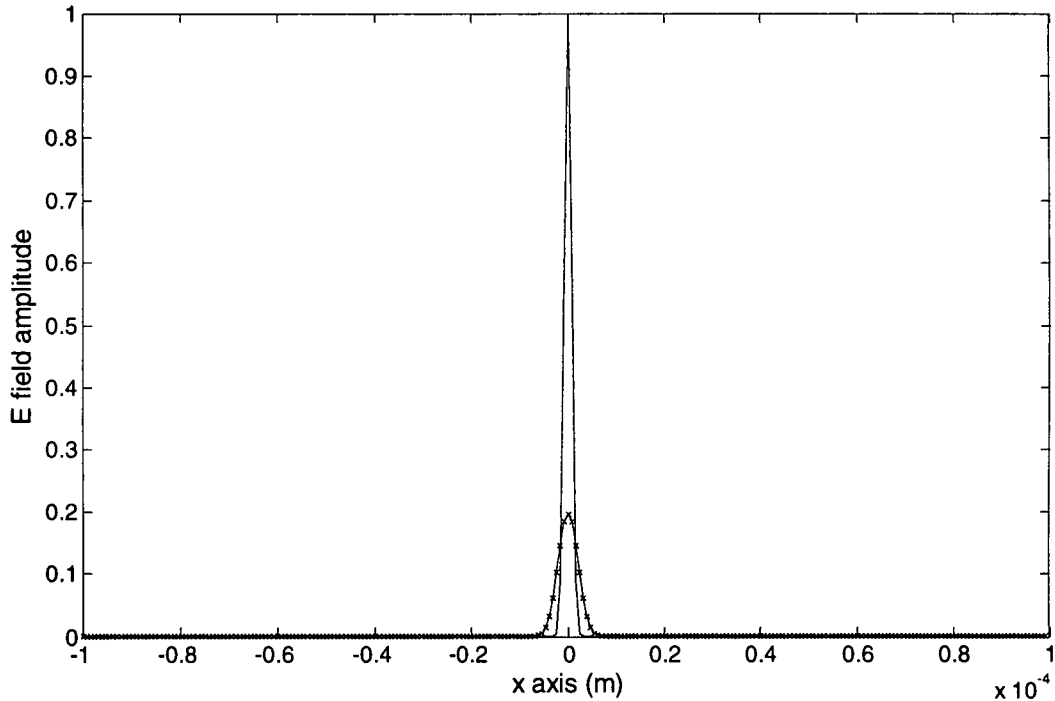


Figure 9.1: The transverse Gaussian profile of a 1 μm pump beam at the front (entrance) face of the crystal (solid line), and the diffracted signal beam coming out through the same crystal boundary (dashed, cross hairs). The crystal is 40 μm long.

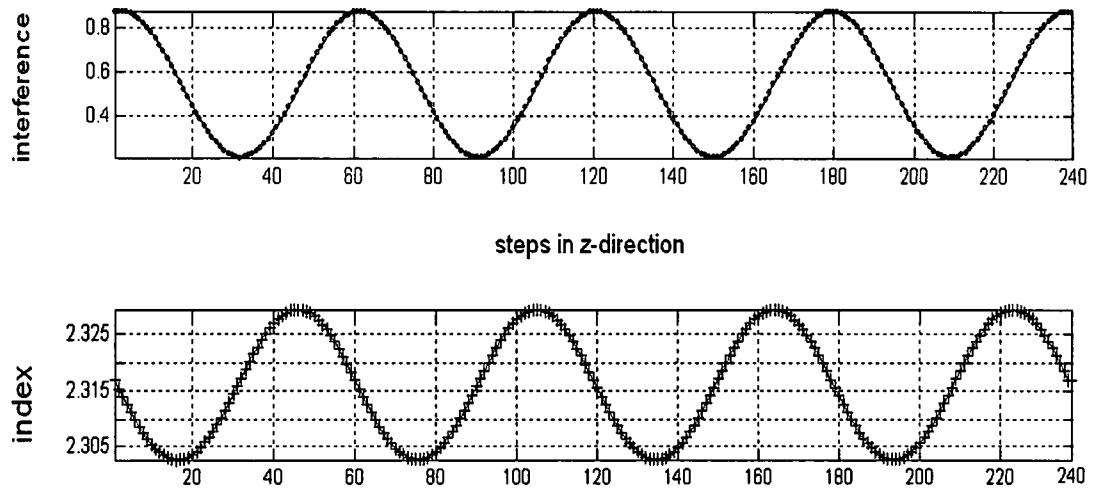


Figure 9.2: Interference pattern (top) and resulting 90° phase shifted index modulation (bottom) for pure diffusion alone. Crystal length is 2 wavelengths inside. Change in index is 0.027.

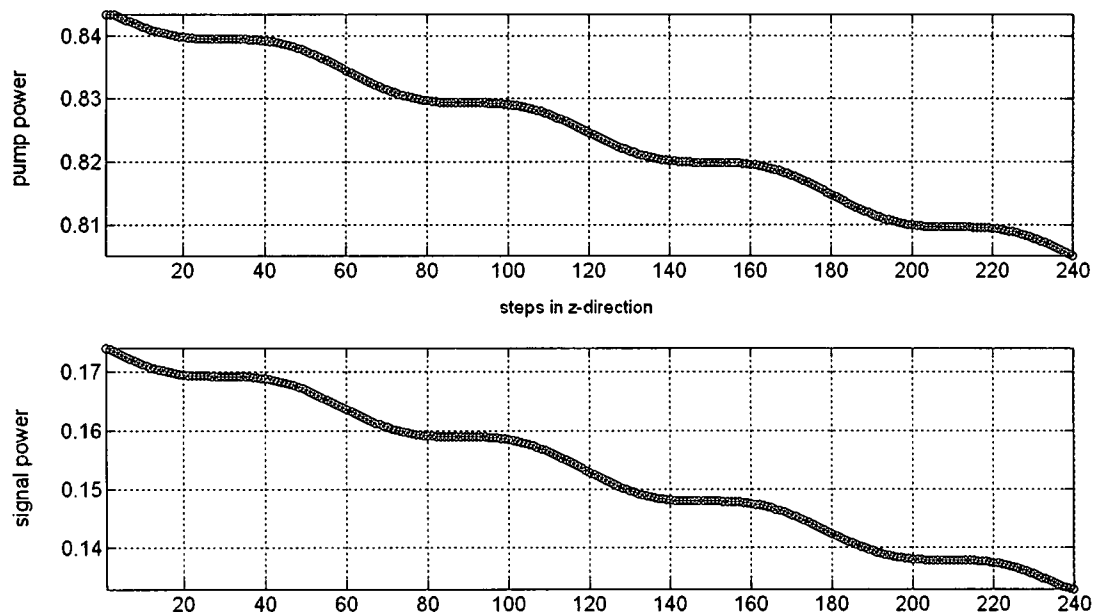


Figure 9.3: Energy exchange between the pump and the signal beam due to the modulated index in Fig. 9.2 due to pure diffusion. Pump power is reduced by about 4% and signal power gains equally. Oscillation in power is artifact.

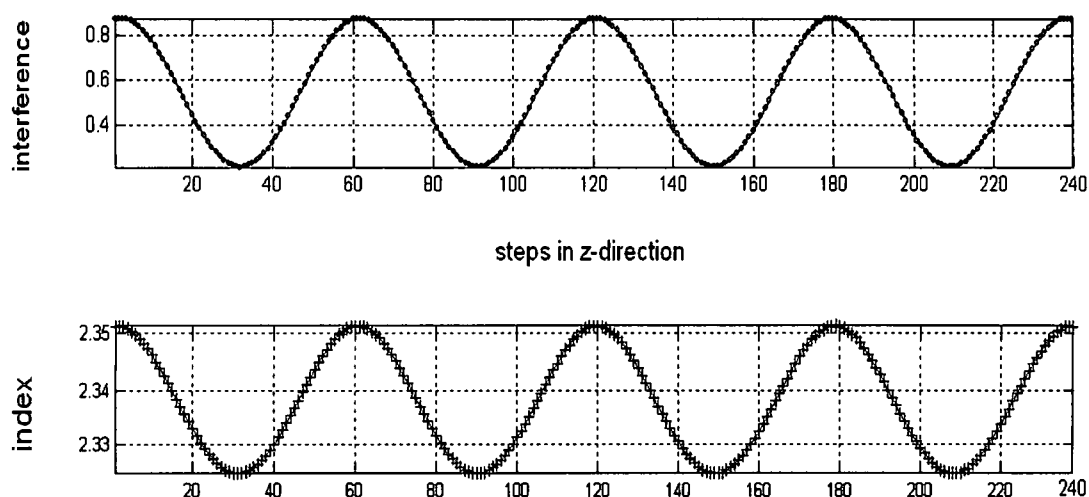


Figure 9.4: Interference pattern (top) and resulting in phase index modulation (bottom). Crystal length is 2 wave lengths inside. Change in index is 0.027, same as Fig. 9.2 for comparison.

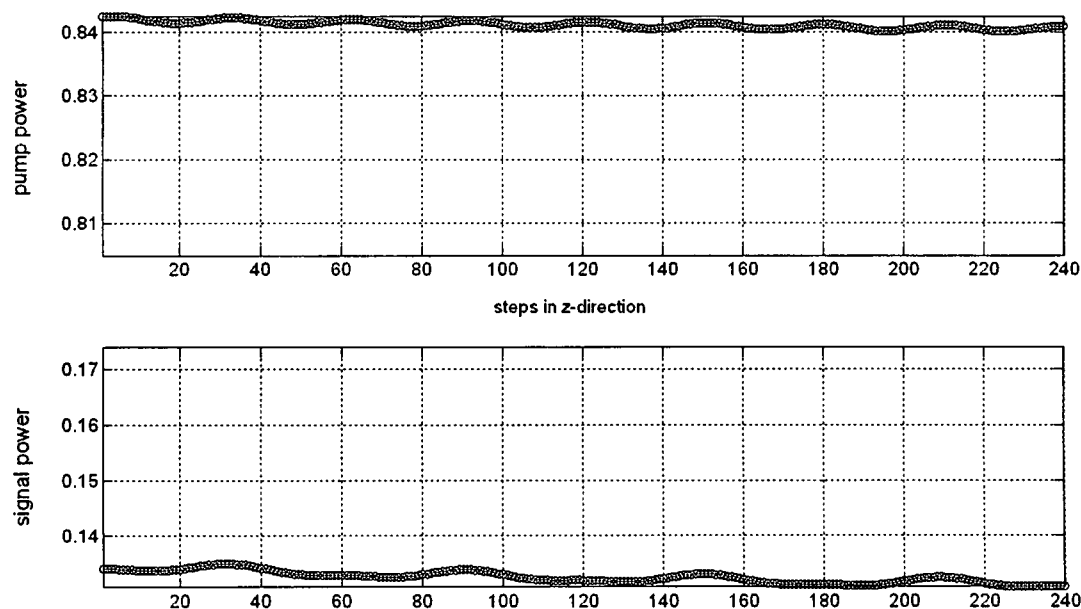


Figure 9.5: No energy exchange between the pump and the signal beam due to the in phase modulated index in Fig. 9.4. Plot is drawn to the same scale as Fig. 9.3. Oscillation is here is artifact.

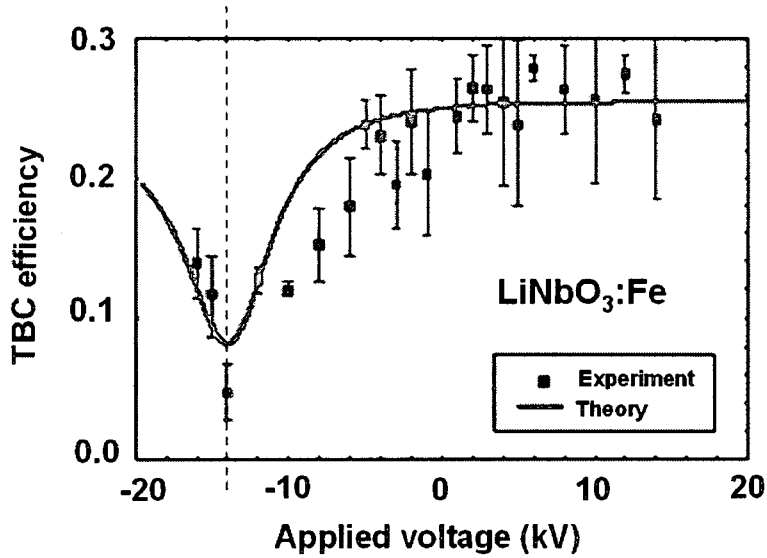


Figure 9.6: Results in LiNbO₃:Fe showing that the negative effect of the grating phase deviation from the optimum 90° is compensated by the positive effect of the larger Δn due to the photovoltaic field that exists in LiNbO₃ [10]

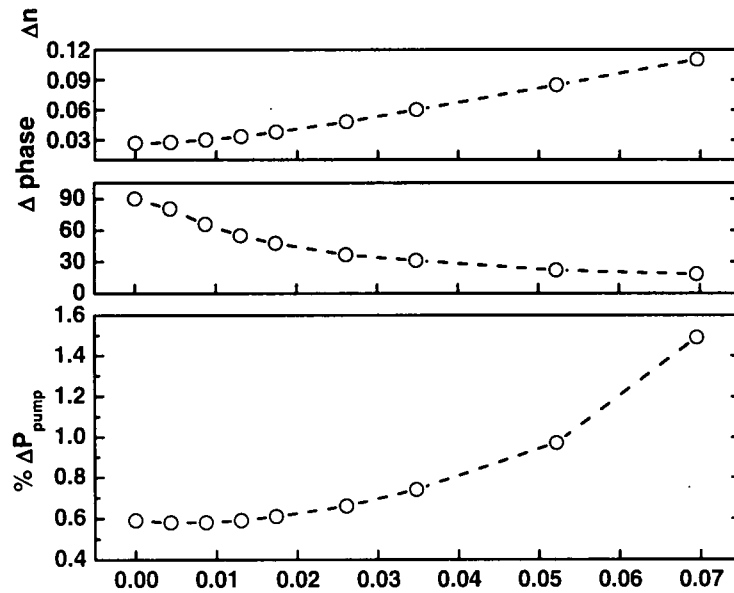


Figure 9.7: The change in refractive index^{pv}(top), the phase difference between interference and index modulation (middle), and the change in pump power (bottom) as the photovoltaic field is varied and the diffusion field is held constant. Result shows that the negative effect of the grating phase deviation from the optimum 90° is compensated by the positive effect of the larger Δn .

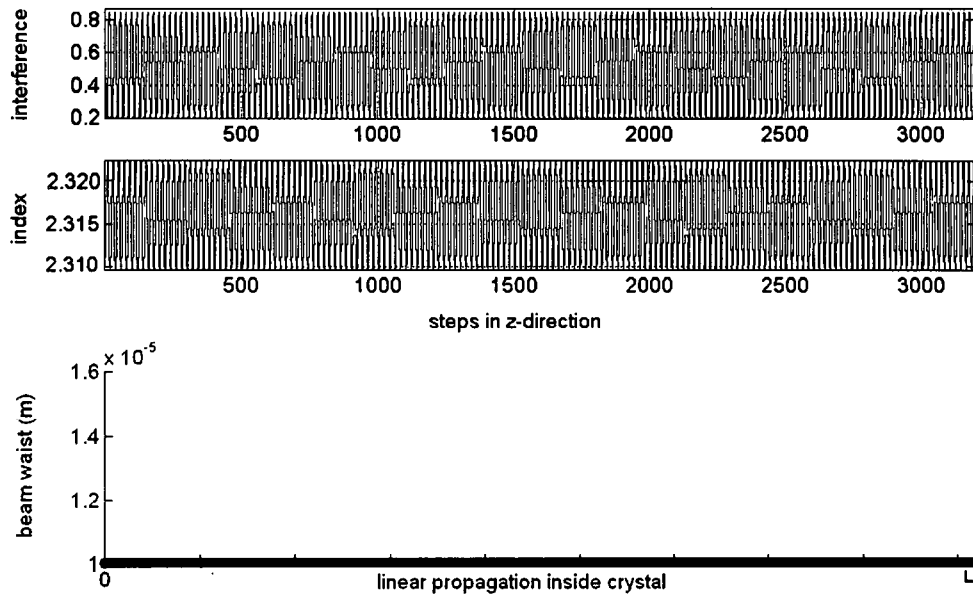


Figure 9.8: Interference pattern (top) and resulting index modulation (middle), and beam waist size for a 10 μm beam propagating in a 40 μm crystal. Beam waist does not change significantly.

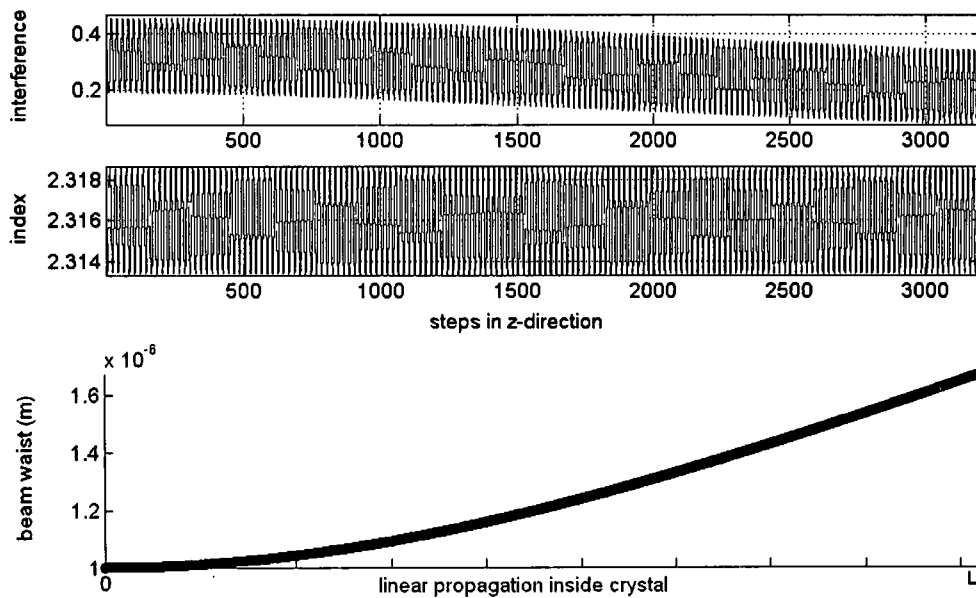


Figure 9.9: Interference pattern (top) and resulting index modulation (middle), and beam waist size for a 1 μm beam propagating in a 40 μm crystal. Beam waist changes significantly. Interference magnitude is smaller, so is the resulting index modulation.

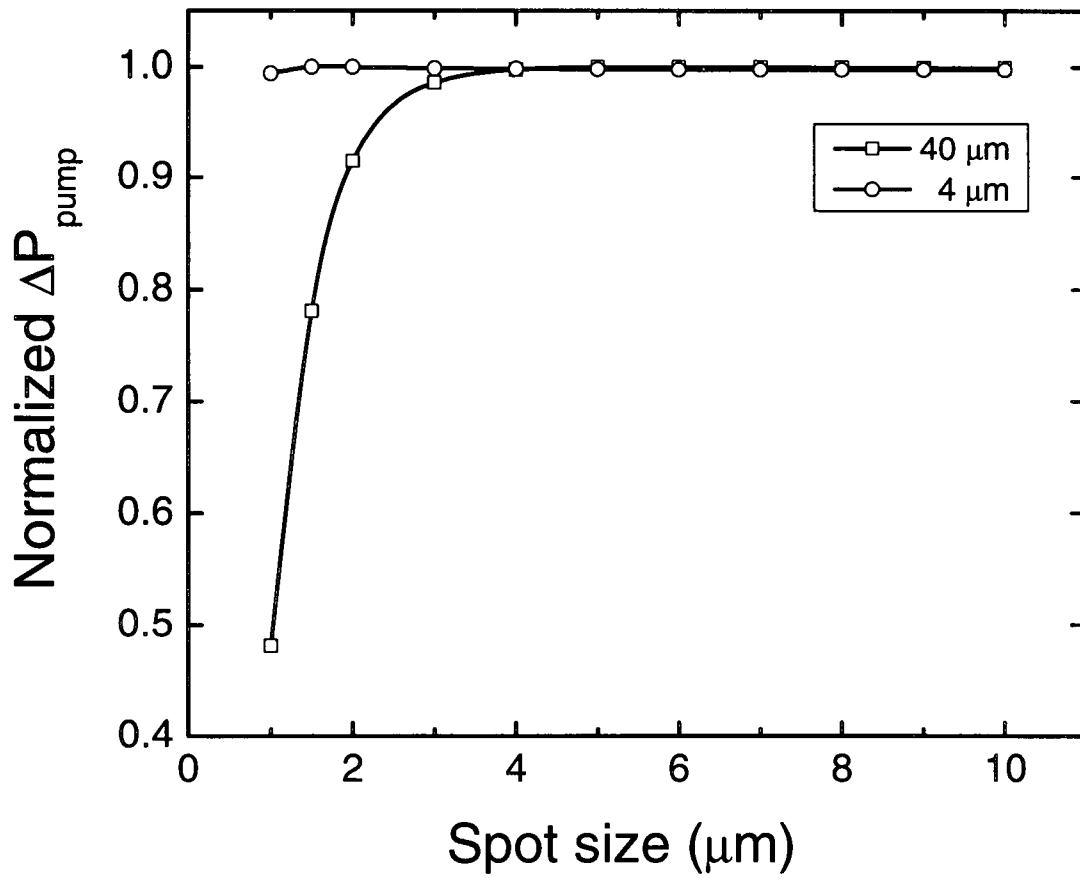


Figure 9.10: Beam coupling as a function of pump spot size for a 40 μm and a 4 μm long crystal. The percent of power loss is normalized (to maximum power loss in percentage) for both graphs. The Rayleigh range for a 1 μm beam in side LiNbO_3 is 27 μm .

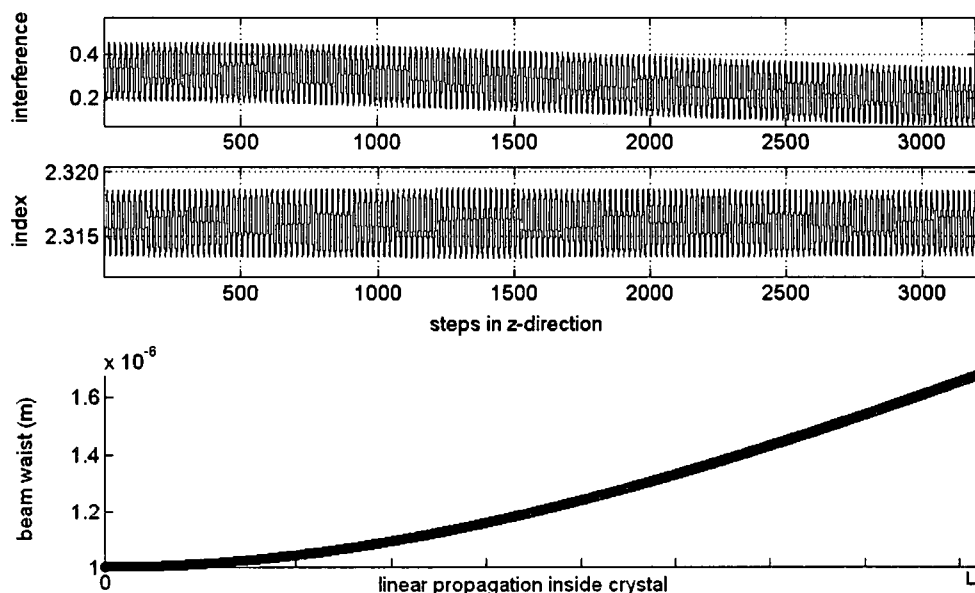


Figure 9.11: Interference pattern (top) and resulting phase index modulation (middle), and beam waist size for a 1 μm beam propagating in a 40 μm crystal and focused at the front. Interference magnitude is smaller compared to beam focus in the middle (Fig. 9.13) or at the end (Fig. 9.12). Same scale is used for Figs. 9.11 – 9.13. This figure is identical to Fig. 9.10. Drawn with new scale to compare with Figs. 9.11 – 9.13.

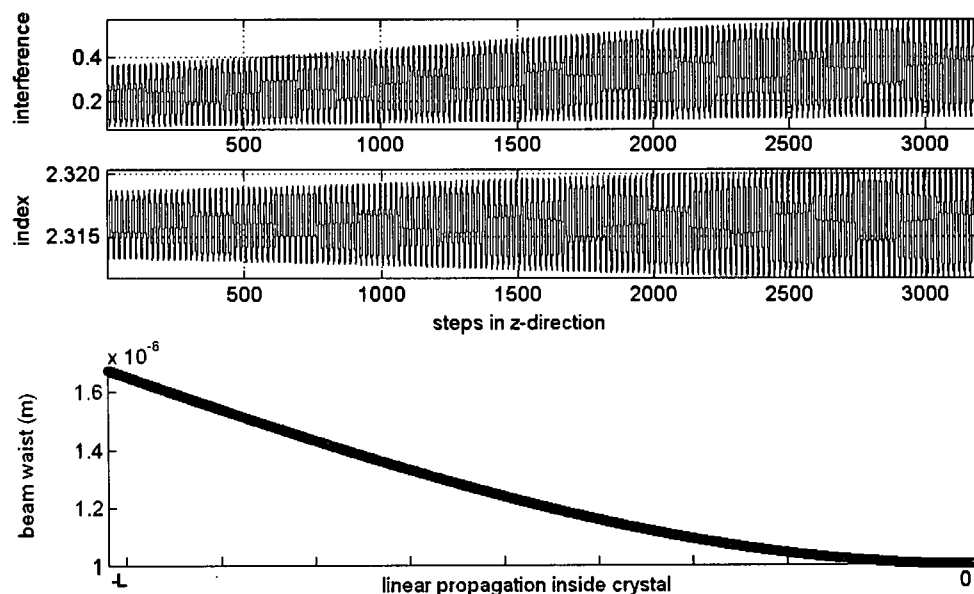


Figure 9.12: Interference pattern (top) and resulting phase index modulation (middle), and beam waist size for a 1 μm beam propagating in a 40 μm crystal and focused at the end. Interference, and index modulation magnitude is larger compared to beam focused at front (Fig. 9.11) or in the middle (Fig. 9.13). Same scale is used for Figs. 9.11 – 9.13.

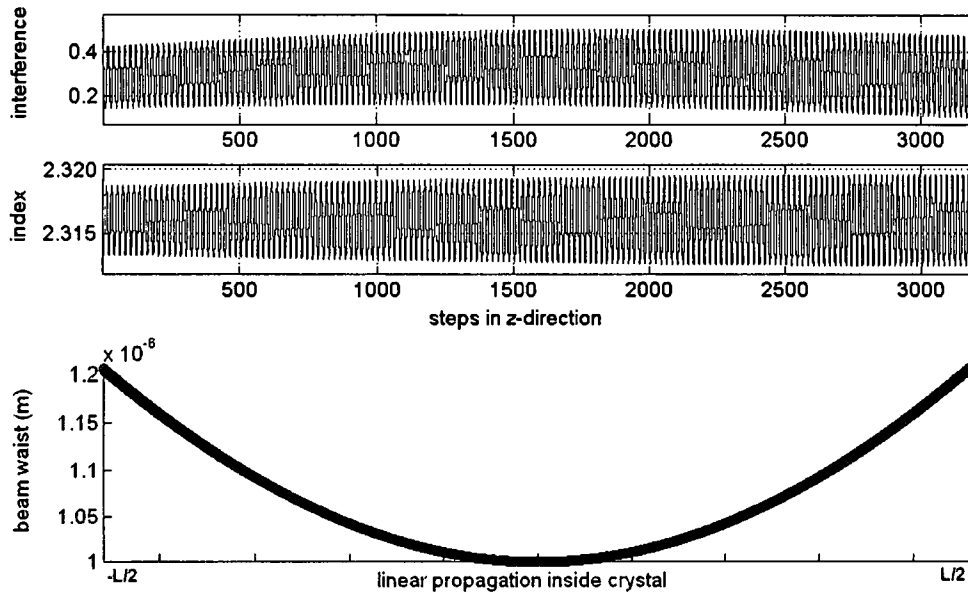


Figure 9.13: Interference pattern (top) and resulting phase index modulation (middle), and beam waist size for a $1\text{ }\mu\text{m}$ beam propagating in a $40\text{ }\mu\text{m}$ crystal and focused in the middle. Interference, and index modulation magnitude is larger compared to beam focused at front (Fig. 9.11) but smaller compared to the beam focused at the end (Fig. 9.12). Same scale is used for Figs. 9.11 – 9.13.

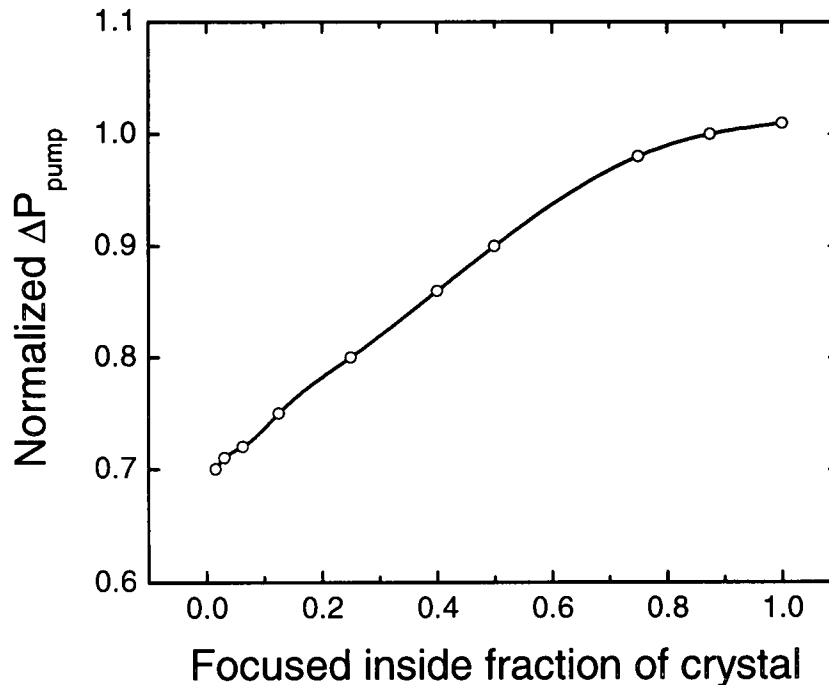


Figure 9.14: Beam coupling as a function of pump beam focus position inside a $40\text{ }\mu\text{m}$ crystal. $x=0$, focused at the entrance, $x=1$, focused at the end. The percent of power loss is normalized (to the maximum power loss in percentage).

CHAPTER X

CONCLUSIONS

10.1 Summary of Work in this Dissertation

In this work, we have focused on two specific aspects of photorefractive effect, the self-pumped contra-directional (SPCD) two-beam coupling (TBC) and a phenomenon that is closely related to SPCD-TBC, called stimulated back-scatter leading to six-wave mixing. We have extended the knowledge on stimulated back scatter and six-wave mixing with detail experimental work on various $\text{LiNbO}_3\text{:Fe}$ crystals. In addition, we have modeled the SPCD-TBC for a Gaussian beam in a PR media.

In Chapter 2 we have described the physics of the photorefractive effect, the band transport model and the theory of beam-coupling for plane waves and Gaussian beams. We have shown that the theoretical formulation for the space-charge field is different for these two cases. For plane-wave coupling, a closed form coupled equation can be formulated. For two-beam coupling such a closed form solution does not exist. In Chapter 3 we have reviewed the earlier work on SPCD-TBC and the earlier work on six-wave mixing.

In Chapter 4 SPBS leading to six-wave mixing is investigated in iron doped lithium niobate crystals of various doping concentrations, coatings, and thicknesses. The

experimental arrangement is discussed in detail. The time evolutions of all six interacting waves are monitored. The SPBS from $\text{LiNbO}_3\text{:Fe}$ is subjected to the well-established image restoration test and compared with a self-pumped phase conjugation from a $\text{BaTiO}_3\text{:Ce}$ sample. The nature of the SPBS is further investigated through an interference experiment.

In Chapter 5 we have discussed a set of coupled wave and material equations that models the observed six-wave mixing. It is shown here that the generated SPBS contains contributions from self diffraction and parametric diffraction, the latter containing the self-phase conjugate of the pump. Expanding on the work by Kukhtarev *et al.* in Ref. 9, a novel order analysis for the steady-state of the six waves is presented here.

In Chapter 6 six-wave mixing in different samples of $\text{LiNbO}_3\text{:Fe}$ with various concentrations, coatings and thicknesses has been investigated for oblique incidence of a 532 nm pump with respect to the c-axis. It is shown that the generated SPBS contains contributions from self diffraction and parametric diffraction, the latter containing the self-phase conjugate of the pump. A consequence of six-wave mixing is the generation of waves traveling along the $\pm c$ axes, whose intensities depend on the amount of scatter along the $\pm c$ axes and the interaction length of the six waves in the crystal. The time dynamics and the steady states for all participating waves have been experimentally studied and reconciled with inferences from approximate heuristic steady state theory. In the process, we have also shown that a reduced set of steady state equations based on a novel order analysis can be used to model six wave interactions in the future. A careful study of the SPBS, which includes image restoration test, interference with the pump, and visibility measurement, suggests that the phase conjugation may be contaminated by the

self diffraction. It is postulated that reduction of self diffraction may significantly improve the phase conjugate in SPBS.

In Chapter 7 we have reviewed the basics of the beam propagation theory and how the discrete Fourier transform could be used to implement the theory into a simulation code. In Chapter 8 we present the novel algorithm for simulating the self-pumped contra-directional (SPCD) two beam coupling (TBC) for a Gaussian beam. A split-step Fourier transform-inverse Fourier transform beam propagation method (FFT-BPM) using MATLAB[®] is used.

In Chapter 9 we have simulated SPCD-TBC using exact diffraction of a Gaussian pump beam. Because of the intense computational load involved, we have considered a crystal that is 40 μm long. For this crystal, we have used amplified change in the magnitude of modulated index in order to produce significant beam coupling. We present two proof-of-concept simulations that show well established characteristics of the PR self-pumped beam coupling. Following that we show beam coupling as a function of spot size and focal position to show that the simulation correctly accounts for beam diffraction. For our simulation in the 40 μm long crystal beam coupling starts to drop off below 4 μm spot size. We also observe that coupling is optimum when the beam is focused at the rear surface.

10.2 Future Work

We propose that future work could be focused along the ideas listed below.

1. Modeling the steady-state of six-waves.
2. Modeling the time dynamics of six-wave mixing.

3. Reducing the self-diffraction to produce SPBS with stronger phase-conjugate characteristics.
4. Examine 6W characteristics in lithium niobate crystals with other dopants besides Iron.
5. Use our simulation model with high gain materials such as photorefractive polymers that are also less than 50 μm in thickness.
6. Parallelize the simulation code to run with multiple processors to be able to simulate longer crystals.

APPENDIX A

SPCD-TBC SIMULATION CODE

A.1 MATLAB® Code

This appendix contains the code to simulate SPCD-TBC using split step beam propagation method. The algorithm is presented in Chapter 8 and simulation results are discussed in Chapter 9.

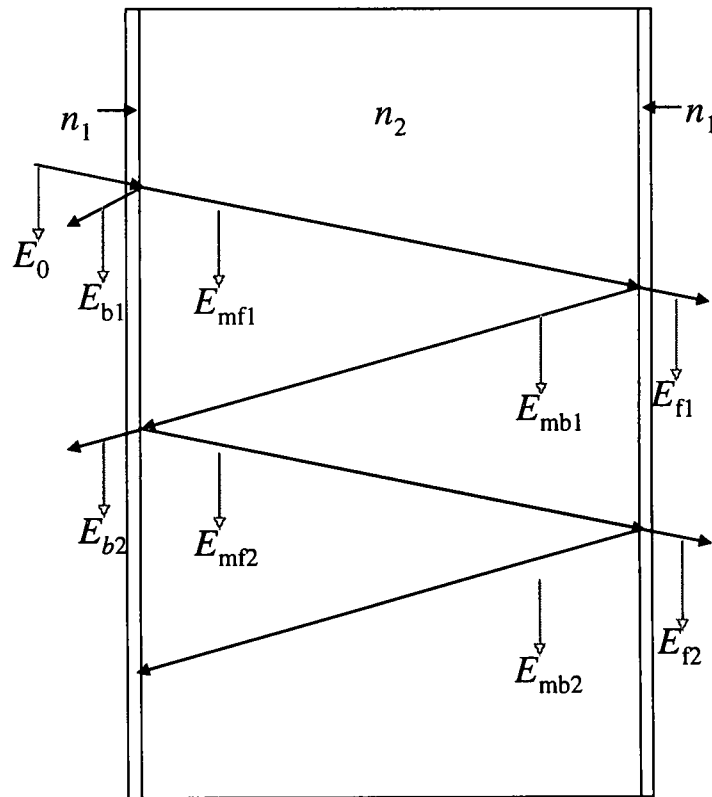


Figure A.1: Schematic representation participating beams and their symbols as used in the code. Beams are normal to crystal surfaces, but shown at an angle for convenience.

```

% CONTRA-DIRECTIONAL TWO-BEAM COUPLING (SELF-PUMPED)
% Written by Mohammad Saleh
% List of important figures
% Peak_Ezs_R1: After linear round—one with x is identical (311 format).
% _R1 for round one. _1,2 corresponds to trip 1 and 2.
% One, Two etc: Interference saved if not converged.
% EzR1_Nz_Nz2_EzFinal: First round Ez and final round Nz (pump,signal), Final Ez.
% Ez_Nz_peaks_conv: Would only be generated if converged. In that case it is
% identical to Ez_Nz_Ez_peaks' last two curves.
% =====END OF
COMMENT=====
%

clear all
error=1;tol=.97; %error initiated, error<tol would converge the NL round.
beta=1; %unit 1/sec)
s=6.2*10^(-5); %m^2/Joule
s=0;
mu=0.1*10^(-4); %unit m^2/(V*sec)
T=300;electron=1.6*10^(-19);
k_b=1.38*10^(-23); %This is joule/kelvin, we need this one
%k_b=8.62*10^(-5); %electron-volt/kelvin. (e*V/T)
Ds=mu*k_b*T/electron; %unit comes out as m^2/sec
r13=9.6; % for trans grating r33 applies(which is called gamma33 In Banerjee paper)
%r33=30.8*10^(-12); %unit m/V
Pf=1; %power factor. 25-->25 mW. Make lower for higher power.
%Cdf=0.01*s*0.5*((2.316)^3)*r33*Ds/mu % Cdf representing diffusion effect
%This is not the whole thing, Grad(I)/(sI+beta)
%is still missing, that part is with nz def.
Cpv=0*8352*10^(-3); %Cpv photovoltaic effet (in old time it was .0174)
%real params not tried yet. When done, use P/A and
%proper index_m factor like Cdf. (=0.48* 0.0174)
Cdf=1*0.27*2.316; % Artificial. MAKE s=0,beta=1,Pf=1;
% index_m and another constant added to get similar dn like before.
display('Purpose: true twostep and no fftshift(nz), any different result? Vary Cpv');
% 0.0174 and 0.270 gives same delta n (0.0268) for lamda in crystal,
% ***IF YOUR MAKE BOTH ZERO THEN ACTIVATE THE nz~=loop,
% otherwise r_k becomes zero at RB (1032 line)
%-----
display('New run started here--to separate between successive runs in command window');
delete log_exp.txt % so that stuffs don't get appended
format compact
format long e
diary log_exp.txt;
string1='DP_NL_T DP_wrtL_T DP_NL_B DP_wrtL_B';% just chose space a dilimeter in Excel.
fid = fopen('result_exp.xls','w');
fprintf(fid,'%38s \n',string1);
%if I used many strings instead, I would have to specify format for each.
fclose(fid);
t0=fix(clock);cpu0=cputime;fix(clock); %for future time ref for figures.
% Option controls
plotyn=1 % most has it 0, convert them to 1 to plot too. Make 3 to plot nothing.
plots=10; % see next line for its use.
nzR1T2=1; % for round 1
nzT1=plots;nzT2=plots;nzT3=plots;
interT1=plots;interT2=plots;interT3=plots; % both lines for final round

```

```

runpower=1;      % make zero if power measure is not needed.
runwaist=1       % make zero if waist measure is not needed. Was needed early to verify code.
movefocus=0     % Moves focus of the beam
mf=1            % 1,2,4,4/3 focusing at end, middle, 1/4, and 3/4 of L, and so on.
thirdtrip=0;
%-----
index_m=2.316; % 2.316 for LNbO3. verified that this=1 produces free space propagation
% if index_m is changed to 1.0000003 to debug, change the number 16 in line 628 to
% number 2 (in 3-15-05 version of code). This gives a good choice of transverse
% gradient (remember for q-lambda only, for others need to find out).
% Just be aware (for debugging) for n>> 1, if assuming 99% back reflection, then
% interference after first RTrip and final interference will be different
% because of Left B. reflection.
index_air=1;
cm=1e-2;mm=1e-3;um=1e-6;nm=1e-9;
t_k=1;          % transmission coefficient at each step. changes at interfaces
alpha=1;        % change to have absorption.

```

% PARAMETERS

```

N=16; % number of quarter wavelengths.
w0=5*um
totaldistance=(N*(0.532/4)*um)/index_m
stepsperQW=10
maxit=N*stepsperQW;% Now maxit and maxiterations are the same, which was not the
% case early on. Does not hurt to leave alone.
% If maxit goes down, the 1 in gradient(Ez_sq,1) should go up by inverse factor.
% automatically makes air before crystal 1/maxit
dz=totaldistance/maxit;% unless wanted spec. dz this is the easiest way. Specially since
% dz maxiteration has to be a multiple of 10 to make thing work.
medium=200*um % width of the medium, should be w0*333 to travel 60 z0.
maxiterations=floor(totaldistance/dz) % do not let this be < 1/crystal, see below.
maxround=30 % do not want to run convergence infinite time.
crystal=1/maxit; % do not make 1/crystal bigger than maxiterations, LBound becomes < 1
% but leftboundary has to be an interger to make the code work.
leftboundary=maxiterations*crystal % The smaller this number, less time wasted
rightboundary=maxiterations*(1-crystal) % Bigger the number, less time wasted
dim=256 % chose 2^n array, makes it faster,
% 1024 is good enough, but you can see trace of the 2nd theor. Wo line, so is 2048
% the first waist(1) value gets closest for 4096, then it does not improve anymore.
n1=index_air*ones(1,dim); % Index array in free space
n2=index_m*ones(1,dim); % Index array in the medium

```

% WAVE SETUP

```

iter=0;j=1;k=1;conv_loop=1;C=1; % Just initializing
lambda=0.532*um;
k0=2*pi/lambda; % Free space wave vector magnitude
k1=2*pi*index_m/lambda; % BEAWARE, n1 goes with k0, n2 goes with k1, late to fix
z0=(pi*index_m*(w0)^2)/lambda; % Rayleigh range inside the crystal.
a=medium/2/pi;
i=sqrt(-1);
k=[0:(dim/2-1)-(dim/2):-1]/a; % k=kx here. See page 249 (Pollock) for justification
% defined in a way that if fftshifted then looks like
% the physical k. Thats how it needs to be.
% Concern about the defs, use plot(fftshift(k)) to plot the array or plot(x,fftshift(k))
% to plot as a function of x to see what is going on.
kmax=max(k);kmin=min(k);

```

```

x=medium*(-0.5+(0:(dim-1))/dim);
% ALL THE APPROXIMATIONS WOULD BE NECESSARY IF WE REALLY USED TOO HIGH A
% FREQUENCY, BUT FOR CONFINING AS SMALL AS A 1 um BEAM NOT NEED TO DO THAT.
theta_i=asin(k./k0); % NO APPROXIMATION, this is incomplete since asin not unique
% IF we really want this, change formulation with a loop
% So that you get unique values.
theta_im=asin(k./k1); % NO APPROXIMATION, this is incomplete since asin not unique
% if in doubt plot the angles and see nothing is funny.
% IF we really want this, change formulation with a loop
% So that you get unique values.
theta_t=asin((n1./n2).*sin(theta_i)); % NO APPROXIMATION, incomplete since asin not unique
% Really want this? change formulation
% with a loop
% So that you get unique values.
theta_tm=asin((n2./n1).*sin(theta_im)); % NO APPROXIMATION, incomplete. asin not unique
% Really want this, change formulation with a loop
% So that you get unique values.
cos_theta_i=cos(theta_i);
cos_theta_im=cos(theta_im);
cos_theta_t=cos(theta_t);
cos_theta_tm=cos(theta_tm);

phase=exp(i*((n1*k0*dz).*(sqrt(1-k.^2./(n1.^2*k0^2))).^(-1)))); % Free space (9.10 Pollock)
%phase=exp(i*((n1*k0*dz))); % linear
phase_m1=exp(i*((n2*k0*dz).*(sqrt(1-k.^2./(n2.^2*k0^2))).^(-1)))); % 1st medium
%phase_m1=exp(i*((n2*k0*dz))); % 1st medium % linear
phase_m2=phase; % 2nd medium (this case freespace)
% above is the phase shift of individual plane waves after propagating the distance dz.

% FIRST ROUND STARTING (EACH ROUND STARTS WITH A NEW INCIDENT BEAM)

% BEAM DEFINED
v=exp(-(x/w0).^2)/Pf;
if plotyn==0
    figure(7);clf
    plot(x,v,'r');grid % no phase, so abs not needed.
    axis([-medium/2 medium/2 0 1]);
    title('The original gaussian at z=0');
    xlabel('x axis (m)');
    ylabel('E field amplitude');
    saveas(7,'E_focus.fig');close
end

powerarray=(v.*conj(v));
initial_onaxis_power=powerarray(dim/2+1)
initial_power=sum(v.*conj(v)) % same as sum(abs(v.^2))
% Normally Power is defined and then field is calculated from the power
% using proper convention. But in our case we will need to use the power
% of the beam again anyway and will have to use the same formula to
% calculate the power. It is then ok to start with the field instead and
% use an arbitrary power (E*conj(E)) formula to find power. If we had some
% constants in the formulation, the field magnitude would just have to be
% readjusted to give us the same power.
% If and when I make the change, use this formula
% I=epselon*(c/n)*E*conj(E)
% where epselon=dielectric constant*epselon_0

```

```

% now for Lithium niobate D.C. are as follows (printout inside Yariv book)
% DC_parallel (eps_33/eps_0) = 29, DC_perpendicular (eps_11/eps_0) = 85
% In this code, we assume perpendicular for the Fresnel r,t, so use that.
display('Adjust Pf up to make initial power higher.')
%pause;

v_k=fft(v); % looking at the frequency spectrum
if plotyn==0
    figure(9);clf
    plot(fftshift(k),abs(fftshift(v_k)));grid % here vk.^2 not needed, want amplitude only
    axis tight; % To see the whole thing
    title('Frequency spectrum amplitude');
    xlabel('k_x (1/m)');
    ylabel('spectrum amplitude');
    saveas(9,'Spc_Am_fo.fig');
end
%display('Done with original beam spot analysis. Press a key ..');pause(5);
%close all

% DEFINING ALTERNATE STARTING POINT
% This is following partha's suggestion. If I want to focus at the end I
% need propagate all the way to the end, using linear propagation, use the
% complex conjugate of that field as the starting point. To adjust for the
% index different between inside and the outside of the crystal, we are
% actually going to use the field after it comes out through the back, take
% the complex-conjugate of that and use that as the starting point of the
% actual linear round.
focus=1; % will be made 3+ if we do not want to move focus.
while focus<3; % Normally we will not repeat this cycle, unless we
    % want to focus somewhere else.
    % Maxiterations takes it all the way to the end and
    % outside. If we want to take halfway we can just make
    % maxiterations half, and the beam will still exit. The
    % virtual crystal then becomes half for this round.
    if movefocus==1 % redefining the travel distance for the pre-run.
        maxiterations=maxiterations/mf
        maxit=maxiterations % They are interchangeable, so this is redefined.
        crystal=1/maxiterations % This has be changed too, to make LB =1
        leftboundary=maxiterations*crystal
        rightboundary=maxiterations*(1-crystal)
        %pause
    end
    if focus==2
        maxiterations=floor(totaldistance/dz)
        maxit=maxiterations % They are interchangeable, so this is redefined.
        crystal=1/maxiterations % This has be changed too, to make LB =1
        leftboundary=maxiterations*crystal
        rightboundary=maxiterations*(1-crystal)
        %display('It works. Press a key ...');pause;
        v=fftshift(conj(Ef1)); % Since Ef1 was fftshifted, but our v needs to be in
        % Gaussian shape not U shape to start the loop.
    clear waist % So that old data does not corrupt
    iter=0 % Otherwise it would not run
end

```



```

if plotyn==0
figure(10);clf
plot(x,abs(v),'r');grid
axis([-medium/2 medium/2 0 1]);
title('The spatial field at the starting point');
xlabel('x axis (m)');
ylabel('E field amplitude');
saveas(10,'E_start.fig');
end
% display('Spatial field at start. Press a key ...');pause(5);
% display('starting progation...iterating...wait for plot to change')
% close
counter=0;
v_max=max(abs(v));
% LOOP TO GET THE ORIGINAL BEAM WAIST
if runwaist==1
while counter<(dim/2+1);
    counter=counter+1;
    if (abs(v_max/exp(1))-abs(v(counter)))<(0.01*abs(v_max/exp(1)));
        counter
        waist(1)=abs((dim/2+1)-counter)*(medium/dim)
        % display('used to see the first waist(1). Type control c to kill');pause;
        % waist(1) value changes strongly with medium (spatial resolution), and dim (sampling)
        counter=(dim/2+1);
    end
end
end
% END OF BEAM WAIST LOOP. If not needed to run, you can skip this step.
powerarray=(v.*conj(v));
onaxispower(1)=powerarray(dim/2+1);
power(1)=sum(v.*conj(v));

% ITERATION LOOP
tic
v=fftshift(v);
%
=====
=====
% FIRST TRIP THROUGH THE MEDIUM (iter=0 now)
while iter<maxiterations;          % The matching end is commented with ITEREND
    t_k=t_k*alpha;
    v_k=t_k.*(fft(v).*phase); % It accounts for transmission loss if any
    % also this simulate the boundary is right
    % after Ez1 line (in tbc.ppt).
%DEFINING INTERMEDIATE FIELDS
%(It is critical that these are done before iter value changes again (follows)
    if iter==leftboundary
        % Emf1=ifft(v_k); %defined for record in early version, superflous
        % Emf1 beam coming out rightward through the 1st interface

        v_kr=r_k.*(fft(v).*phase_m2);%since 'phase' has been redefined
        Eb1=ifft(v_kr);
        % Eb1 beam reflected leftward off the 1st interface, this is now at grid 0
    end
    if iter==rightboundary;
        Ef1=ifft(v_k); % Beam coming out rightward through the 2nd interface

```

```

v_kr=r_k.*(fft(v).*phase_m1);
Emb1=ifft(v_kr); % Beam reflected leftward off the 2nd interface
v_kr=r_k.*(fft(v));
Emb0=ifft(v_kr); %Emb1 without the step, right on Ez9 for maxiteration 10.
end
v=ifft(v_kr); %doing this in two steps allows me to define other beams
%at the boundaries conveniently.
t_k=1; % so T loss happens once only after being defined at the interface
%v=ifft(fft(v).*phase); % This was the easy way, no transmission coefficient.
iter=iter+1;
% To avoid future headache let us write an example here. As soon as the
% first two lines of above while loop is executed, beam is updated. As it
% is if the iter value at that point is 4 (or N), beam would reside on the
% position (in the TBC.ppt file) where Ez5 (or Ez(N+1)) resides. However as
% soon as the "iter=iter+1" is executed, things change. Now if iter value
% at any point is 4 (or N), beam would reside on the position where Ez4
% (or EzN) resides.

% LEFT BOUNDARY
if iter==leftboundary;
    % display('left boundary at'),iter
    phase=phase_m1; % takes effect from the next iteration
    % TRANSMISSION COEF. Considering perpendicular polarization only now
    %t_k=(2*n1.*cos_theta_i)/(n1.*cos_theta_i+n2.*cos_theta_t); %from n1 to n2
    t_k=(2*n1.*1)/(n1.*1+n2.*1); %from n1 to n2
    % theta_t is defined by theta_i, so no need to use theta_tm here
    % VERIFIED: Offcourse agrees for normal. For 30deg, inc angle calculated
    % theoretical to be .5476 for n2=2.36. Then found the point of k vector
    % where theta_i appears to be 30deg (apprx k=3.25e7). Then found that
    % t_k is aprx 0.55 around k=3.25e7
    % REFLECTION COEF. Considering perpendicular polarization only now
    %r_k=(n1.*cos_theta_i-n2.*cos_theta_t)/(n1.*cos_theta_i+n2.*cos_theta_t);
    r_k=(n1.*1-n2.*1)/(n1.*1+n2.*1);
    % VERIFIED: for normal matches upto 8th digit
    % r_k(1)=4.047661925139398e-001=r_k(1024)
    % Next fourlines would verify if coeffs are preserving power.
    %r_k(1)
    %t_k(1)
    % (r_k(1))^2+index_m*(t_k(1))^2 % for derivation see note on 6-2-04
    %display('LB r,t pause(5)'),pause(5);
end
% RIGHT BOUNDARY
if iter==rightboundary;
    % display('right boundary at'),iter
    phase=phase_m2; % takes effect from the next iteration
    % TRANSMISSION COEF. Considering perpendicular polarization only now
    % theta_tm is defined by theta_im, so need to use theta_tm even though it
    % is in free space at the 2nd interface n1,n2 are exchanged, and angle
    % variable are redefined since k0 changed to k1
    %t_k=(2*n2.*cos_theta_im)/(n2.*cos_theta_im+n1.*cos_theta_tm); %n2 to n1
    t_k=(2*n2.*1)/(n2.*1+n1.*1); %n2 to n1
    % use t_k=sqrt(index_m) if want full transmission.
    % Since the field is multiplied by t_k and field gets
    % squared, and the power inside crystal has the index_m
    % multiplicative factor, to keep the power same need

```

```

    % this extra factor outside the crystal.
    % multiply r_k by 2.519 if we want same signal
    % (84.25%). That is sqrt(sqrt because field is squared)
    % of 6.349 (which is the ratio of 84.25 and 13.27, normal signal).
    % t_k=0.001; % to test with constant, put 0.001 for interference null
    % tk2=t_k; % so I can look at the array later
    % REFLECTION COEF. Considering perpendicular polarization only now
    %r_k=(n2.*cos_theta_im-n1.*cos_theta_tm)./(n2.*cos_theta_im+n1.*cos_theta_tm);
    r_k=(n2.*1-n1.*1)./(n2.*1+n1.*1);
    %r_k=0.999; % to test with constant, put 0.999 for interference null
    %rk2=r_k; % so I can look at the array later
    r_kg=r_k; % for final step of the scattered beam, leaving crystal
    %r_k(1)
    %t_k(1)
    %(r_k(1))^2+(t_k(1))^2/index_m % derivation? note on 6-2-04
    %display('RB r,t pause(5)'),pause(5);
    end

    vv=fftshift(v); % The wave is v, vv is defined (with fftshift) temporarily to find
    % waist etc..or to plot it without using fftshift all the time.
    % Was unnecessary but may cause confusion if I try to use just v
    % for power, waist calculation. So, just keep as is.
% LOOP TO GET THE BEAM WAIST
    v_max=max(abs(vv));
    counter=0;
    if runwaist==1
        while counter<(dim/2+1);
            counter=counter+1;
            if (abs(v_max/exp(1))-abs(vv(counter)))<(0.01*abs(v_max/exp(1)));
                waist(iter+1)=abs((dim/2+1)-counter)*(medium/dim); % The first loop will give waist(2)
                counter=(dim/2+1);
            end
        end
    end
% END OF BEAM WAIST LOOP. If not needed to run, you can skip this step.
% POWER CALCULATION
% Going through the exact definition of power, I figured that the power
% between inside and outside of the crystal (air) differs by the index
% factor. So, instead of using the complex formula, using this factor to
% keep track of power. Now P_in is unity. For quantitative, need to
% change that.
    if runpower==1
        if iter>leftboundary
            C=index_m; %Power is different by this index factor
        end
        if iter>rightboundary
            C=1;
        end
        powerarray=C*(vv.*conj(vv));
        onaxispower(iter+1)=powerarray(dim/2+1); % The first loop will give onaxispower(2)
        % In reality this is the first point since propagation, but since we calcuted power
        % early before any propagation, the total number of points are maxiteration+1. So,
        % just beaware of this one extra point in the very first leg of the
        % trip. The very first point corresponds to the initial field, which is
        % not part of any other array in the simulation. This is ok, if the
        % beam takes n steps, array should be of length n+1.

```

```

power(iter+1)=C*sum(vv.*conj(vv));
end
% DEFINING INTERMEDIATE PLOTS
%%%%%%%%%%%%%%%%%%%%%%%%%%%%%%%%%%%%%%%%%%%%%%%%%%%%%%%%%%%%%%%%%%%%%%%%
Ez(iter,1)=v(1); % so first one will be Ez1, since iter become 1 at this point.
%if mod(iter,(maxit/plots))==0 % for intermediate plots, denom number of plots
if plotyn==0
    figure(iter);clf
    plot(x,abs(vv),'r');grid % no need to use fftshift since using vv
    axis([-medium/2 medium/2 0 1]);
    title('The spatial field R1/T1 after Figure.No steps');
    xlabel('x axis (m)');
    ylabel('E field amplitude');
    display('showing spatial field R1/T1 after Figure.No steps');pause(5);
    close(iter)
end
%if mod(iter,(maxit/5))==0 % for intermediate plots, denom number of plots
if plotyn==0
    vv_k=fft(vv); % looking at the frequency spectrum at this stage
    figure(iter+1);clf
    plot(fftshift(k),abs(fftshift(vv_k)));grid
    axis tight; % To see the whole thing
    title('Frequency spectrum amplitude after Figure.No steps');
    xlabel('k_x (1/m)');
    ylabel('spectrum amplitude');
    display('showing frequency spectrum at this Figure.No steps');%pause(5);
    close(iter+1)
end

end % ITEREND (ends the main iter loop)
%Ef1f=v; % Renamed the transmitted plot at the end of the 2nd medium

% DEFINING steps of propagation, to plot z-dependent things.
if runwaist==1
%Beaware that unless the Length is not many times z0, the simulated
%waist will look very much off from the theoretical waist. For the 1 um
%spot, I have to go to 400 um (N3200)to generate decent plot. z0 only 27
%um. To travel such great length (not possible in NL round), make dz big
%(1/quarter wave used for N3200).
z=linspace(0, totaldistance, (maxiterations+1));
w=w0*sqrt(1+(z/z0).^2);
if movefocus==2 % made 2 at the end of pre-run
if mf==2
    if movefocus==1 %executed during the pre-run bp
        z=linspace(0, totaldistance/2, (maxiterations+1));
    else %executed during the real bp
        z=linspace(-totaldistance/2, totaldistance/2, (maxiterations+1));
    end
    w=w0*sqrt(1+(z/z0).^2);
end
if mf==1
    if movefocus==1 %executed during the pre-run bp
        z=linspace(0, totaldistance, (maxiterations+1));
    else %executed during the real bp
        z=linspace(-totaldistance, 0, (maxiterations+1));
    end
end

```

```

w=w0*sqrt(1+(z/z0).^2);
end
if mf==4
    if movefocus==1 %executed during the pre-run bp
        z=linspace(0, totaldistance/4, (maxiterations+1));
    else %executed during the real bp
        z=linspace(-totaldistance/4, totaldistance*(3/4), (maxiterations+1));
    end
w=w0*sqrt(1+(z/z0).^2);
end
if mf==4/3
    if movefocus==1 %executed during the pre-run bp
        z=linspace(0, totaldistance*(3/4), (maxiterations+1));
    else %executed during the real bp
        z=linspace(-totaldistance*(3/4), totaldistance/4, (maxiterations+1));
    end
w=w0*sqrt(1+(z/z0).^2);
end
end
figure(11);
if N>2000
    plot(z,waist,'r--'); %plotting for small N would look staircase like.
    %plot(z,waist,'go');
else
    end
hold on
    %plot(z,w,'r--');
    plot(z,w,'go');
% swapped the plotting symbol, style. See explanation in log of June23,07
axis tight
title('The beam waist linear propagation');
xlabel('travelled distance (m)');
ylabel('Beam waist (m)');
saveas(11,'waist.fig');close
end
if runpower==1
if plotyn==1
    figure(12);
        %plot(z,onaxispower,'c. ');grid
        plot(onaxispower,'c. ');grid
        axis tight
        title('Original on axis power = 1 unit');
        %xlabel('travelled distance (m)');
        ylabel('On axis power');grid
        saveas(12,'On_axis1_R1.fig');close
end
    % display('Press a key ...');%pause(5);
if plotyn==1
    figure(13);
    power=power./initial_power;
        %plot(z,power,'r. ');grid
        plot(power,'r. ');grid
        axis tight
        title('Power during First Trip, normalized to initial');
        %xlabel('travelled distance (m)');
        ylabel('Total beam power');grid

```

```

    saveas(13,'Power_1_R1.fig');close
end
end
    power_R1B1=sum(Eb1.*conj(Eb1))/initial_power
    power_R1MB1=index_m*sum(Emb1.*conj(Emb1))/initial_power
    Err_LB=1-(power_R1B1+power(3))% power(2) is before boundary.
    Err_RB=power(maxit)-(power_R1MB1+power(maxit+1))
if plotyn==0
    figure(14);
    plot(x,abs(fftshift(Ef1)), 'r');grid
    axis([-medium/2 medium/2 0 1]);
    title('Field after crystal end of first trip (Ef1)');
    xlabel('x axis (m)');
    ylabel('E field amplitude');
    saveas(14,'Ef1_R1.fig');close
end
if plotyn==0
    figure(15);
    plot(x,abs(fftshift(Ef1f)), 'r');grid
    axis([-medium/2 medium/2 0 1]);
    title('Field after complete end of first trip (Ef1f)');
    xlabel('x axis (m)');
    ylabel('E field amplitude');
    saveas(15,'Ef1f_R1.fig');close
end
    display('=====END OF FIRST TRIP');
    %display('type plot(x,abs(fftshift(Ef1))) or similar to see specific fields')
    %display('saved fields are Eb1,Emf1,Emb1,Ef1,Ef1f');
    % pause(5)
    close all
    if movefocus==1
        focus=2 % less than 3
        movefocus=2 % so that it only runs once
        %display('It works. Press a key ...');pause;
        open waist.fig
        saveas(1,'waist_prerun.fig');close
    else
        focus=4 % bigger than 3
    end
end
% =====END OF FIRST TRIP
toc
%=====

tic
% SECOND TRIP THROUGH THE MEDIUM
    %remember now the journey begins on the right crystal surface, going left
C=index_m; % since starting in medium
iter2=0; % reinitializing
% To know how we decided on this boundary, see notes in Feb 04, May 04, Mar
% 15 of 2005. This is changed from FP1D and for good reasons.
leftboundary=(maxiterations*(1-2*crystal)) % until hits the left interface
rightboundary=(maxiterations*(2-4*crystal)) % after travelling back rightward
% Abover two lines uses the old maxiteration value, below we redefine for this trip.
maxiterations=(maxiterations*(2-3*crystal)) %taking trans. beam to same distance
v=Emb1; % now we have Emb0 defined also, we could use that,

```

```

% but then all Ez formula would require change
phase=phase_m1;
% NOTE: Since we are starting with EmbX, we are already in n2 index.
while iter2<maxiterations;      % The matching end commented with ITEREND
    t_k=t_k*alpha;
    v_k=t_k.*(fft(v).*phase);    % It accounts for transm. loss if any
    %DEFINING INTERMEDIATE FIELDS
    if iter2==0 % I call this dummy step.
        % since Emb2 is already a step ahead by definition, having the regular
        % BPM makes the first E-field here two steps away from the interface
        % For maxiteration=10, Ez1 of this trip coincides with Ez8 of first trip.
        % By using this loop we keep Ez1==Emb1 and allow it to coincide with Ez8
        v_k=fft(v);
    end
    %(It is critical that these are done before iter changes again (follows)
    if iter2==leftboundary
        % at this point beam is already at Ez1 position (tbc.ppt),
        % but still inside the crystal.
        % the phase_m2, makes the next step in air.
        Eb2=ifft(t_k.*(fft(v).*phase_m2));% Leftward through 1st interface
        v_kr=r_k.*(fft(v).*phase);
        Emf2=ifft(v_kr); % (archaic) defined for bookkeeping purpose.
        v_k=v_kr; % Now need the reflected beam, not transmitted
        % This is different from trip one
    end
    if iter2==rightboundary
        Ef2=ifft(v_k); % Rightward through the 2nd interface
        v_kr=r_k.*(fft(v).*phase_m1);
        Emb2=ifft(v_kr); % Reflected leftward off the 2nd interface
        % no need to define Emb0_2 since it would not be added to Ez.
    end
    v=ifft(v_k);
    t_k=1; % so T loss happens once only after being defined at the interface
    %v=ifft(fft(v).*phase);% This was the easy way, no transmission coefficient.

    iter2=iter2+1;
% thanks to the dummy step after the "iter2=iter2+1" value of iter will be
% exactly as the blue numbers in tbc.ppt, when beam is located at that
% longitudinal position (marked by the vertical bars inside the box).

% LEFT BOUNDARY (n2 in/n1 out) (for detail see the first trip)
    if iter2==leftboundary;
        %display('left boundary at'),iter2
        % phase=phase_m1; % not needed now since we were already in n2
        %t_k=(2*n2.*cos_theta_im)./(n2.*cos_theta_im+n1.*cos_theta_tm); % n2 to n1
        t_k=(2*n2.*1)./(n2.*1+n1.*1); % n2 to n1
        %r_k=(n2.*cos_theta_im-n1.*cos_theta_tm)./(n2.*cos_theta_im+n1.*cos_theta_tm);
        r_k=(n2.*1-n1.*1)./(n2.*1+n1.*1);
    end
% RIGHT BOUNDARY (again n2 in/n1 out!) (for detail see the first trip)
    if iter2==rightboundary;
        %display('right boundary at'),iter2
        phase=phase_m2; % takes effect from the next iteration
        %t_k=(2*n2.*cos_theta_im)./(n2.*cos_theta_im+n1.*cos_theta_tm); %n2 to n1
        t_k=(2*n2.*1)./(n2.*1+n1.*1); %n2 to n1
        %r_k=(n2.*cos_theta_im-n1.*cos_theta_tm)./(n2.*cos_theta_im+n1.*cos_theta_tm);

```



```

% this fixes the last point of Ez for index_m=2.316
% since for intensity we use abs(Ez) anyway, it does not hurt to use it here. Also
% because Ez is complex, above linear eqs does not give smooth curve for all N.

for j = 1:(maxit)
    Ezmax(j)=max(abs(Ez((j),1).^2));
    % unless beam gets two peaks this should work. Could try Ez((j),1,1) also.
end
if plotyn==1
    figure(23);clf
    subplot(3,1,1),plot(Ezmax,'ro-');grid
    ylabel('Interference');
    title('Interference, index and interference');
    axis tight
    saveas(23,'Interference.fig');close all
    % This one we are plotting everything--but in NL round we plot only
    % 2-99 because that is where the NL effects are. (do not delete)
    %display('Press a key ...');pause
end

%=====
% This is here to check if my code is still correct, for Cdf,Cpv=0,it should
% produce the same fabry perot effect as by fp1d.m. After any major modification
% to the code, should make sure that nothing is screwed up. (may not match
% with fp1d anymore, since the boundary conditions were chagned (may 26th,04)
% EbT=Eb1+Eb2;
if plotyn==0
    figure(51);clf
    EbTfft=fft(EbT);
    % Exploiting the fact that fft is same as far field profile
    plot(fftshift(k),fftshift(abs(EbTfft)), 'r');grid
    title('Fft of backward sum vs k-vector');
    xlabel('k_x (1/m)');
    ylabel('FFT after multiple pass');
    saveas(51,'Fft_bSum_vs_k_R1.fig');close
end
% MISC POWER CALC.
%plot(x,abs(fftshift(Ef1)), 'b');grid
%title('Ef1 end of first trip, round one');pause(5)
%plot(x,abs(fftshift(Ef2)), 'b');grid
%title('Ef2 end of second trip, round two');pause(5)
%display('These powers normalized with respect to initial power');
% Ef1,2,3 are outside the crystal, so no need for C.
power_R1T1=sum(Ef1.*conj(Ef1))/initial_power
power_R1B2=sum(Eb2.*conj(Eb2))/initial_power
power_R1B1=sum(Eb1.*conj(Eb1))/initial_power
power_R1MF2=index_m*sum(Emf2.*conj(Emf2))/initial_power
%display('Sum_field back and frontal should add up close to 1');
%onaxis_R1T1=fftshift(Ef1.*conj(Ef1)); %result same if fft on product/individual
%onaxis_R1T1= onaxis_R1T1(dim/2+1); %result verified with on_axis_1_R1.fig
%onaxis_R1T2=fftshift((Ef2.*conj(Ef2)));
%onaxis_R1T2=onaxis_R1T2(dim/2+1);
Total_Power=power_R1T1+power_R1B2+power_R1B1+power_R1MF2
Loss=1-Total_Power
display('=====END OF FIRST ROUND');
display('strike any key to continue');

```



```

% TO nz(j,:). Not sure if that will cost huge CPU time or not.
% Also more things need to be changed below this point.
% No, may be best would be using the gaussian when nz is used, not here.

nz(j)=index_m+(Cpv*index_m*(Ez(j,1).*conj(Ez(j,1)))+Cdf*py(j))./(s*index_m*(Ez(j,1).*conj(Ez(j,1)))/(p
i*(waist(j)^2))+beta);
end
if r==1

nz(j)=index_m+(Cpv*index_m*(Ez(j,2).*conj(Ez(j,2)))+Cdf*py(j))./(s*index_m*(Ez(j,2).*conj(Ez(j,2)))/(p
i*(waist(j)^2))+beta);
end
% this defines nz(1,r=1) and nz(maxit,r=1) wrongly, but they are not used.
end

% START OF NON LINEAR ROUND, NEW BEAM.
% Similar to the first round first trip.
% open Peak_Ezs_R1.fig % if desired to compare Ez and nz plots
maxiterations=floor(totaldistance/dz)
leftboundary=maxiterations*crystal
rightboundary=maxiterations*(1-crystal)

iter=0;jj=1;kk=1; % Just initializing
C=1;EgbT=0;TP_Egb=0; % Just initializing
for j = 1:maxit % Just initializing
Ez(j,r)=0; % Just initializing, maintains matrix form
Es(j,r)=Ez(j,r); % Initializing, with same form
%Defined the whole array (for new 'r') so that grating loop can update
end

phase=exp(i*((n1*k0*dz).*((sqrt(1-k.^2./(n1.^2*k0^2))).^(-1)))); % Free space, nonparaxial
%phase=exp(i*((n1*k0*dz))); %linear
phase_m1=exp(i*((n2*k0*dz).*((sqrt(1-k.^2./(n2.^2*k0^2))).^(-1)))); % 1st medium (crystal)
%phase_m1=exp(i*((n2*k0*dz))); % 1st medium (crystal) linear
phase_m2=phase; % 2nd medium (this case air)
phase_sp=1; % used to multiply in spatial domain, equals 1 until defined
% above is the phase shift of individual plane waves after propagating the distance dz.

% BEAM REDEFINED (for convenience nothing is redefined, only final plots are renamed)

v=exp(-(x/w0).^2)/Pf;

powerarray=(v.*conj(v));
onaxispower(1)=powerarray(dim/2+1);
power(1)=sum(v.*conj(v));
% ITERATION LOOP

v=fftshift(v);
tic
%
=====
=====
% FIRST TRIP THROUGH THE MEDIUM (iter=0 now)
while iter<maxiterations; % The matching end is commented with ITEREND
t_k=t_k*alpha;
v_k=t_k.*(fft(v).*phase); % It accounts for transmission loss if any

```

```

% DEFINING INTERMEDIATE FIELDS
%(It is critical that these are done before iter changes again (follows)
if iter==leftboundary
    % Emf1=ifft(v_k); % defined for record in early version
    % Emf1 beam coming out rightward through the 1st interface

    v_kr=r_k.*(fft(v).*phase_m2);%since 'phase' has been redefined
    Eb1=ifft(v_kr);
    % Reflected leftward off the 1st interface, this is now at grid 0
end
if iter==rightboundary;
    Ef1=ifft(v_k); % Rightward through the 2nd interface
    v_kr=r_k.*(fft(v).*phase_m1);
    Emb1=ifft(v_kr); % Reflected leftward off the 2nd interface
    v_kr=r_k.*(fft(v));
    Emb0=ifft(v_kr); %Emb1 without the step, right on Ez9 for maxiteration 10.
end
v=(ifft(v_k)).*phase_sp; % doing this in two step allows me to define other beams
% at the boundaries conveniently.

t_k=1; % so T loss happens once only after being defined at the interface
% v=ifft(fft(v).*phase); % This was the easy way, no tranmission coefficient.
iter=iter+1;
if iter==10
    CPU_time_iter10_NL=cputime-cpu0
end

% To avoid future headache let us write an example here. As soon as the
% first two lines of above while loop is executed, beam is updated. As it
% is if the iter value at that point is 4 (or N), beam would reside on the
% position (in the TBC.ppt file) where Ez5 (or Ez(N+1)) resides. However as
% soon as the "iter=iter+1" is executed, things change. Now if iter value
% at any point is 4 (or N), beam would reside on the position where Ez4
% (or EzN) resides.

% DEFINING MODIFIED INDEX (has to be done before new Ez is defined)
if iter<rightboundary % so that the right interface does not behaves as nonlinear step.
% Ez10 does not play any role in propagation at all. Right now, right boundary is treated
% a the linear case. Even if Ez9 is close to the edge, it would be improper to assume the
% boundary t_k changes (it would if we used the Ez9 modified index.)
if iter>leftboundary % so first mod index in going from Ez2 --> Ez3 (when iter=2)
    % Because Ez2 is the first field inside the material we could only
    % introduce nonlinearity at that point and not before.
    nznw=nz(iter);
    nznext=nz(iter+1);
    %plot to check if index and field aligned or not.
    %plot((nznw));pause;
    %plot((nznext));pause;
    %plot(x,abs((v)), 'r. ');pause;
    kz=2*pi*nznw./lambda;
    phase_sp=exp(i*k0*(nznw-index_m).*dz);
    % this is defined following Eq. 9.13 in Pollock.

    % plot(fftshift(real(phasez))) %name above phasez to run
    % display('new correct phase')
    % pause(5)

```

```

% Plotting modified index
% if mod(iter,(maxit/nzT1))==0 % for intermediate plots, denom number of plots
if plotyn==0
figure(iter);clf
subplot(3,1,1),plot(x,fftshift(py(iter)),'r');grid
ylabel('Grad Int.');
```

if r==2

```

subplot(3,1,2),plot(x,fftshift(Ez(iter,1).*conj(Ez(iter,1))),'r');grid
end
if r==1
subplot(3,1,2),plot(x,fftshift(Ez(iter,2).*conj(Ez(iter,2))),'r');grid
end
ylabel('Intensity');
```

subplot(3,1,3),plot(x,fftshift(nznw));grid

```

xlabel('x-axis');
ylabel('Modified index');
saveas(iter,'Mod_nznw.fig');close
display('showing intermediate index/Ez trip one');
display('i^(th) plot here correspond to (i-1)^th point on Peak_Ezs_R1.fig');pause(5);
close(iter)
end
```

=====

```

=====
% GRATING REFLECTIONS
    % Simulating first left boundary kind of picture.
    % LOCAL TRANSMISSION COEF.
        %theta_iz=asin(k./kz);
        %theta_tz=asin((nznext./nznw).*sin(theta_iz));
        %cos_theta_iz=cos(theta_iz);
        %cos_theta_tz=cos(theta_tz);
    %t_k=(2*nznw.*cos_theta_iz)./(nznw.*cos_theta_iz+nznext.*cos_theta_tz);%nznw to nznext(new)
    t_k=(2*nznw)./(nznw.*1+nznext.*1); %non spect. identical to spect. upto 15 decimals.
    %plot to check if t_k and field aligned or not.
    %plot(t_k);pause;
    %plot(x,abs((v)), 'r. ');pause;
        % since the "BOUNDARY" handling section comes below this, t_k
        % will be overwritten at the boundary with proper t_k.

% DEBUGGING TOOL: detect the loss due to each k, by changing number from 1 to maxit.
%if iter<6
    %t_k=1;
%end
    % LOCAL REFLECTION COEF.
        %plot(fftshift(t_k));pause(5) % shows what's happening
        %plot(fftshift(nznw));pause(5)
        r_k=(nznw.*1-nznext.*1)./(nznw.*1+nznext.*1);
        %plot to check if r_k and field aligned or not.
        %plot(r_k);pause;
        %plot(x,abs((v)), 'r. ');pause;
        %plot(r_k)
    %r_k=(nznw.*cos_theta_iz-nznext.*cos_theta_tz)./(nznw.*cos_theta_iz+nznext.*cos_theta_tz);
    v_gr=r_k.*(fft(v).*phase);% grating reflected beam, moved a step (due to the phase)
    Egb=(ifft(v_gr)).*phase_sp; % Beam reflected leftward
```



```

Ezmax(j)=max(abs(Ez((j),r).^2));
end
plot(Ezmax,'ro-');grid
ylabel('Interference');
title('Developement of Ezs in NL first trip');
axis tight
saveas(77,'Last_Ez_NL_firsttrip');%close
% pause(5) % can see almost a movie in progress.
end

if mod(iter,(maxit/interT1))==0 % for intermediate plots, denom number of plots
    iter
    cputime
    if plotyn==0
        figure(iter);clf
        plot(x,abs(vv),'r');grid % no need to use fftshift since using vv
        axis([-medium/2 medium/2 0 1]);
        title('The spatial field final round trip one after Figure.No steps');
        xlabel('x axis (m)');
        ylabel('E field amplitude');
        display('showing spatial field trip one after Figure.No steps');%pause(5);
        close(iter)
    end
    if plotyn==0
        vv_k=fft(vv); % looking at the frequency spectrum at this stage
        figure(iter+1);clf
        plot(fftshift(k),abs(fftshift(vv_k)));grid
        axis tight; % To see the whole thing
        title('Frequency spectrum amplitude after Figure.No steps');
        xlabel('k_x (1/m)');
        ylabel('spectrum amplitude');
        display('showing frequency spectrum at this Figure.No steps');%pause(5);
        close(iter+1)
    end
end
end
% LEFT BOUNDARY
if iter==leftboundary;
    % display('left boundary at'),iter
    phase=phase_m1; % as phase_m1
    % TRANSMISSION COEF. Considering perpendicular polarization only now
    %t_k=(2*n1.*cos_theta_i)./(n1.*cos_theta_i+n2.*cos_theta_t); %from n1 to n2
    %t_k=(2*n1.*1)./(n1.*1+n2.*1); %n1 to n2 (for NL need nznext)
    nznext=nz(iter+1);
    t_k=(2*n1.*1)./(n1.*1+nznext.*1); %n1 to nznext
    %plot to check if nznext, t_k and field aligned or not.
    %plot(nznext);pause;
    %uu=1068
    %plot(x,abs((v)), 'r. ');pause;
    %plot(t_k);pause;
    % REFLECTION COEF. Considering perpendicular polarization only now
    %r_k=(n1.*cos_theta_i-n2.*cos_theta_t)./(n1.*cos_theta_i+n2.*cos_theta_t);
    % r_k=(n1.*1-n2.*1)./(n1.*1+n2.*1);
    r_k=(n1.*1-nznext.*1)./(n1.*1+nznext.*1);%n1 to nznext
end
% RIGHT BOUNDARY
if iter==rightboundary;

```



```

    % display('right boundary at'),iter
    phase=phase_m2; % takes effect from the next iteration
    % TRANSMISSION COEF. Considering perpendicular polarization only now
    %t_k=(2*n2.*cos_theta_im)./(n2.*cos_theta_im+n1.*cos_theta_tm); %n2 to n1
    % t_k=(2*n2.*1)./(n2.*1+n1.*1); %n2 to n1 (for NL need nznw)
    nznw=nz(iter);
    t_k=(2*nznw.*1)./(nznw.*1+n1.*1); %nznw to n1
    % t_k=0.001; % to test with constant, put 0.001 for interference null
    % REFLECTION COEF. Considering perpendicular polarization only now
    %r_k=(n2.*cos_theta_im-n1.*cos_theta_tm)./(n2.*cos_theta_im+n1.*cos_theta_tm);
    %r_k=(n2.*1-n1.*1)./(n2.*1+n1.*1); % (for NL need nznw)
    r_k=(nznw.*1-n1.*1)./(nznw.*1+n1.*1);
    % r_k=0.999; % to test with constant, put 0.999 for interference null
    r_kg2=r_k; % for the exiting for diffraction, instead of calculating again.
end

% POWER CALCULATION
    vv=fftshift(v); % The wave is v, vv is defined (with fftshift) temporarily to find
    % waist etc..or to plot it without using fftshift all the time.
    % This was unnecessary but may cause confusion if I try to use just
    % v for power, waist calculation. So, just keep as is.
    if runpower==1
        if iter>leftboundary
            % C=1;% After trying various things, we realized the best thing is
            % to calculate field squared, not power, since this is inside
            % and does not matter. I went back to C=fftshift(nz) since that gives a
            % good sense of power calculation compared to the linear case. Otherwise
            % I will have to change the label of all the figures. Plus, I have a
            % sense of what is expected, as far as power is concerned. Now if I move
            % away, it will be confusing. I can always, re-label it if I want to.
            C=fftshift(nznex);% see note below
            % For a long time it was a mystery, why fftshift was needed.
            % Today realized that since vv=fftshift(v), C needs fftshift.
            % See log of aug 22, 05 to see why nznw is used instead of nznex.
            end

            if iter>rightboundary
                C=1;
            end
            powerarray=C.*(vv.*conj(vv));
            onaxispower(iter+1)=powerarray(dim/2+1); % The first loop will give onaxispower(2)
            % In reality this is the first point since propagation, but since we calcuted power
            % early before any propagation, the total number of points are maxiteration+1. So,
            % just beaware of this one extra point in the very first leg of the
            % trip. The very first point corresponds to the initial field, which is
            % not part of any other array in the simulation.
            power(iter+1)=sum(powerarray);
            end
        end
        % ITEREND (ends the main iter loop)
    close all
    %E1f=v; % Renamed the transmitted plot at the end of the 2nd medium
    %normally no other use, so definition and plot commented out.
    if runpower==1
        if plotyn==1
            figure(12);clf
            %plot(z,onaxispower,'c');grid

```

```

plot(onaxispower,'c. ');grid
axis tight
title('Original on axis power = 1 unit');
xlabel('travelled distance (m)');
ylabel('On axis power');grid
saveas(12,'On_axis1.fig');close
end
%display('Press a key ...');%pause(5);
if plotyn==1
figure(13);clf
power=power./initial_power;
%plot(z,power,'r. ');grid
plot(power,'r. ');grid
axis tight
title('Power during First Trip, normalized to initial');
xlabel('travelled distance (m)');
ylabel('Depleting pump without signal scatter');grid
saveas(13,'Power_1.fig');close
end
end

if plotyn==0
figure(14);clf
plot(x,abs(fftshift(Ef1)), 'r. ');grid
axis([-medium/2 medium/2 0 1]);
title('Field after crystal end of first trip (Ef1), final round');
xlabel('x axis (m)');
ylabel('E field amplitude');
saveas(14,'Ef1.fig');close
end
if plotyn==0
figure(15);clf
plot(x,abs(fftshift(Ef1f)), 'r. ');grid
axis([-medium/2 medium/2 0 1]);
title('Field after complete end of first trip (Ef1f)');
xlabel('x axis (m)');
ylabel('E field amplitude');
saveas(15,'Ef1f.fig');close
end
display('=====END OF FIRST TRIP');
%display('type plot(x,abs(fftshift(Ef1))) or similar to see specific fields')
%display('saved fields are Eb1,Emf1,Emb1,Ef1,Ef1f');
%pause(5)
close all
% =====END OF FIRST TRIP
toc
%pause

tic
%=====
% SECOND TRIP THROUGH THE MEDIUM
%remember now the journey begins on the right crystal surface, going left
C=index_m; % since starting in medium
iter2=0; % reinitializing
% THE MINUS 2 AT THE END WAS ADDED AFTER REALIZING THAT WITHOUT IT 2ND TRIP

```

% BOUNDARIES TAKES ADDITIONAL STEPS LEFTWARD, COMPARED TO THE FIRST TRIP.
(TBC.PPT)

```

leftboundary=(maxiterations*(1-2*crystal)) % until hits the left interface
rightboundary=(maxiterations*(2-4*crystal)) % after travelling back rightward
% Above lines still uses the old maxiteration value, below we redefine for this trip.
maxiterations=(maxiterations*(2-3*crystal)) % takes the tran. beam to the same distance
v=Emb1;Egb2T=0;TP_Egb2=0;
phase=phase_m1;
phase_sp=1; % until defined again, overwrites on trip1 value
% NOTE: Since we are starting with EmbX, we are already in n2 index.
while iter2<maxiterations; % The matching end is commented with ITEREND
    t_k=t_k*alpha;
    v_k=t_k.*(fft(v).*phase); % It accounts for transmission loss if any
    %DEFINING INTERMEDIATE FIELDS
    if iter2==0
        % since Emb1 is already a step ahead by definition, having the regular
        % BPM formula makes the first E-field here two steps away from the interface
        % For maxiteration=10, Ez1 of this trip coincides with Ez8 of first trip.
        % By using this loop we keep Ez1==Emb1 and allow it to coincide with Ez8
        v_k=fft(v); % without the phase term, ifft(fft) reproduces (v)
    end
    % (It is critical that these are done before iter value changes again (follows)
    if iter2==leftboundary % remember that in this case LB is not so near.
        % at this point beam is already at Ez1 position (tbc.ppt),
        % but still inside the crystal.
        % the phase_m2, makes the next step in air.
        Eb2=ifft(t_k.*(fft(v).*phase_m2)); % Leftward through the 1st interface
        v_kr=r_k.*(fft(v).*phase);
        Emf2=ifft(v_kr); % Reflected rightward off the 1st interface
        v_k=v_kr; % Want the reflected beam, not transmitted
        % This is different from trip one
    end
    if iter2==rightboundary
        Ef2=ifft(v_k); % Rightward through the 2nd interface
        v_kr=r_k.*(fft(v).*phase_m1);
        Emb2=ifft(v_kr); % Reflected leftward off the 2nd interface
        % no need to define Emb0_2 since it would not be added to Ez.
    end
    v=(ifft(v_k)).*phase_sp;
    t_k=1; % so T loss happens once only after being defined at the interface
    %v=ifft(fft(v).*phase); % This was the easy way, no transmission coefficient.

    iter2=iter2+1;
    % thanks to the dummy step after the "iter2=iter2+1" value of iter will be
    % exactly as the blue numbers in tbc.ppt, when beam is located at that
    % longitudinal position (marked by the vertical bars inside the box).

    % DEFINING MODIFIED INDEX (has to be done before Ezs are redefined)
    if iter2<rightboundary % unless more than 1% of crystal use, this is useless.
        % make a large number if loop not desired
        % no lower bound., so first mod index in going from Ez1->Ez2
    if iter2>(maxit-3) % for rightward, for leftward see 'else'
        nznz=nz(iter2-(maxit-3)); % see tbc.ppt, if beam is at 11, nznz is from Ez4
        nznz=nz((iter2+1)-(maxit-3)); % if beam is at 11, nznz is from Ez5
        % PLOTTING MODIFIED INDEX
        % if mod(iter2,(maxit/nzT2))==0 % nzT2 plots in rightbound only

```

```

if plotyn==0
figure(iter2);clf
iter2,display('rightbound')
if r==2
subplot(2,1,1),plot(x,fftshift(Ez(iter2-(maxit-3),1)).*conj(Ez(iter2-(maxit-3),1))), 'r');grid
end
if r==1
subplot(2,1,1),plot(x,fftshift(Ez(iter2-(maxit-3),2)).*conj(Ez(iter2-(maxit-3),2))), 'r');grid
end
ylabel('abs(Ez^2)');
subplot(2,1,2),plot(x,fftshift(nznw));grid
title('Ez and nznw modified by Ez, final round trip two (Ez.FigureNo)');
xlabel('x-axis');
ylabel('Modified index');
saveas(iter2,'Mod_nznw.fig');close
display('showing intermediate index/Ez trip two');
display('for iter=i, compare [(i-(maxit-3))-1] point on interfer. plot');
% that -1 comes because two edges are not plotted.
close(iter2)
end
else % going leftward (not invoked once iter2 becomes (maxit-2)
if iter2==1
nznw=nznw;% using the old one from trip 1 thus power is conserved.
nznxt=nz(maxit-(iter2+2));% if beam is at 4, nznxt is from Ez4
% see log of aug 22, 05 to see why nznw is used instead of nznxt.
elseif iter2==(maxit-3)
nznw=nz(maxit-(iter2+1));
nznxt=nznw;
% this was done to avoid Ez(1) which has error.
% see note on Aug22, 05
else
nznw=nz(maxit-(iter2+1)); % see tbc.ppt, if beam is at 4, nznw is from Ez5
nznxt=nz(maxit-(iter2+2));% if beam is at 4, nznxt is from Ez4
end
% PLOTTING MODIFIED INDEX
% if mod(iter2,(maxit/nzT2))==0 % nzT2 plots in rightbound only
if plotyn==0
figure(iter2);clf
iter2,display('leftbound')
if r==2
subplot(2,1,1),plot(x,fftshift(Ez(maxit-(iter2+1),1)).*conj(Ez(maxit-(iter2+1),1))), 'r');grid
end
if r==1
subplot(2,1,1),plot(x,fftshift(Ez(maxit-(iter2+1),2)).*conj(Ez(maxit-(iter2+1),2))), 'r');grid
end
ylabel('abs(Ez^2)');
subplot(2,1,2),plot(x,fftshift(nznw));grid
title('Ez and nznw modified by Ez, final round trip two (Ez.FigureNo)');
xlabel('x-axis');
ylabel('Modified index');
saveas(iter2,'Mod_nznw.fig');close
display('showing intermediate index/Ez trip two');
display('for iter=i, compare [(maxit-(i+1))-1] point on interference plot');
close(iter2)
end
end
end

```

```

kz=2*pi*nznw./lambda;
phase_sp=exp(i*k0*(nznw-index_m).*dz);
% this is defined following Eq. 9.13 in Pollock.

%plot(fftshift(real(phasez)))
%display('new phase')
%pause(5)
%=====
=====
% GRATING REFLECTIONS %CHANGE THEM WITH NZNOW AND NZNEXT
    %theta_iz=asin(k./kz);
    %theta_tz=asin((nznw./nznw).*sin(theta_iz));
    %cos_theta_iz=cos(theta_iz);
    %cos_theta_tz=cos(theta_tz);
    % LOCAL TRANS. COEF.
    %t_k=(2*nznw.*cos_theta_iz)./(nznw.*cos_theta_iz+nznw.*cos_theta_tz);
    t_k=(2*nznw)./(nznw.*1+nznw.*1); % from nznw to nznw (new)
    %if iter2==(maxit-3)
        % t_k=ones(1,dim);
    %end
    % since the "BOUNDARY" handling section comes below this, t_k
    % will be overwritten at the boundary with proper t_k.

% FOR GATHERING THE DIFFRACTED BEAMS FROM THE SIGNAL.
    if iter2<leftboundary % thus ignoring the later part of second trip
        % LOCAL REFLECTION COEF.
        %r_k=(nznw.*cos_theta_iz-
nznw.*cos_theta_tz)./(nznw.*cos_theta_iz+nznw.*cos_theta_tz);
        r_k=(nznw.*1-nznw.*1)./(nznw.*1+nznw.*1);
        v_gr=r_k.*(fft(v).*phase); % grating reflected beam
        Egb2=(ifft(v_gr).*phase_sp); % Reflected off the grating in 2nd trip
        iter2=1; % redefining before everyloop
        while iter2<iter2 %makes iter2-1 # steps, to go to screen
            Ez((maxit-(iter2+1))+iter2,r)=Ez((maxit-(iter2+1))+iter2,r)+Egb2(1);
            kz_g=2*pi*nz((maxit-(iter2+1))+iter2)/lambda;
            phase_gsp=exp(i*k0*((nz((maxit-(iter2+1))+iter2))-index_m).*dz);
            Egb2=(ifft(fft(Egb2).*phase)).*phase_gsp;
            % In this trip phase is already defined as being inside crystal
            iter2=iter2+1;
        end
        Egb2=r_kg2.*ifft(fft(Egb2).*phase_m2); %last step outside crystal
        % taking it to the same place where Ef1 is located.
        %P_Egb2=sum(Egb2.*conj(Egb2));
        P_Egb2=sum(Egb2.*conj(Egb2));
    end % note that this loop does not exist for iter.
    Egb2T=Egb2T+Egb2; % All in the plane outside, adding up
    TP_Egb2=TP_Egb2+P_Egb2;
    %iter2
    %plot(x,abs(fftshift(Egb2T)), 'b');grid
    %title('diffraction from the grating transmitted');
    %Power_Signal_Diff=sum(Egb2T.*conj(Egb2T))
    %pause(5)
    % Next fourlines would verify if coeffs are preserving power.
    %r_k(1)
    %t_k(1)
    %(r_k(1))^2+(t_k(1))^2*(nznw(1)/nznw(1)) %(Test if = 1)

```

```

        %pause(5),display('pause(5)d');
end
% DEFINING NZ_peaks (for 2nd trip)
%%%%%%%%%%%%%%%%%%%%%%%%%%%%%%%%%%%%%%%%%%%%%%%%%%%%%%%%%%%%%%%%%%%%%%%%
% if iter2<(leftboundary+1)
if iter2<(leftboundary+1)
    if min(nznw)<index_m
        nzmax2(iter2)=min(nznw);
    else
        nzmax2(iter2)=max(nznw);
        %synchronized with Ezmax, in case want to plot together.
    end
end
%%%%%%%%%%%%%%%%%%%%%%%%%%%%%%%%%%%%%%%%%%%%%%%%%%%%%%%%%%%%%%%%%%%%%%%%
% DEFINING EZs
%%%%%%%%%%%%%%%%%%%%%%%%%%%%%%%%%%%%%%%%%%%%%%%%%%%%%%%%%%%%%%%%%%%%%%%%
if iter2<(maxit-1) % upto the left boundary, see tbc.ppt
    Es(maxit-(iter2+1),r)=Es(maxit-(iter2+1),r)+v(1);
    if iter2==1
        Es((maxit-1),1)=Es((maxit-1),1)+Emb0(1); %this is to fix the right edge
        %The Emb0 is before phase was added to the reflected beam.
        %Note, since iter2=1 adds the right fields to both Ez8 and Ez9.
    end
end
if iter2>(maxit-2)
    Es((iter2-(maxit-3)),r)=Es((iter2-(maxit-3)),r)+0;%v;
end
%%%%%%%%%%%%%%%%%%%%%%%%%%%%%%%%%%%%%%%%%%%%%%%%%%%%%%%%%%%%%%%%%%%%%%%%
% if mod(iter2,(maxit/interT2))==0 % for intermediate plots, denom # of plots
if plotyn==0
    figure(iter2);clf
plot(x,abs(vv),'r');grid % no need to use fftshift since using vv
axis([-medium/2 medium/2 0 1]);
title('The spatial field final round trip two Figure.No steps');
xlabel('x axis (m)');
ylabel('E field amplitude');
display('showing spatial field trip two after Figure.No steps');%pause(5)
close(iter2)
end

% LEFT BOUNDARY (n2 in/n1 out) (for detail see the first trip)
if iter2==leftboundary;
    %display('left boundary at',iter2
    % phase=phase_m1; % not needed now since we were already in n2
    %t_k=(2*n2.*cos_theta_im)/(n2.*cos_theta_im+n1.*cos_theta_tm);%n2 to n1
    %t_k=(2*n2.*1)/(n2.*1+n1.*1);%n2 to n1
    %nznw=fftshift(nz((maxit-(iter2+1)),:));%before, aug22, 05
    nznw=(nz(maxit-(iter2)));
    %nznw is not needed, but If I call for it it will use the one defined last
    % time, which is defined for (iter2==leftboundary-3).
    % see note on Aug22,05
    t_k=(2*nznw.*1)/(nznw.*1+n1.*1);%n2 to n1
    %r_k=(n2.*cos_theta_im-n1.*cos_theta_tm)/(n2.*cos_theta_im+n1.*cos_theta_tm);

```

```

        %r_k=(n2.*1-n1.*1)/(n2.*1+n1.*1);
        r_k=(nznw.*1-n1.*1)/(nznw.*1+n1.*1);
    end
% RIGHT BOUNDARY (again n2 in/n1 out!) (for detail see the first trip)
    if iter2==rightboundary;
        %display('right boundary at'),iter2
        phase=phase_m2; % takes effect from the next iteration
        %t_k=(2*n2.*cos_theta_im)/(n2.*cos_theta_im+n1.*cos_theta_tm); %n2 to n1
        %t_k=(2*n2.*1)/(n2.*1+n1.*1); %n2 to n1
        nznw=nz((iter2-(maxit-3))); % This is for second part of trip.
        t_k=(2*nznw.*1)/(nznw.*1+n1.*1); %n2 to n1
        %r_k=(n2.*cos_theta_im-n1.*cos_theta_tm)/(n2.*cos_theta_im+n1.*cos_theta_tm);
        %r_k=(n2.*1-n1.*1)/(n2.*1+n1.*1);
        r_k=(nznw.*1-n1.*1)/(nznw.*1+n1.*1);
    end

%=====
% POWER CALCULATION
        vv=fftshift(v); % The wave is v, vv is defined (with fftshift) temporarily to find
        % waist etc..or to plot it without using fftshift all the time.
        % This was unnecessary but may cause confusion if I try to use just
        % v for power, waist calculation. So, just keep as is.

    if runpower==1
        if iter2>0
            % C=1;% After trying various things, we realized the best thing is
            % to calculate field squared, not power, since this is inside
            % and does not matter. I went back to C=fftshift(nz) since that gives a
            % good sense of power calculation compared to the linear case. Otherwise
            % I will have to change the label of all the figures. Plus, I have a
            % sense of what is expected, as far as power is concerned. Now if I move
            % away, it will be confusing. I can always, re-label it if I want to.
            C=fftshift(nznw); % see note below
            % For a long time it was a mystery, why fftshift was needed.
            % Today realized that since vv=fftshift(v), C needs fftshift.
            % See log of aug 22, 05 to see why nznw is used instead of nznext.
            end
            if iter2>rightboundary
                C=1; end
            powerarray2=C.*(vv.*conj(vv));
            onaxispower2(iter2)=powerarray2(dim/2+1);
            power2(iter2)=sum(powerarray2);
            end
        end

        % ITEREND (ends the main iter loop)
        %Ef2f=v; % Renamed the transmitted plot at the end of the 2nd medium

    if runpower==1
        z=linspace(0, maxiterations*dz, (maxiterations)); %m..s*dz is the new distance
    if plotyn==0
        figure(212);clf
        %plot(z,onaxispower2,'c.');
```

```

        %plot(z,onaxispower2,'c.');
```



```

% this fixes the last two points of Ez for index_m=2.316
% since for intensity we use abs(Ez) anyway, it does not hurt to use it here.
% also, because Ez is complex, the above linear eqs does not give smooth
% curve for all N.
Es((1),r)=Es((2),r);
Es((maxit-2),r)=Es((maxit-3),r);
Es((maxit-1),r)=Es((maxit-2),r);
Es((maxit),r)=Es((maxit-1),r);

% CALCULATING THE PUMP/SIGNAL FIELDS AFTER COUPLING
%%%%%%%%%%%%%%%%%%%%%%%%%%%%%%%%%%%%%%%%%%%%%%%%%%%%%%%%%%%%%%%%%%%%%%%%
for j = 1:(maxit)
    P_pump(j)=sum(fftshift(nz(j)).*(exp(-(x/w0).^2).*abs(Ez((j),r))).^2)/initial_power;
    P_signal(j)=sum(fftshift(nz(j)).*(exp(-(x/w0).^2).*abs(Es((j),r))).^2)/initial_power;
    %P_pump(j)=sum((fftshift(nz(j))).*(((exp(-(x/w0).^2)*abs(Ez((j),r))).^2))/initial_power;
    %P_signal(j)=sum((fftshift(nz(j))).*(((exp(-(x/w0).^2)*abs(Es((j),r))).^2))/initial_power;
end
if plotyn==1
figure(71);clf
subplot(2,1,1),plot(P_pump,'bo-');grid,axis tight;hold on
ylabel('Pump power');
subplot(2,1,2),plot(P_signal,'ro-');grid,axis tight;hold on
ylabel('signal power');
axis tight
saveas(71,'Pump_Signal_power.fig'); % Ez, nz and resulting Ez all in one.
display('Press a key ...');%pause;
end

% RECALCULATING Ezmax (INTERFERENCE) AFTER THE NL round
%%%%%%%%%%%%%%%%%%%%%%%%%%%%%%%%%%%%%%%%%%%%%%%%%%%%%%%%%%%%%%%%%%%%%%%%
Esmax(j)=max(abs(Es((j),r).^2));
for j = 1:(maxit)
    Ezmax(j)=max(abs(Ez((j),r).^2));
    Esmax(j)=max(abs(Es((j),r).^2));
    % unless beam gets two peaks this should work. Could try Ez((j),1,1) also.
end
% Replotting Ez and Nz after the NL
round%%%%%%%%%%%%%%%%%%%%%%%%%%%%%%%%%%%%%%%%%%%%%%%%%%%%%%%%%%%%%%%%%%%%%%%%
if plotyn==0
    open Interference.fig
    subplot(4,1,2),plot(nzmax,'bo-');grid,axis tight;hold on
    ylabel('{\delta}n pump');
    subplot(4,1,3),plot(nzmax2,'bo-');grid,axis tight;hold on
    ylabel('{\delta}n signal');
    subplot(4,1,4),plot(Ezmax,'ro-');grid % to put together. (this should be left Ezmax) Modify
    ylabel('Int. post-NL');
    axis tight
    %pause(5);
    saveas(1,'EzR1_Nz_Nz2_EzFinal.fig');close % Ez, nz and resulting Ez all in one.
    close all
end
%=====
% Error calculation (error should be zero if there is no-nonlinearity)
for j = 1:(maxit-2)
    % below is average percent error at each peak between two steps

```

```

% here the two troubling points at the ends are excluded.
err(j)=abs(abs(max(abs(Ez(j+1,2)))-max(abs(Ez(j+1,1))))/max(abs(Ez(j+1,1))))*100;
% since r alternates between 1,2 this will work in either case.
end
error=(sum(err)/maxit); % this is to average out, err is already in percent.
%-----
if plotyn==1
if error>tol;
%saving the nzmax and Ezmax for unconverged loops.
open Interference.fig % since all closed, will open in figure(1)
subplot(3,1,2),plot(nzmax,'bo-');grid,axis tight;hold on
ylabel('\delta n pump');
subplot(3,1,3),plot(nzmax2,'bo-');grid,axis tight;hold on
ylabel('\delta n signal');

if conv_loop==1
    saveas(1,'shows_all.fig');
end
if conv_loop==2
    saveas(1,'two.fig');
end
if conv_loop==3
    saveas(1,'three.fig');
end
if conv_loop==4
    saveas(1,'four.fig');
end
if conv_loop==5
    saveas(1,'five.fig');
end
if conv_loop==6
    saveas(1,'six.fig');
end
if conv_loop==7
    saveas(1,'seven.fig');
end
if conv_loop==8
    saveas(1,'eight.fig');
end
if conv_loop==9
    saveas(1,'nine.fig');
end
if conv_loop==10
    saveas(1,'ten.fig');
end
if conv_loop==15
    saveas(1,'fifteen.fig');
end
if conv_loop==20
    saveas(1,'twenty.fig');
end
    %pause(5);
    close all
end
end
%=====

```

```

% This is here to check if my code is still correct, for Cdf,Cpv=0,it should
% produce the same fabry perot effect as by fp1d.m. After any major modification
% to the code, should make sure that nothing is screwed up. (may not match
% with fp1d anymore, since the boundary conditions were chagned (may 26th,04)
% EbT=Eb1+Eb2;
if plotyn==0
    figure(51);clf
    EbTfft=fft(EbT);
    % Exploiting the fact that fft is same as far field profile
    plot(fftshift(k),fftshift(abs(EbTfft)), 'r');grid
    title('Fft of backward sum vs k-vector');
    xlabel('k_x (1/m)');
    ylabel('FFT after multiple pass');
    saveas(51,'Fft_bSum_vs_k.fig');close
end
close all
%=====
if plotyn==0
    plot(x,abs(fftshift(Ef1)), 'b');grid
    title('Ef1 end of first trip NL round');pause(5)
    plot(x,abs(fftshift(Ef2)), 'b');grid
    title('Ef2 end of first trip NL round');pause(2)
    % Ef1,2,3 are outside the crystal, so no need for C.
    % display('These powers normalized with respect to initial power');
end
power_T1=sum(Ef1.*conj(Ef1))/initial_power
DPower_T1=(power_T1-power_R1T1)
% would be zero for linear case, otherwise does not mean anything.
% display('=====');
Power_Diffr_Signal=sum(Egb2T.*conj(Egb2T))/initial_power
Power_Diffr_Signal_NI=TP_Egb2/initial_power
Diffr_added=Ef1+Egb2T;
Power_diffr_added_T=sum(Diffr_added.*conj(Diffr_added))/initial_power
DP_W_Diffr_T=Power_diffr_added_T-power_T1
display('In Excel DP_inNL (Front). Negative=depletion,positive=gain of pump')
DP_W_Diffr_T_comR1=Power_diffr_added_T-power_R1T1
display('In Excel DP_wrtL (Front). Negative=depletion,positive=gain of pump')
% this is the actual coupling, since comparing to linear case. However DP_W_Diffr
% shows the effect of interference alone--if that is of interest.
display('=====');

power_B2=sum(Eb2.*conj(Eb2))/initial_power
DPower_B2=(power_B2-power_R1B2)
Power_Diffr_Pump=sum(EgbT.*conj(EgbT))/initial_power
Power_Diffr_Pump_NI=TP_Egb/initial_power
Diffr_added_B=Eb2+EgbT;
Power_diffr_added_B=sum(Diffr_added_B.*conj(Diffr_added_B))/initial_power
DP_W_Diffr_B=Power_diffr_added_B-power_B2
display('In Excel DP_inNL (Back). positive=gain, negative=depletion of signal')
DP_W_Diffr_B_comR1=Power_diffr_added_B-power_R1B2
display('In Excel DP_wrtL (Back). positive=gain, negative depletion of signal')
% this is the actual coupling, since comparing to linear case. However DP_W_Diffr
% shows the effect of interference alone--if that is of interest.

power_B1=sum(Eb1.*conj(Eb1))/initial_power
power_MF2=index_m*sum(Emf2.*conj(Emf2))/initial_power %index_m is approximate

```

```

%display('Sum_field back and frontal should add up close to 1');
%onaxis_R1T1=fftshift(Ef1.*conj(Ef1)); %result same if fft on product/individual
%onaxis_R1T1= onaxis_R1T1(dim/2+1); %result verified with on_axis_1_R1.fig
%onaxis_R1T2=fftshift((Ef2.*conj(Ef2)));
%onaxis_R1T2=onaxis_R1T2(dim/2+1);
Total_Power_NL=power_T1+power_B2+power_B1+power_MF2
Loss_NL=1-Total_Power_NL
display('strike any key to continue');
%pause(5);
fid = fopen('result_exp.xls','a');
fprintf(fid,'%17.17e \t %17.17e \t %17.17e \t %17.17e\n'
,DP_W_Diffr_T,DP_W_Diffr__T_comR1,DP_W_Diffr_B,DP_W_Diffr_B_comR1);
fclose(fid);
display('=====END OF NON LINEAR ROUND');
error
display('Error is already in percent. Do not multiply with 100');
conv_loop
%-----
%onaxis_T1=fftshift(Ef1.*conj(Ef1));
%onaxis_T1=onaxis_T1(dim/2+1);
%Delta_onaxis_T1=100*(onaxis_T1-onaxis_R1T1)/onaxis_R1T1;
%onaxis_T2=fftshift((Ef2.*conj(Ef2)));
%onaxis_T2=onaxis_T2(dim/2+1);
%Delta_onaxis_T2=100*(onaxis_T2-onaxis_R1T2)/onaxis_R1T2;
%-----
if error<tol
display('Converged, Yahhhhhooo!!!!!!!!!!');
figure(53)
plot(err)
title('Error array');
xlabel('General index array');
ylabel('Error between Ez max of last two loops');
saveas(53,'Err_con.fig');close
r=3 % converged, loop ends
else % loop continues, Ez(:,1) being defined again
if r==2
r=1;
else
r=2;
end
end
conv_loop=conv_loop+1;
if conv_loop>maxround
figure(23);clf
subplot(2,1,1),plot(nzmax,'bo-');grid;axis tight;hold on
ylabel('Index modulation');
subplot(2,1,2),plot(Ezmax,'ro-');grid % to put together.
ylabel('Interference');
% n_compare=index_m*ones(1,(maxit-2));plot(n_compare,'g*');
title('Converged solution');
axis tight
% pause(5);
saveas(23,'Ez_Nz_peaks_uncon.fig');close
r=3 % trying for too long, so forced break
figure(55)
plot(err)

```

```

    title('Error array');
    xlabel('General index array');
    ylabel('Error between Ez max of last two loops');
    saveas(55,'Err_uncon.fig');close
    display('did not converge, see the Err_uncon.fig');
end
r=r+3;
end                                     % matching r loop

Cdf,Cpv,N,dim,stepsperQW % to keep record in log file
Real_time=fix(clock)-t0 % tells time elapsed
CPU_time=cputime-cpu0
display('type plot(x,abs(fftshift(Ef2))) or similar to see specific fields')
display('saved fields are Eb1,2;,Ef1,2;Emb0,1,2'); %Emf1,2 are commented out.
diary off
close all

```

APPENDIX B

ANALYSIS OF GAUSSIAN BEAMS AND FABRY-PEROT CAVITY SIMULATION

B.1 Gaussian Beam in Free Space

In order to simulate contra-directional two-beam coupling involving Gaussian beams, we need to start with the simplest form of BPM, simulating the propagation of a Gaussian beam in free space. In addition to being the basic building block of most BPM simulations, this also helps to verify the accuracy of the code by comparing the simulation result with the free space analytical result. Specifically, by comparing the change in beam waist as a function of propagation distance one can check the accuracy of the code. Conservation of power is an additional way to check the validity of the code. Appendix A shows the Matlab code for the one dimensional Gaussian Beam propagation.

In what follows, we show some simulations of Gaussian free space propagation. A beam of $5\text{ }\mu\text{m}$ focal waist (e^{-1} radius) at $z = 0$ is assumed to be traveling through a medium (index = 1) that is $200\text{ }\mu\text{m}$ along the x -axis. Figure B.1 is the initial Gaussian field at the focus, with unit amplitude and with the e^{-1} radius being $5\text{ }\mu\text{m}$. The width along the x -axis (x -window) determines the range of the spatial frequency space (as

discussed in Chapter 4). For a given beam waist, if the x -window is chosen too large, the spatial frequency range becomes too small for the frequency content of the beam and higher frequencies are truncated from the simulation. In order to maintain the exact degree of accuracy if the x -window is doubled, the sampling number (dim in this code) needs to be doubled as well, which would increase the computation time. We have used 1024 (dim in code) number of sampling points for all of our calculations in our 2D simulation.

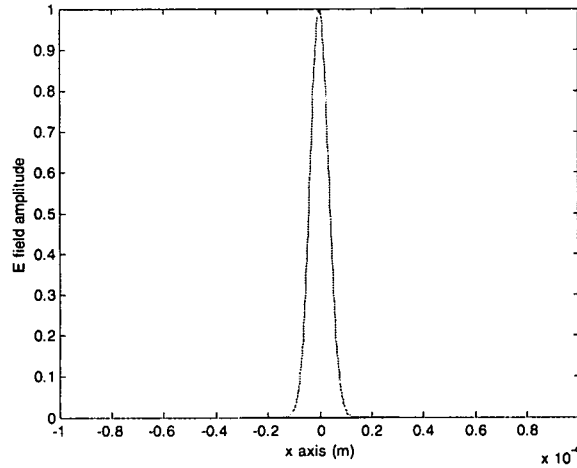


Figure B.1: Beam of $5 \mu\text{m}$ (e^{-1}) focal waist at $z = 0$, using $200 \mu\text{m}$ x -window.

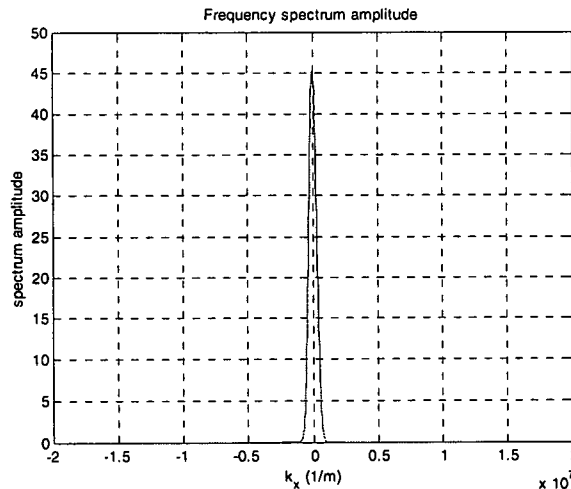


Figure B.2: The frequency spectrum using $200 \mu\text{m}$ x -window.

For free space propagation a smaller sampling may be sufficient, but when interference of multiple reflections in the photorefractive crystals are simulated, a minimum sampling of 1024 is required to produce the correct interference pattern. For the chosen x -window ($200\ \mu\text{m}$) in Fig. B.1, the $5\ \mu\text{m}$ waist beam is well confined in the frequency space, as shown in Fig. B.2. The x -window size plays a very important role in simulating the beam propagation inside the photorefractive crystal. Hence we will explore this issue here for the free space propagation.

We first propagate the beam shown in Fig. B.1 a distance of 1 mm, and the resulting field is shown in Fig. B.2. It can be seen that the beam has expanded so much that we could not simulate another 1 mm of propagation using the $200\ \mu\text{m}$ x -window. During the simulation it is important to make sure that at no time the beam tail crosses

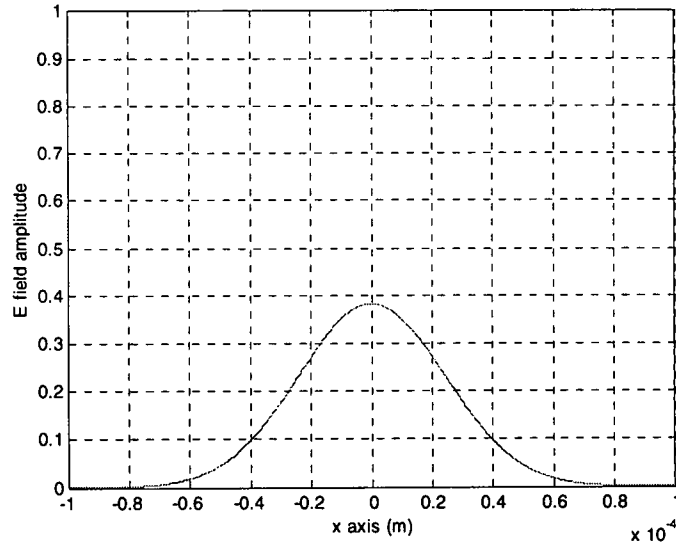


Figure B.3: The field shown in Fig. B.1 at $z = 1\ \text{mm}$, with $200\ \mu\text{m}$ x -window.

the boundaries at the left and right edges of the spatial window, since this would cause numerical errors. Hence, if we are to propagate the beam for much longer distance the spatial window of $200\ \mu\text{m}$ has to be increased. We demonstrate this by simulating 10

mm propagation of the beam, where the x -window had to be increased to $2000\ \mu\text{m}$. The original field, the frequency spectrum, and the end field are shown in Fig. B.4, B.5, and B.6 respectively.

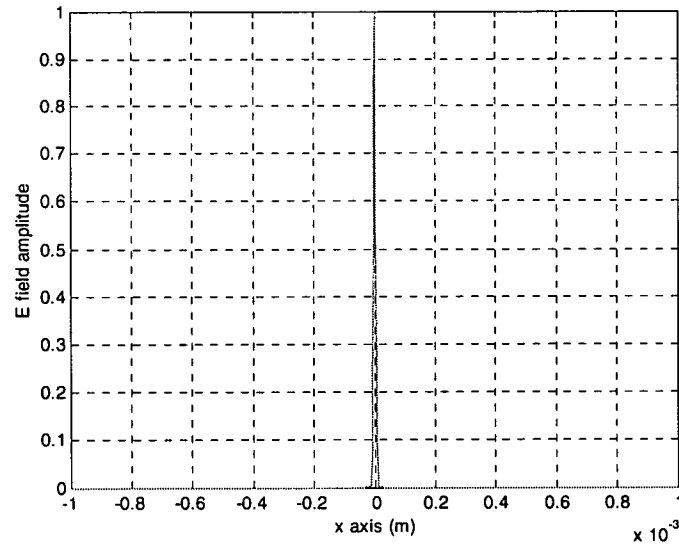


Figure B.4: Beam of $5\ \mu\text{m}$ (e^{-1}) focal waist at $z = 0$, using 2 mm x -window.

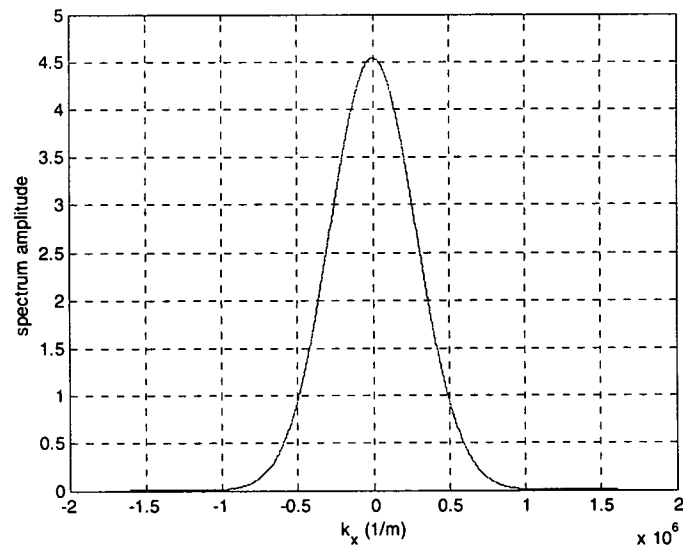


Figure B.5: The frequency spectrum using 2 mm x -window.

Figure B.5 shows that for the 2 mm *x-window* the frequency spectrum is barely contained. At $z = 10$ mm, the beam is also barely contained spatially. So, propagating a beam with $5 \mu\text{m}$ focal waist longer than 10 mm would require an *x-window* larger than 2 mm and would require sampling more than 1024. This restricts us from looking at the beam at the far field after it has traveled through the crystal. We circumvent this problem by invoking the fact that the far field pattern of a beam is just the Fourier transform of the beam (with a scaling factor) [41].

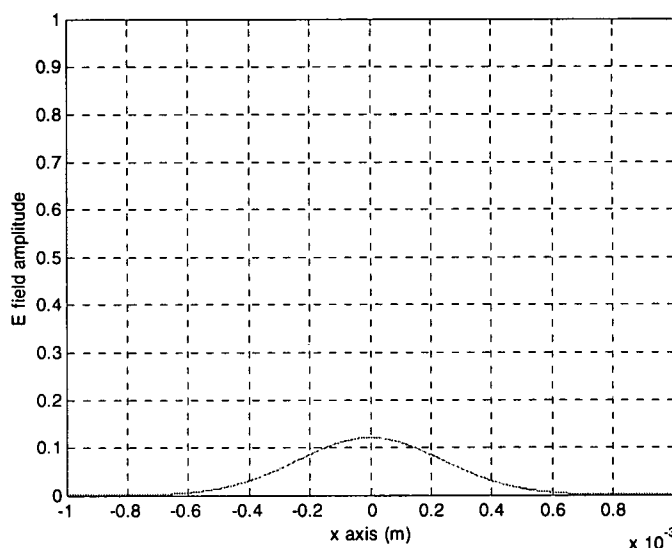


Figure B.6: The field shown in Fig. B.1 at $z = 10$ mm, with 2 mm *x-window*.

We have first used the Gaussian free space propagation as a way to verify the accuracy of the simulation. Figure B.7 shows the agreement between the analytical and simulated e^{-1} beam radius for the Gaussian beam of $5 \mu\text{m}$ focal waist traveling a distance of 10 mm. The total energy (arbitrary units) was calculated by multiplying the E field array with its complex conjugate and then summing the array. The result presented in

Figure B.8 shows that energy is conserved even though the beam has expanded, which further validates the accuracy of the simulation.

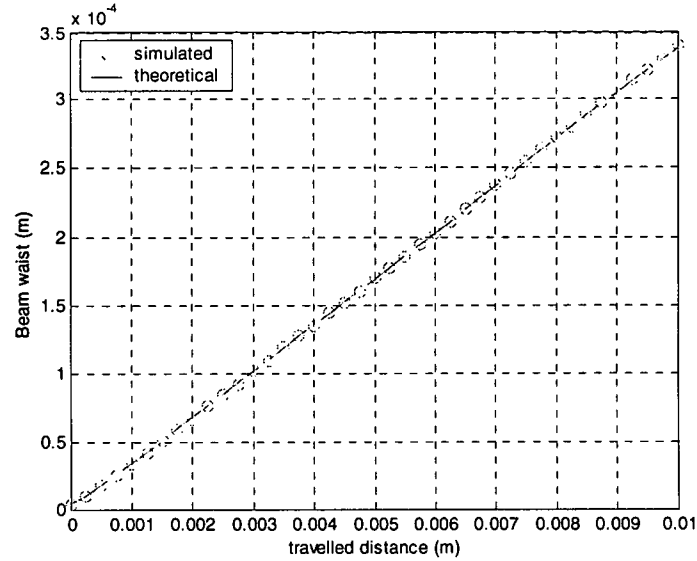


Figure B.7: $5\ \mu\text{m}$ focal waist beam propagating 10 mm through air.

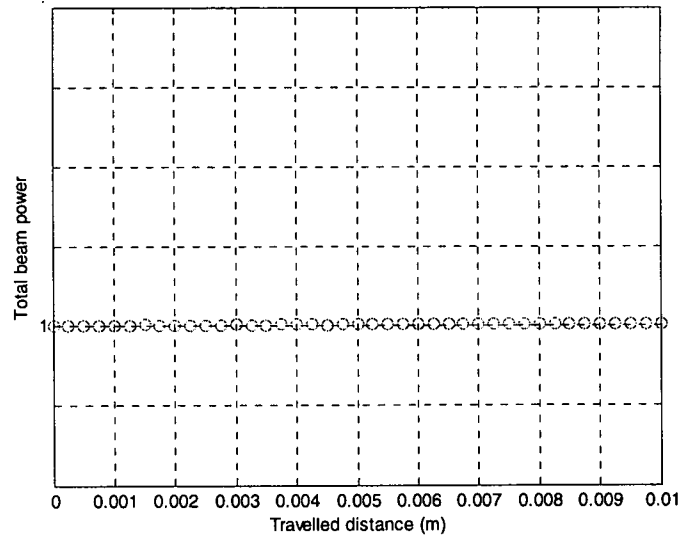


Figure B.8: Energy is conserved (normalized with respect to initial beam energy).

B.2 The Fabry-Perot Cavity

The parallel surfaces of the photorefractive crystal form a Fabry-Perot cavity, which plays an important role in the ring formation through self-organization [42]. Simulating the photorefractive two-beam coupling would also require accounting for the multiple reflections inside the crystal. Since the result for the Fabry-Perot cavity is well understood [34, 43], we simulate this as the first step toward simulating the two-beam coupling and self-organization. This is achieved by extending the basic code of the Gaussian free space propagation.

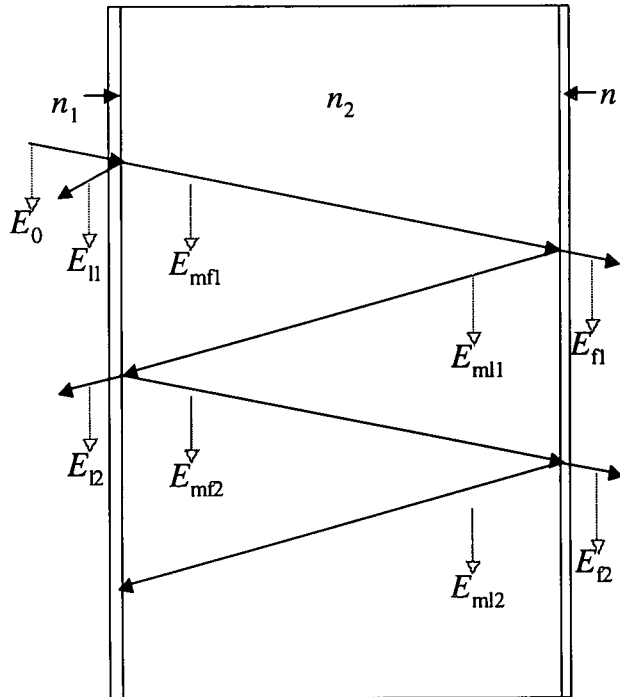


Figure B.9: Schematic representation participating beams and their symbols as used in this code. Beams are normal to crystal surfaces, but shown at an angle for convenience.

The total traveled path is divided into three sections. The first and third sections (for convenience each taken as 1/100 of the total distance) are considered to be air, and the mid section is considered to be the crystal (we considered LiNbO_3 with a refractive index

of 2.36). Figure B.9 shows a schematic representation of the geometry of the slab and also shows the multiple beam interference. The subscripts m, l, and f stands for “inside the medium”, “traveling leftward”, and “traveling forward” respectively. For the sake of clarity, the path of the beam is shown slanted in Fig. B.9. In the simulation all the beams are nominally perpendicular to the crystal surfaces. To account for the Fresnel reflection and refraction at each interface, the Fresnel coefficients are derived in terms of the spatial frequencies of the beams incident at an interface. For the sake of simplicity, only vertical polarization was assumed. For a beam traveling from index of n_1 to index of n_2 the general field reflection and transmission coefficients are given by [43]

$$r = \frac{n_1 \cos \theta_i - n_2 \cos \theta_t}{n_1 \cos \theta_i + n_2 \cos \theta_t}$$

$$t = \frac{2n_1 \cos \theta_i}{n_1 \cos \theta_i + n_2 \cos \theta_t}, \quad (\text{B.1})$$

where θ_t and θ_i related through Snell's law.

For our Fabry-Perot simulation we define the angles as shown in Fig. B.10.

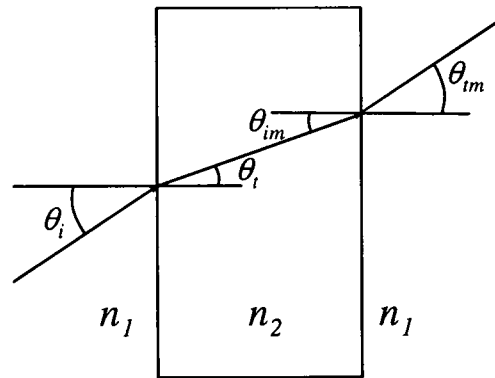


Figure B.10: The angles are defined as shown in this diagram.

In our simulation θ_i was derived as function of spatial frequency k_x using

$$\theta_i(k_x) = \sin^{-1}\left(\frac{k_x}{k_0}\right) \quad (\text{B.2})$$

where, k_0 is the free space wave vector. Using the Fresnel refraction law, θ_i is calculated from

$$\theta_i(k_x) = \sin^{-1}\left(\frac{n_1}{n_2} \sin(\theta_i)\right). \quad (\text{B.3})$$

When traveling from the slab of index of n_2 to index of n_1 , the incident angle inside the material can be derived as function of spatial frequency k_x

$$\theta_{im}(k_x) = \sin^{-1}\left(\frac{k_x}{k_m}\right), \quad (\text{B.4})$$

where, k_m is the wave number inside the material. Index n_1, n_2 are interchanged in Eq. B.1 when calculating the reflection and transmission coefficients at the left and right interfaces of the crystal.

As the beam is reflected and refracted multiple times at each interface, all fields reflected at the front surface ($E_{11}, E_{12} \dots$) and transmitted field out the rear surface ($E_{f1}, E_{f2} \dots$) are saved for future calculations. Even though the internal reflected fields ($E_{m11}, E_{m12} \dots$) propagate in the opposite direction, they are simulated as though they are still going forward, since the diffraction of the beam would be similar for both cases. For example, after the field E_{m11} is calculated, we assume that it is still going in the positive z direction within a material of index n_2 until it travels a distance equal to the crystal length, at which point the right reflection and transmission coefficients are used to calculate E_{mf2} and E_{12} . Again, we propagate E_{mf2} in the same manner, going in the

positive direction, until another crystal path length is traveled, at which point E_{m2} and E_{f2} are calculated using the right reflection and transmission coefficients. The code is presented in Appendix B and has been commented thoroughly.

In an actual Fabry-Perot cavity like this, a circular ring would form at the far field in both forward and backward directions as a result of interference between waves that have traveled different distances and thus have different accumulated phases [34, 43]. Since we have first simulated in one transverse dimension, we expect to see dark and bright fringes. In our simulation we calculate three passes only (since by the end of 3rd pass, E_{f3} is only $\approx 1/1400$ of E_{f1} and same is true for E_{l3} and E_{l1}). Furthermore accounting for more reflections would result in a final beam that would expand outside the maximum size *x-window* that could be used for the simulation. In the future, we plan to dynamically change the *x-window* by redefining the beam when it is too expanded.

Three different focal waist radii are used (5, 10, 30 microns) in our simulation. The length of the crystal is assumed to be 10mm and wavelength of the light beam is taken as 532 nm. The *x-window* is optimally chosen at 2 mm for the smallest beam size. In order to have a better visual comparison, all three simulations are done with the same *x-window*. We first look at the result for the 5 μm waist beam. The transmitted fields and the reflected fields are summed together to calculate the total transmitted ($E_{fT} = E_{f1} + E_{f2} + E_{f3}$) and total reflected ($E_{lT} = E_{l1} + E_{l2} + E_{l3}$) fields. These two summed fields are shown in Fig. B.11 and B.12 respectively. We can see signs of interference in both of these near field plots. To confirm that these interference effects are truly due to different phase accumulation by plane wave components, we plot the sum of the absolute field

$E_{\text{fabs_T}} = \text{abs}(E_{f1}) + \text{abs}(E_{f2}) + \text{abs}(E_{f3})$ in Fig. B.13. Lack of any interference pattern in Fig.

B.13 proves that the accumulated phase is the cause of interference.

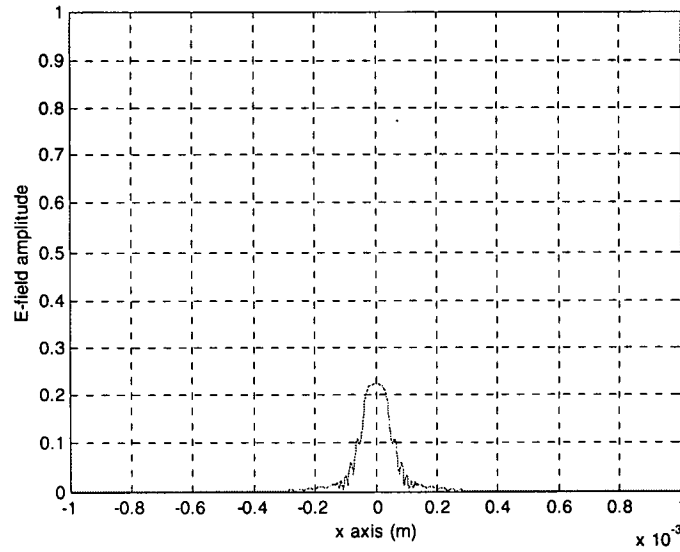


Figure B.11: Sum of the transmitted fields for the original beam of $5 \mu\text{m}$ waist.

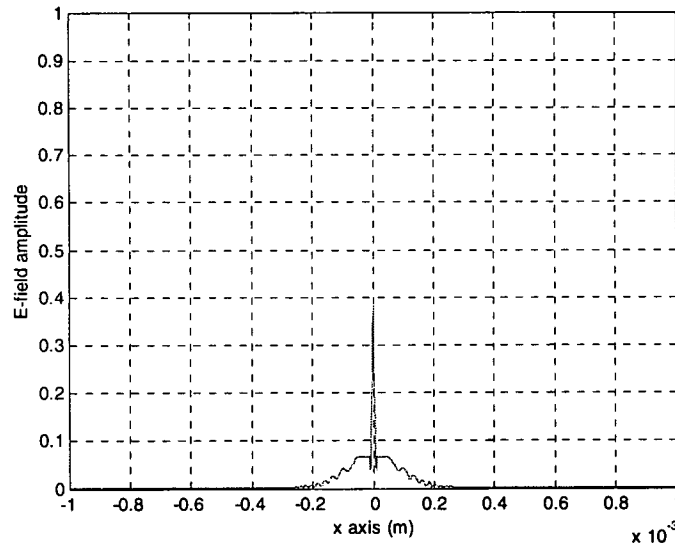


Figure B.12: Sum of the reflected fields for the original beam of $5 \mu\text{m}$ waist.

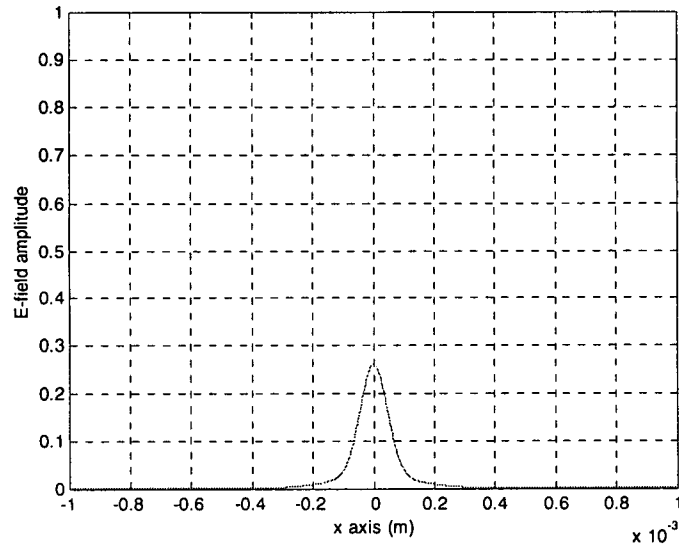


Figure B.13: Sum of the absolute reflected field for the beam of $5\ \mu\text{m}$ waist.

In order to look at the far field pattern of these total fields we take the Fourier transform of these total fields (E_{RT} and E_{IT}) and plot them as functions of spatial frequency k_x in Fig. B.14 and B.15. As expected, interference fringes are observed for both transmitted

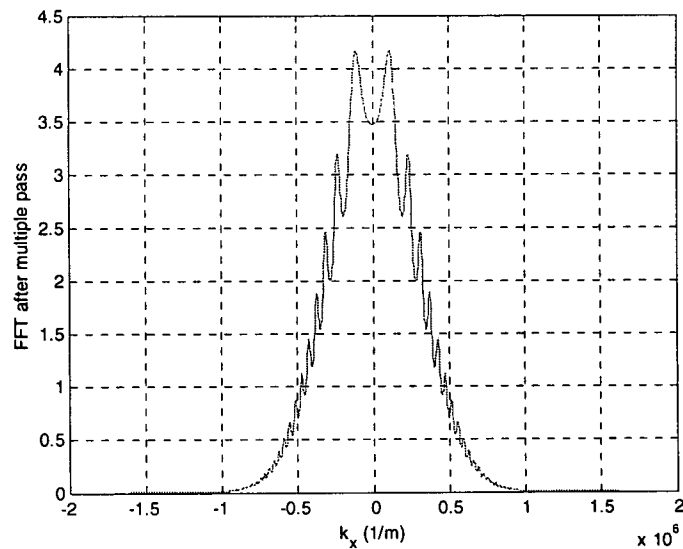


Figure B.14: FFT of sum of the transmitted fields for the original beam of $5\ \mu\text{m}$ waist.

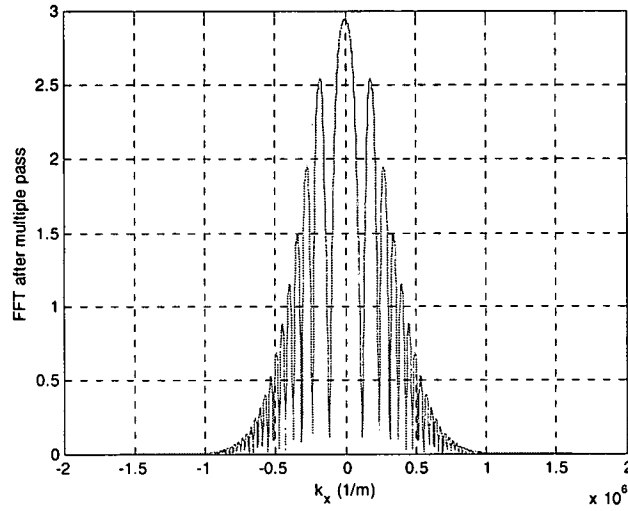


Figure B.15: FFT of sum of the reflected fields for the original beam of $5\ \mu\text{m}$ waist and reflected beams. Since in our simulation the beam is always focused at the left interface of the crystal, the frequency content is higher on the reflected side and stronger interference patterns are observed compared to the transmitted beam through the right interface.

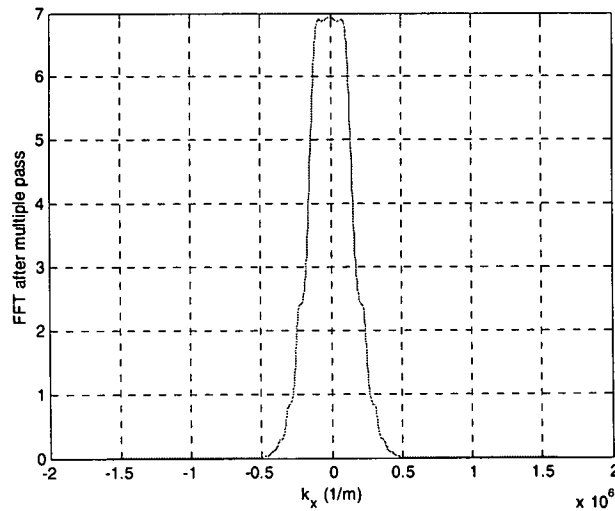


Figure B.16: FFT of sum of the transmitted fields for a beam of $10\ \mu\text{m}$ waist.

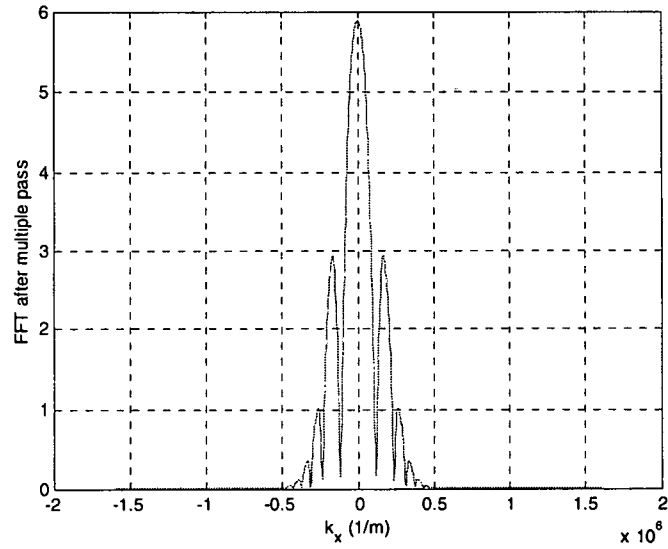


Figure B.17: FFT of sum of the reflected fields for a beam of $10 \mu m$ waist.

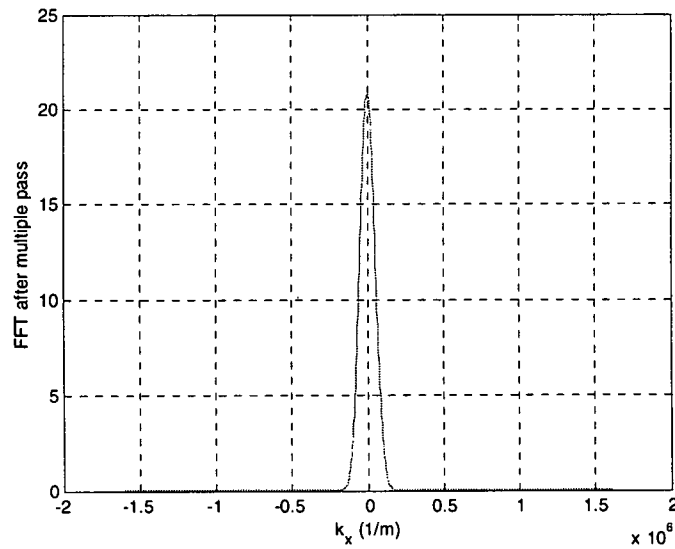


Figure B.18: FFT of sum of the transmitted fields for a beam of $30 \mu m$ waist.

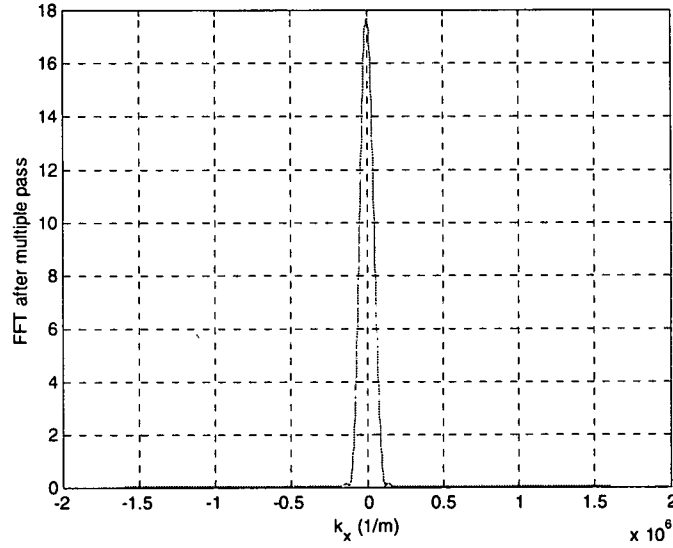


Figure B.19: FFT of sum of the reflected fields for a beam of $30\ \mu\text{m}$ waist.

Similarly, we produced the far field interference patterns for the transmitted and reflected sum of field for $10\ \mu\text{m}$ and $30\ \mu\text{m}$ beam waists and the results are shown in Fig. B.16, B.17 and Fig. B.18, B.19 respectively.

We observe that the interference fringes are reduced in numbers with increasing beam focal waist, totally disappearing for a beam of $30\ \mu\text{m}$ waist. This is not in accordance with experimental observation of ring formation in photorefractive crystals. Ring formation has been observed (for a $10\ \text{mm}$ crystal, as is used in our simulation) routinely for beam waist close to $100\ \mu\text{m}$. We conclude that in the experimental case, the scattering of the light introduces the higher spatial frequencies that are absent in a large beam waist.

We check the validity of our simulation by comparing the position of peaks and valleys for the $5\ \mu\text{m}$ and $10\ \mu\text{m}$ beams. We look at the fringes in the reflected light,

since it is more pronounced than the fringes in the transmitted light. It has been shown [42] that for a Gaussian beam traveling through a Fabry-Perot cavity formed by the parallel faces of the photorefractive material the angular position of the circular rings are only determined by the length of the cavity. If we assume that a radially symmetric beam $C(r)$, where r represents the radial distance in the transverse plane, is normally incident onto a Fabry-Perot cavity, then the far field intensity profile can be shown to be given by $|\hat{C}(\theta)S(\theta)|$, where $S(\theta)$ is a shaping function, which, to a first approximation can be shown to be [41]

$$S(\theta) \propto \frac{1}{1 + F(\theta) \sin^2(k_0 \theta^2 L / 2)} \quad (B.5)$$

Also $\hat{C}(\theta)$ represents the Fourier transform of $C(r)$, with $\theta = k_r / k_0$, where k_r is the spatial frequency corresponding to r and k_0 is the propagation constant of light in the medium. In the above relation F is the cavity Finesse and L is the thickness of the cavity. From Eq. B.5 it can be seen that the angular position of the circular rings are only determined by the length of the cavity.

Since in our 2D (only one transverse direction) simulation the angles are related to the spatial frequencies through Eqs. B.2 and B.3, we look at the position of the fringes on k_x space in Figs. B.15 and B.17. These figures correspond to far field patterns of the reflected light from a 10 mm LiNbO₃ crystal for beams of 5 and 10 μm focal waists. The results are shown in Table 1. It is observed that the fringes do appear at almost identical k_x values for both 5 and 10 μm beams. Since the peaks are unsymmetrical and are not as

sharply defined as the valleys, there is a minor difference in the calculated positions of the peaks, compared to the exactly identical positions of the valleys.

e^{-1} waist	1 st peak	2 nd peak	3 rd peak	1 st valley	2 nd valley	3 rd valley
5 μm	1.78	2.75	3.44	1.18	2.37	3.14
10 μm	1.75	2.72	3.42	1.18	2.37	3.14

Table B.1: Location of bright and dark patterns for the 5 and 10 micron focal waist beams observed at the far field of the reflected light from a 10mm long LiNbO₃ crystal. The numbers correspond to the spatial frequency (k_x) and each has a multiplicative factor of 10^5 .

The absence of a comparable interference pattern for the 30 μm focal waist beam is easily understood to be due to the absence of any significant amount of light at the higher characteristic frequencies where the fringes occur. The 10 mm length of the crystal used in above simulation is equivalent to 67 Rayleigh ranges for the 5 μm focal waist beam. If the 30 μm focal waist beam is also simulated to travel an equivalent distance of 67 Rayleigh ranges, interference fringes appear very strongly (not shown). However the position of peaks and valleys are at different (much lower) frequencies, since the crystal length is different.

By repeating the simulation presented above for a 5 mm length crystal we show that the characteristic spatial frequencies (where peaks and valleys occur) change with crystal length, but remain independent of the waist size of the incident beam. We are able to add a smaller focal waist beam (3 μm), by using a smaller x -window, (1500 μm compared to 2mm before) to contain all of the frequency content of the beam.

e^{-1} waist	1 st peak	2 nd peak	3 rd peak	1 st valley	2 nd valley	3 rd valley
3 μm	2.36	3.79	4.78	1.38	3.22	4.33
5 μm	2.35	3.76	4.77	1.38	3.22	4.33
10 μm	2.20	3.70	4.70	1.38	3.22	4.33

Table B.2: Location of bright and dark patterns for the 5 and 10 micron focal waist beams observed at the far field of the reflected light from a 5mm long LiNbO₃ crystal. The numbers correspond to the spatial frequency (k_x) and each has a multiplicative factor of 10^5 .

The same x -window was used for the other two (5 and 10) focal waists also. To verify that the change in the characteristic frequency was not due to the change in x -window, we also simulated the 3 μm focal waist beam with the 2mm x -window as well by doubling the sampling number to 2048. It was concluded that the change in characteristic frequency is due to the crystal length change only. The result from the 5mm crystal simulation is presented in Table B.2. We can see that position of the peaks and valleys are all at the characteristic frequencies.

APPENDIX C

GAUSSIAN BEAM PROPAGATION CODE

C.1 MATLAB® Code

This appendix contains the code to simulate propagation of a Gaussian beam through free space using split step beam propagation method. The simulation results are shown in Appendix B from Fig. B.1 through B.8. The comments are shown in a reduced size font.

% Gaussian 1D BEAMPROPAGATION

```
clear all
format compact
format long e
```

% Option controls

```
runwaist=1      % make zero if waist measure is not needed.
runpower=1      % make zero if power measure is not needed.
stepseen=1      % no of step that will be plotted during propagation.
```

% UNITS DEFINED

```
cm=1e-2;mm=1e-3;um=1e-6;nm=1e-9;
```

% PARAMETERS

```
medium=2000*um;      % width of the medium.
w0=5*um,totaldistance=10*mm,dz=250*um
dim=1024;             % chose 2^n array, makes it faster,
index=1;n=index*ones(1,dim);
```

% WAVE SETUP

```
iter=0;              % Just initializing
```



```

lambda=0.532*um;
k0=2*pi/lambda;
z0=(pi*(w0)^2)/lambda; Nz0=floor(totaldistance/z0)
maxiterations=floor(totaldistance/dz)
a=medium/2/pi;
i=sqrt(-1);
k=[0:(dim/2-1) -(dim/2):-1]/a; % k=kx
x=medium*(-0.5+(0:(dim-1))/dim);
figure(1)
plot(x,fftshift(k),'r');
title('The tranverse k vector as defined');
xlabel('x axis (m)');
ylabel('tranverse k');
saveas(1,'k_vector.fig')

phaserterm=(n*k0*dz).*(1+k.^2./(2*n.^2*k0^2));
phase=exp(i*((n*k0*dz).*(1+k.^2./(2*n.^2*k0^2)))); % Free space

figure(2)
plot(fftshift(k),fftshift(phaserterm),'r');
title('The phase change at dz for each plane wave');
xlabel('k (1/m)');
ylabel('phaserterm change');
saveas(2,'phase_change.fig')
% above is the phase shift of individual plane waves after propagating the distance dz.

theta_i=asin(k./k0);
figure(21);
plot(fftshift(k),fftshift(180*theta_i/pi));grid
title('{\theta}_i(deg)');
xlabel('k (1/m)');
ylabel('{\theta}_i(deg)');
saveas(21,'theta_i.fig')

% BEAM DEFINED
v=exp(-(x/w0).^2);
figure(3)
plot(x,v,'r');grid
axis([-medium/2 medium/2 0 1]);
title('The original gaussian at z=0');
xlabel('x axis (m)');
ylabel('E field amplitude');
saveas(3,'E_focus.fig')
powerarray=(v.*conj(v));
initial_onaxis_power=powerarray(dim/2+1)
initial_power=sum(v.*conj(v))

```

```

v_k=fft(v);    % looking at the frequency spectrum
figure(4);
plot(fftshift(k),abs(fftshift(v_k)));grid
title('Frequency spectrum amplitude');
xlabel('k (1/m)');
ylabel('spectrum amplitude');
saveas(4,'Spc_Am_fo.fig')
counter=0;
v_max=max(abs(v));
    % LOOP TO GET THE ORIGINAL BEAM WAIST
    if runwaist==1
        while counter<=(dim/2+1);
            counter=counter+1;
            if (abs(v_max/exp(1))-abs(v(counter)))<(0.01*abs(v_max/exp(1)));
                waist(1)=abs((dim/2+1)-counter)*(medium/dim)
                counter=(dim/2+1);
            end
        end
    end
powerarray=(v.*conj(v));
onaxispower(1)=powerarray(dim/2+1);
power(1)=sum(v.*conj(v));
figure(5)
plot(x,abs(v),'r');
axis([-medium/2 medium/2 0 1]);
title('The spatial field at the starting point');
xlabel('x axis (m)');
ylabel('E field amplitude');
saveas(5,'E_start.fig')

% ITERATION LOOP
v=fftshift(v);
while iter<maxiterations;
    v=ifft(fft(v).*phase);
    iter=iter+1;
    counter=0;
    vv=fftshift(v); % The wave is v, vv is defined (with fftshift)
                    % temporarily to find waist etc..
    v_max=max(abs(vv));
    % LOOP TO GET THE BEAM WAIST
    if runwaist==1
        while counter<=(dim/2+1);
            counter=counter+1;
            if (abs(v_max/exp(1))-abs(vv(counter)))<(0.01*abs(v_max/exp(1)));
                waist(iter+1)=abs((dim/2+1)-counter)*(medium/dim);    % The first loop will
give waist(2)
                counter=(dim/2+1);

```

```

        end
    end
end
if runpower==1
    powerarray=(vv.*conj(vv));
    onaxispower(iter+1)=powerarray(dim/2+1);
    power(iter+1)=sum(vv.*conj(vv));
end
    if mod(iter,(maxiterations/stepseen))==0 % this would show you in between plots
        figure(iter)
        plot(x,abs(vv),'r');grid
        axis([-medium/2 medium/2 0 1]);
        title('The spatial field at this (dz*iter) z position');
        xlabel('x axis (m)');
        ylabel('E field amplitude');
        saveas(iter,'E_end.fig')
        Total_power=sum(vv.*conj(vv))
        %display('showing profile at this (dz*iter) z position,;pause
    end
end
    z=linspace(0, totaldistance, (maxiterations+1));
    figure(6)
    if runwaist==1
        plot(z,waist,'go');
        hold on;
    end
    w=w0*sqrt(1+(z/z0).^2);
    plot(z,w,'r--');
    title('The beam waist, Theoretical(red) and BPM(green)');
    xlabel('travelled distance (m)');
    ylabel('Beam waist (m)');
    saveas(6,'waist.fig')
    if runpower==1
        figure(7)
        plot(z,onaxispower,'r-.');
        title('Original on axis power = 1 unit');
        xlabel('travelled distance (m)');
        ylabel('On axis power');grid;
        saveas(7,'On_axis.fig')
        figure(8);
        power=power./initial_power;
        plot(z,power,'ro');
        title('Beam power, normalized to initial power');
        xlabel('travelled distance (m)');
        ylabel('Total beam power');
        saveas(8,'Power.fig')
    end
end

```

APPENDIX D

FABRY-PEROT CAVITY SIMULATION CODE

D.1 MATLAB[®] Code

This appendix contains the code to simulate propagation of a Gaussian beam through a slab of material and produce the interference of multiple reflections. The simulation results are shown in Fig. B.9 through B.19.

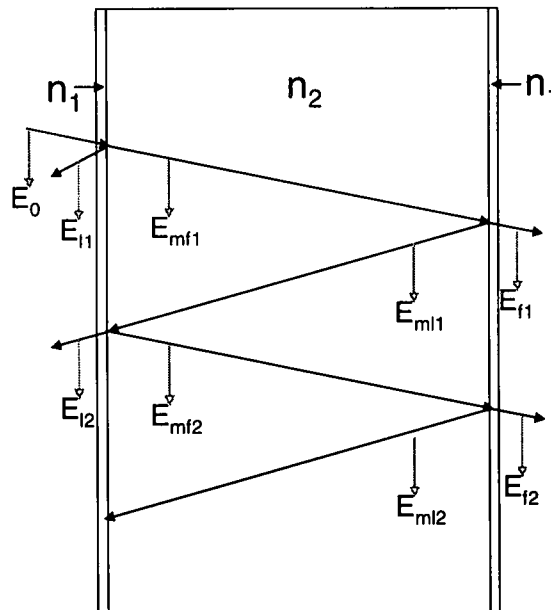


Figure D.1: Schematic representation participating beams and their symbols as used in the code. (Same as Fig. B.9).

% Fabry-Perot for Gaussian 1D beam using BEAMPROPAGATION

```
clear all
format compact
format long e
diary log1D.txt;
t0=fix(clock);cpu0=cputime;fix(clock) %for future time ref for figures.
% Option controls
plotyn=1           % make 1 with low dim to see plot, to see one plot only make that change to 0
runpower=1         % make zero if power measure is not needed.
runwaist=1         % make zero if waist measure is not needed.
stepseen=1         % do not type 0! no of step that will be plotted during propagation.
intermediate=0     % make 1 to plot intermediate steps
phaseseen=2        % do not type 0! no of step that will be plotted during propagation.
interphase=0       % make 1 to plot intermediate steps
frontpattern=1     % make 1 to see front pattern
rearpattern=1      % make 1 to see rear pattern
```

% UNITS DEFINED

```
index_m=2.36;      % verified that this=1 produces free space propagation
index_air=1;
cm=1e-2;mm=1e-3;um=1e-6;nm=1e-9;
crystal=1/100;
t_k=1;            % transmission coefficient at each step. changes at interfaces
```

% PARAMETERS

```
w0=3*um,totaldistance=5*mm,dz=1*um
medium=2000*um
maxiterations=floor(totaldistance/dz)
leftboundary=maxiterations*crystal
rightboundary=maxiterations*(1-crystal)
dim=2048           % chose 2^n array, makes it faster,
n1=index_air*ones(1,dim); % Index array in free space
n2=index_m*ones(1,dim);  % Index array in the medium
```

% WAVE SETUP

```
iter=0;jj=1;kk=1;C=1; % Just initializing
lambda=0.532*um;
k0=2*pi/lambda;      % free space wave vector magnitude
k1=2*pi*index_m/lambda; % BEAWARE, n1 goes with k0, n2 goes with k1
z0=(pi*(w0)^2)/lambda; Nz0=floor(totaldistance/z0)
a=medium/2/pi;
i=sqrt(-1);
k=[0:(dim/2-1) -(dim/2):-1]/a; % k=kx here.
kmax=max(k);kmin=min(k);
```

```

x=medium*(-0.5+(0:(dim-1))/dim);
figure(1);clf
plot(x,fftshift(k),'r');grid
axis tight;
title('The tranverse k vector as defined');
xlabel('x axis (m)');
ylabel('tranverse k');
saveas(1,'k_vector.fig')
phaseterm=(n1*k0*dz).*(1+k.^2./(2*n1.^2*k0^2)); % Just to have a picture of phase change

```

```

figure(2);clf
plot(fftshift(k),fftshift(phaseterm),'r');grid
axis tight;
title('The phase change at dz for each plane wave');
xlabel('k_x (1/m)');
ylabel('phaseterm change');
saveas(2,'phase_change.fig')

```

```

theta_i=asin(k./k0);
theta_im=asin(k./k1);

```

```

figure(3);clf
plot(fftshift(k),fftshift(180*theta_i/pi));grid %in deg
axis tight;
title('{\theta}_i (deg)');
xlabel('k_x (1/m)');
ylabel('{\theta}_i (deg)');
saveas(3,'theta_i.fig')

```

```

figure(31);clf
plot(fftshift(k),fftshift(180*theta_im/pi));grid %in deg
axis tight;
title('{\theta}_{im} (deg)');
xlabel('k_x (1/m)');
ylabel('{\theta}_{im} (deg)');
saveas(31,'theta_im.fig')

```

```

theta_t=asin((n1./n2).*sin(theta_i));
theta_tm=asin((n2./n1).*sin(theta_im));
figure(4);clf
plot(fftshift(k),fftshift(180*theta_t/pi));grid %in deg
axis tight;
title('{\theta}_t (deg)');
xlabel('k_x (1/m)');
ylabel('{\theta}_t (deg)');
saveas(4,'theta_t.fig')

```

```

figure(41);clf
plot(fftshift(k),fftshift(180*theta_tm/pi));grid %in deg
axis tight;
title('\theta}_{tm} (deg)');
xlabel('k_x (1/m)');
ylabel('\theta}_{tm} (deg)');
saveas(41,'theta_tm.fig')

cos_theta_i=cos(theta_i);
cos_theta_im=cos(theta_im);
figure(5);clf
plot(fftshift(k),fftshift(cos_theta_i));grid %in deg
axis tight;
title('cos(\theta}_i)');
xlabel('k_x (1/m)');
ylabel('cos(\theta}_i)');
saveas(5,'cos_th_i.fig')
cos_theta_t=cos(theta_t);
cos_theta_tm=cos(theta_tm);

figure(6);clf
plot(fftshift(k),fftshift(cos_theta_t));grid
axis tight;
title('cos(\theta}_t)');
xlabel('k_x (1/m)');
ylabel('cos(\theta}_t)');
saveas(6,'cos_th_t.fig')
phase=exp(i*((n1*k0*dz).*(1+k.^2./(2*n1.^2*k0^2)))); % Free space
phase_m1=exp(i*((n2*k1*dz).*(1+k.^2./(2*n2.^2*k1^2)))); % 1st medium
phase_m2=phase; % 2nd medium (this case air)
% above is the phase shift of individual plane waves after propagating the distance dz.

% BEAM DEFINED
v=exp(-(x/w0).^2);
figure(7);clf
plot(x,v,'r');grid
axis([-medium/2 medium/2 0 1]);
title('The original gaussian at z=0');
xlabel('x axis (m)');
ylabel('E field amplitude');
saveas(7,'E_focus.fig')
powerarray=(v.*conj(v));
initial_onaxis_power=powerarray(dim/2+1)
initial_power=sum(v.*conj(v))

v_k=fft(v); % looking at the frequency spectrum

```

```

figure(8);clf
plot(fftshift(k),angle(fftshift(v_k))*180/pi);grid %in deg
axis([kmin/100 kmax/100 -180 180]);
title('Frequency spectrum phase (degree), done with angle!');
xlabel('k vector, section of it');
ylabel('fft(original field)');
saveas(8,'Spc_Phs_fo.fig')

figure(9);clf
plot(fftshift(k),abs(fftshift(v_k)));grid
%axis tight; % To see the whole thing
title('Frequency spectrum amplitude');
xlabel('k_x (1/m)');
ylabel('spectrum amplitude');
saveas(9,'Spc_Am_fo.fig')

display('Done with original beam spot analysis');pause;
close all

counter=0;
v_max=max(abs(v));

% LOOP TO GET THE ORIGINAL BEAM WAIST
if runwaist==1
    while counter<=(dim/2+1);
        counter=counter+1;
        if (abs(v_max/exp(1))-abs(v(counter)))<(0.01*abs(v_max/exp(1)));
            waist(1)=abs((dim/2+1)-counter)*(medium/dim);
            counter=(dim/2+1);
        end
    end
end
powerarray=(v.*conj(v));
onaxispower(1)=powerarray(dim/2+1);
power(1)=sum(v.*conj(v));
angle_v=angle(v);
if plotyn==1
    figure(10);clf
    plot(x,abs(v),'r');grid
    axis([-medium/2 medium/2 0 1]);
    title('The spatial field at the starting point');
    xlabel('x axis (m)');
    ylabel('E field amplitude');
    saveas(10,'E_start.fig')
end

```


% ITERATION LOOP

```
v=fftshift(v);
```

% FIRST TRIP THROUGH THE MEDIUM

```
while iter<maxiterations;
```

```
    v_k=t_k.*(fft(v).*phase);    % It accounts for transmission loss if any
```

```
        if iter==leftboundary
```

```
            Emf1=ifft(v_k);    % Beam coming out rightward through the 1st interface
```

```
            v_kr=r_k.*(fft(v).*phase);
```

```
            El1=ifft(v_kr);    % Beam reflected leftward off the 2nd interface
```

```
        end
```

```
        if iter==rightboundary
```

```
            Ef1=ifft(v_k);    % Beam coming out rightward through the 2nd interface
```

```
            v_kr=r_k.*(fft(v).*phase);
```

```
            Eml1=ifft(v_kr);    % Beam reflected leftward off the 2nd interface
```

```
        end
```

```
v=ifft(v_k);
```

```
t_k=1;    % so T loss happens once only after being defined at the interface
```

```
    iter=iter+1;
```

% OPTIONAL INTERMEDIATE PLOTTING OF PHASE

```
if interphase==1
```

```
if mod(iter,(maxiterations/phaseseen))==0
```

```
    iter;
```

```
    figure(iter);clf
```

```
    max_v_k=max(abs(v_k));
```

```
    plot(x,fftshift(angle(v)), 'r');
```

```
    hold on
```

```
    plot(x,abs(fftshift(v)));grid
```

```
    title('Making sure phase is ok for the field round one');
```

```
    xlabel('x-axis');
```

```
    ylabel('phase (radian), field amplitude');
```

```
    saveas(iter,'Field_phase_R1.fig')
```

```
    display('Phase for the field after Figure.No steps');pause;clf
```

```
end
```

```
end
```

% LEFT BOUNDARY

```
    if iter==leftboundary;
```

```
        display('left boundary at'),iter
```

```
        phase=phase_m1; % takes effect from the next iteration
```

```
    % TRANSMISSION COEF. Considering perpendicular polarization only now
```

```
        t_k=(2*n1.*cos_theta_i)/(n1.*cos_theta_i+n2.*cos_theta_t); %from n1 to n2
```

```
    if plotyn==1
```

```
        figure(iter+1);clf
```

```

    plot(fftshift(k),fftshift(t_k));grid
    axis([kmin kmax -1 1]);
    title('field transmission coefficient at first interface');
    xlabel('k_x (1/m)');
    ylabel('transmission coefficient');
    saveas(iter+1,'tk_left.fig')
end
    tk1=t_k; % so I can look at the array later
% REFLECTION COEF. Considering perpendicular polarization only now
    r_k=(n1.*cos_theta_i-n2.*cos_theta_t)./(n1.*cos_theta_i+n2.*cos_theta_t);
if plotyn==1
    figure(iter+2);clf
    plot(fftshift(k),fftshift(r_k));grid
    axis([kmin kmax -1 1]); % change as desired to see the central part
    title('field reflection coefficient at first interface');
    xlabel('k_x (1/m)');
    ylabel('reflection coefficient');
    saveas(iter+2,'rk_left.fig')
end
    rk1=r_k; % so I can look at the array later
end
% RIGHT BOUNDARY
if iter==rightboundary;
    display('right boundary at'),iter
    phase=phase_m2; % takes effect from the next iteration
    % TRANSMISSION COEF. Considering perpendicular polarization only now
    t_k=(2*n2.*cos_theta_im)./(n2.*cos_theta_im+n1.*cos_theta_tm); % from n2 to n1

if plotyn==1
    figure(iter+1);clf
    plot(fftshift(k),fftshift(t_k));grid
    axis([kmin kmax -2 2]); % change as desired to see the central part
    title('field transmission coefficient at 2nd interface');
    xlabel('k_x (1/m)');
    ylabel('transmission coefficient');
    saveas(iter+1,'tk_right.fig')
end
    tk2=t_k; % so I can look at the array later
    % REFLECTION COEF. Considering perpendicular polarization only now
    r_k=(n2.*cos_theta_im-n1.*cos_theta_tm)./(n2.*cos_theta_im+n1.*cos_theta_tm);
if plotyn==1
    figure(iter+2);clf
    plot(fftshift(k),fftshift(r_k));grid
    axis([kmin kmax -1 1]); % change as desired to see the central part
    title('field reflection coefficient at 2nd interface');
    xlabel('k_x (1/m)');
    ylabel('reflection coefficient');

```

```

        saveas(iter+2,'rk_right.fig')
    end
    rk2=r_k; % so I can look at the array later
end

    counter=0;
    vv=fftshift(v); % The wave is v, vv is defined (with fftshift)
                    % temporarily to find waist etc..or to plot it
    v_max=abs(vv(dim/2+1));
% LOOP TO GET THE BEAM WAIST
    if runwaist==1
        while counter<(dim/2+1);
            counter=counter+1;
            if (abs(v_max/exp(1))-abs(vv(counter)))<(0.01*abs(v_max/exp(1)));
                waist(iter+1)=abs((dim/2+1)-counter)*(medium/dim); % The first loop will
give waist(2)
                counter=(dim/2+1);
            end
        end
    end
    if runpower==1
        if iter>leftboundary
            C=index_m; %Power is different by this index factor
        end
        if iter>rightboundary
            C=1;
        end
        powerarray=C*(vv.*conj(vv));
        onaxispower(iter+1)=powerarray(dim/2+1); % The first loop will give onaxispower(2)
        power(iter+1)=C*sum(vv.*conj(vv));
    end
% OPTIONAL INTERMEDIATE PLOTTING
    if intermediate==1
        if mod(iter,(maxiterations/stepseen))==0 % this would show you 10 in between
plots
            figure(iter);clf
            plot(x,abs(vv),'r');grid
            axis([-medium/2 medium/2 0 1]);
            title('The spatial field after Figure.No steps');
            xlabel('x axis (m)');
            ylabel('E field amplitude');
            %display('showing spatial field after Figure.No steps');pause;clf

            vv_k=fft(vv); % looking at the frequency spectrum at this stage
            figure(iter+1);clf
            plot(fftshift(k),abs(fftshift(vv_k)));grid
            axis tight; % To see the whole thing

```

```

        title('Frequency spectrum amplitude after Figure.No steps');
        xlabel('k_x (1/m)');
        ylabel('spectrum amplitude');
        %display('showing frequency spectrum at this Figure.No steps');pause;clf
    end
end

end

% alpha

z=linspace(0, totaldistance, (maxiterations+1));
if plotyn==1
    figure(11);clf
    if runwaist==1
        plot(z,waist,'g. ');grid
        axis tight
        hold on;
    end
    w=w0*sqrt(1+(z/z0).^2);
    plot(z,w,'r. '); grid
    axis tight
    title('The beam waist, Theoretical(red) and BPM(green)');
    xlabel('travelled distance (m)');
    ylabel('Beam waist (m)');
    saveas(11,'waist.fig');grid
end
if runpower==1
if plotyn==1
    figure(12);clf
    plot(z,onaxispower,'c. ');grid
    axis tight
    title('Original on axis power = 1 unit');
    xlabel('travelled distance (m)');
    ylabel('On axis power');grid
    saveas(12,'On_axis1.fig')
end
if plotyn==1
    figure(13);clf
    power=power./initial_power;
    plot(z,power,'r. ');grid
    axis tight
    title('Power during First Trip, normalized to initial');
    xlabel('travelled distance (m)');
    ylabel('Total beam power');grid
    saveas(13,'Power_1.fig')
end
end
if plotyn==1

```

```

figure(14);clf
plot(x,abs(fftshift(Ef1)), 'r');grid
axis([-medium/2 medium/2 0 1]);
title('Field after crystal end of first trip (Ef1)');
xlabel('x axis (m)');
ylabel('E field amplitude');
saveas(14,'Ef1.fig')
end
display('End of first trip, now all plots will close with next key');
display('type plot(x,abs(fftshift(Ef1))) or similar to see specific fields')
display('saved fields are El1,Emf1,Eml1,Ef1');
close all
% END OF FIRST TRIP

% SECOND TRIP THROUGH THE MEDIUM
%remember now the journey begins on the right crystal surface, going left
C=index_m; % since starting in medium
itEl2=0; % reinitializing
leftboundary=maxiterations*(1-2*crystal); % until hits the left interface, air space excluded
rightboundary=maxiterations*(2-4*crystal); % after travelling back rightward,
maxiterations=maxiterations*(2-3*crystal); %we take the transmitted beam to the same distance
v=Eml1;
phase=phase_m1;
% NOTE: Since we are starting with EmrX, we are already in n2 index.
while itEl2<maxiterations; % The matching end is commented with alpha
    v_k=t_k.*(fft(v).*phase); % It accounts for transmission loss if any
    %DEFINING INTERMEDIATE FIELDS
    %(It is critical that these are done before iter value changes again (follows)
    if itEl2==leftboundary
        El2=ifft(v_k); % Beam coming out leftward through the 1st interface
        v_kr=r_k.*(fft(v).*phase);
        Emf2=ifft(v_kr); % Beam reflected rightward off the 1st interface
        v_k=v_kr; % At this point we want the reflected beam, not
transmitted
    end
    if itEl2==rightboundary
        Ef2=ifft(v_k); % Beam coming out rightward through the 2nd
interface
        v_kr=r_k.*(fft(v).*phase);
        Eml2=ifft(v_kr); % Beam reflected leftward off the 2nd interface
    end
    v=ifft(v_k);
    t_k=1; % so T loss happens once only after being defined at the
interface

    itEl2=itEl2+1;
% OPTIONAL INTERMEDIATE PLOTTING OF PHASE

```

```

if interphase==1
if mod(itEl2,(maxiterations/phaseseen))==0
    figure(maxiterations+itEl2);clf
    max_v_k=max(abs(v_k));
    plot(x,fftshift(angle(v)),'r');
    hold on
    plot(x,abs(fftshift(v_k/max_v_k)));grid
    title('Making sure phase is ok for the field round two');
    xlabel('x-axis');
    ylabel('phase (radian), field amplitude');
    saveas(maxiterations+itEl2,'Field_phase_R2')
    display('Phase change round two after Figure.No steps');pause
    clf
end
end

% LEFT BOUNDARY (n2 in/n1 out) (for detail see the first trip)
    if itEl2==leftboundary;
        display('left boundary at'),itEl2
        % phase=phase_m1; % not needed now since we were already in n2
        t_k=(2*n2.*cos_theta_im)./(n2.*cos_theta_im+n1.*cos_theta_tm); % from n2
to n1
        if plotyn==1
            figure(maxiterations+itEl2+1);clf
            plot(fftshift(k),fftshift(t_k));grid
            axis([kmin kmax -2 2]); % change as desired to see the central part
            title('field transmission coefficient at first interface');
            xlabel('k_x (1/m)');
            ylabel('transmission coefficient');
            saveas(maxiterations+itEl2+1,'tk2_left.fig')
        end
        r_k=(n2.*cos_theta_im-n1.*cos_theta_tm)./(n2.*cos_theta_im+n1.*cos_theta_tm);
        if plotyn==1
            figure(maxiterations+itEl2+2);clf
            plot(fftshift(k),fftshift(r_k));grid
            axis([kmin kmax -1 1]);
            title('field reflection coefficient at first interface');
            xlabel('k_x (1/m)');
            ylabel('reflection coefficient');
            saveas(maxiterations+itEl2+2,'rk2_left.fig')
        end
    end
end

% RIGHT BOUNDARY (again n2 in/n1 out!) (for detail see the first trip)
    if itEl2==rightboundary;
        display('right boundary at'),itEl2
        phase=phase_m2; % takes effect from the next iteration

```

```

        t_k=(2*n2.*cos_theta_im)./(n2.*cos_theta_im+n1.*cos_theta_tm); % from n2
to n1
    if plotyn==1
        figure(maxiterations+itEl2+1);clf
        plot(fftshift(k),fftshift(t_k));grid
        axis([kmin kmax -2 2]);
        title('field transmission coefficient at 2nd interface');
        xlabel('k_x (1/m)');
        ylabel('transmission coefficient');
        saveas(maxiterations+itEl2+1,'tk2_right.fig')
    end
    r_k=(n2.*cos_theta_im-n1.*cos_theta_tm)./(n2.*cos_theta_im+n1.*cos_theta_tm);
    if plotyn==1
        figure(maxiterations+itEl2+2);clf
        plot(fftshift(k),fftshift(r_k));grid
        axis([kmin kmax -1 1]); % change as desired to see the central part
        title('field reflection coefficient at 2nd interface');
        xlabel('k_x (1/m)');
        ylabel('reflection coefficient');
        saveas(maxiterations+itEl2+2,'rk2_right.fig')
    end
end

        vv=fftshift(v); % The wave is v, vv is defined (with fftshift)
                        % temporarily to find waist etc..or to plot it

    if runpower==1
        if itEl2>rightboundary
            C=1;
        end
        powerarray2=C*(vv.*conj(vv));
        onaxispowEl2(itEl2)=powerarray2(dim/2+1); % The first loop will give
onaxispower(2)
        powEl2(itEl2)=C*sum(vv.*conj(vv));
    end

end

    if runpower==1
        z=linspace(0, maxiterations*dz, (maxiterations)); %m..s*dz is the new distance
    if plotyn==1
        figure(212);clf
        plot(z,onaxispowEl2,'c. ');grid
        axis tight
        title('2nd trip on axis power');
        xlabel('From right boundary to left, back again, through to end');
    end
end

```

```

        ylabel('On axis power');grid
        saveas(212,'On_axis2.fig')
    end
    if plotyn==1
        figure(213);clf
        powEl2=powEl2./initial_power;
        plot(z,powEl2,'r. ');grid
        axis tight
        title('2nd trip--total power, normalized to initial');
        xlabel('From right boundary to left, back again, through to end');
        ylabel('Total beam power');
        saveas(213,'Power_2.fig')
    end
    end
    if plotyn==1
        figure(17);clf
        plot(x,abs(fftshift(Ef2)), 'r. ');grid
        axis([-medium/2 medium/2 0 1]);
        title('Field after crystal end of 2nd trip (Ef2)');
        xlabel('travelled distance (m)');
        ylabel('E field amplitude');
        saveas(17,'Ef2.fig')
    end
    display('type plot(x,abs(fftshift(Ef2))) or similar to see specific fields')
    display('saved fields are El2,Emf2,Eml2,Ef2');
    display('End of 2nd trip, now all plots will close with next key');
    %pause
    close all
    maxiterations=floor(totaldistance/dz); % redifing since it got changed in this round.
    % END OF 2ND TRIP

```

% THIRD TRIP THROUGH THE MEDIUM

```

C=index_m; % since starting in medium
itEl3=0; % reinitializing
leftboundary=maxiterations*(1-2*crystal);% until hits the left interface, air space excluded
rightboundary=maxiterations*(2-4*crystal); % after travelling back rightward,
maxiterations=maxiterations*(2-3*crystal); %we will the transmitted beam to the same distance
v=Eml2;
phase=phase_m1;
% NOTE: Since we are starting with EmrX, we are already in n2 index.
while itEl3<maxiterations;
    v_k=t_k.*(fft(v).*phase); % It accounts for transmission loss if any
    % DEFINING INTERMEDIATE FIELDS
    % (It is critical that these are done before iter value changes again (follows)
    if itEl3==leftboundary
        El3=ifft(v_k); % Beam coming out leftward through the 1st interface
        v_kr=r_k.*(fft(v).*phase);
    end
    itEl3++;
end

```



```

        Emf3=ifft(v_kr);          % Beam reflected rightward off the 1st interface
        v_k=v_kr;                % At this point we want the reflected beam, not
transmitted
    end
    if itEl3==rightboundary
        Ef3=ifft(v_k);          % Beam coming out rightward through the 2nd
interface
        v_kr=r_k.*(fft(v).*phase);
        Eml3=ifft(v_kr);        % Beam reflected leftward off the 2nd interface
    end
    v=ifft(v_k);
    t_k=1;                      % so T loss happens once only after being defined at the interface
    itEl3=itEl3+1;
% OPTIONAL INTERMEDIATE PLOTTING OF PHASE
    if interphase==1
    if mod(itEl3,(maxiterations/phaseseen))==0
        figure(3*maxiterations+itEl3);clf
        max_v_k=max(abs(v_k));
        plot(x,fftshift(angle(v)), 'r');
        hold on
        plot(x,abs(fftshift(v_k/max_v_k)));grid
        title('Making sure phase is ok in round three');
        xlabel('x-axis');
        ylabel('phase (radian), Field amplitude(norm)');
        saveas(3*maxiterations+itEl3,'Field_phase_R3.fig')
        display('Phase change for round three after Figure.No steps');pause
        clf
    end
end
end

```

% LEFT BOUNDARY (n2 in/n1 out) (for detail see the first trip)

```

    if itEl3==leftboundary;
        display('left boundary at'),itEl3
        % phase=phase_m1; % not needed now since we were already in n2
        t_k=(2*n2.*cos_theta_im)./(n2.*cos_theta_im+n1.*cos_theta_tm); % from n2 to n1
    if plotyn==1
        figure(3*maxiterations+itEl3+1);clf
        plot(fftshift(k),fftshift(t_k));grid
        axis([kmin kmax -2 2]); % change as desired to see the central part
        title('field transmission coefficient at first interface');
        xlabel('k_x (1/m)');
        ylabel('transmission coefficient');
        saveas(3*maxiterations+itEl3+1,'tk3_left.fig')
    end
    r_k=(n2.*cos_theta_im-n1.*cos_theta_tm)./(n2.*cos_theta_im+n1.*cos_theta_tm);
    if plotyn==1
        figure(3*maxiterations+itEl3+2);clf

```

```

    plot(fftshift(k),fftshift(r_k));grid
    axis([kmin kmax -1 1]);
    title('field reflection coefficient at first interface');
    xlabel('k_x (1/m)');
    ylabel('reflection coefficient');
    saveas(3*maxiterations+itEl3+2,'rk3_left.fig')
end
end
% RIGHT BOUNDARY (again n2 in/n1 out!) (for detail see the first trip)
if itEl3==rightboundary;
    display('right boundary at'),itEl3
    phase=phase_m2; % takes effect from the next iteration
    t_k=(2*n2.*cos_theta_im)./(n2.*cos_theta_im+n1.*cos_theta_tm); % from n2 to n1
    if plotyn==1
        figure(3*maxiterations+itEl3+1);clf
        plot(fftshift(k),fftshift(t_k));grid
        axis([kmin kmax -2 2]);
        title('field transmission coefficient at 2nd interface');
        xlabel('k_x (1/m)');
        ylabel('transmission coefficient');
        saveas(3*maxiterations+itEl3+1,'tk3_right.fig')
    end
    r_k=(n2.*cos_theta_im-n1.*cos_theta_tm)./(n2.*cos_theta_im+n1.*cos_theta_tm);
    if plotyn==1
        figure(3*maxiterations+itEl3+2);clf
        plot(fftshift(k),fftshift(r_k));grid
        axis([kmin kmax -1 1]);
        title('field reflection coefficient at 2nd interface');
        xlabel('k_x (1/m)');
        ylabel('reflection coefficient');
        saveas(3*maxiterations+itEl3+2,'rk3_right.fig')
    end
end
end

    vv=fftshift(v); % The wave is v, vv is defined (with fftshift)
                    % temporarily to find waist etc..or to plot it

if runpower==1
    if itEl3>rightboundary
        C=1;
    end
    powerarray3=C*(vv.*conj(vv));
    onaxispowEl3(itEl3)=powerarray3(dim/2+1);
    powEl3(itEl3)=C*sum(vv.*conj(vv));
end

end

```

```

    if runpower==1
        z=linspace(0, maxiterations*dz, (maxiterations)); %m..s*dz is the new distance
    if plotyn==1
        figure(312);clf
        plot(z,onaxispowEl3,'c. ');grid
        axis tight
        title('3rd trip on axis power');
        xlabel('From right boundary to left, back again, through to end');
        ylabel('On axis power');grid
        saveas(312,'On_axis3.fig')
        %display('Press a key ...');%pause;
    end
    if plotyn==1
        figure(313);clf
        powEl3=powEl3./initial_power;
        plot(z,powEl3,'r. ');grid
        axis tight
        title('3rd trip--total power, normalized to initial');
        xlabel('From right boundary to left, back again, through to end');
        ylabel('Total beam power');
        saveas(313,'Power_3.fig')
    end
    end
    if plotyn==1
        figure(20);clf
        plot(x,abs(fftshift(Ef3)), 'r. ');grid
        axis([-medium/2 medium/2 0 1]);
        title('Field after crystal end of third trip (Ef3)');
        xlabel('travelled distance (m)');
        ylabel('E field amplitude');
        saveas(20,'Ef3.fig')
    end
    end
    figure(21);clf
    plot(x,abs(fftshift(Ef3)), 'r. ');grid
    axis([-medium/2 medium/2 0 1]);
    hold on
    Ef3_max=max(abs(Ef3));Ef3_norm=Ef3./Ef3_max;
    plot(x,abs(fftshift(Ef3_norm)), 'r. ');grid
    title('Last field (Ef3), normalized (red) to see confinement');
    xlabel('travelled distance (m)');
    ylabel('E field amplitude');
    saveas(21,'Ef3_norm.fig')
    display('End of 3rd trip, now all plots will close with next key');
    display('type plot(x,abs(fftshift(Ef3))) or similar to see specific fields')
    display('saved fields are El3,Emf3,Eml3,Ef3,Ef3');
    %pause
    close all

```

```

maxiterations=floor(totaldistance/dz); % redifing since it got changed in this round.
% END OF 3RD TRIP

```

```

if frontpattern==1

```

```

    ET=Ef1+Ef2+Ef3;

```

```

    figure(31);clf

```

```

    ETfft=fft(ET);

```

```

    % Exploiting the fact that fft is same as far field profile

```

```

    plot(fftshift(k),fftshift(abs(ETfft)), 'r');grid

```

```

    title('Fft of Transmitted sum vs k-vector');

```

```

    xlabel('k_x (1/m)');

```

```

    ylabel('FFT after multiple pass');

```

```

    saveas(31,'Fft_TSum.fig')

```

```

    figure(34);clf

```

```

    plot(fftshift(k),fftshift(abs(ETfft)), 'r'); hold on

```

```

    plot(fftshift(k),fftshift(abs(E1fft)), 'r')

```

```

    title('two plots together, vs k-vector (T)');

```

```

    xlabel('k_x (1/m)');

```

```

    saveas(34,'Fft_all_T.fig')

```

```

    % comparing with vs. x-axis, should be similar but scaled

```

```

    figure(35);clf

```

```

    plot(x,fftshift(abs(ETfft)), 'r'); hold on

```

```

    plot(x,fftshift(abs(E1fft)), 'r')

```

```

    title('two plots together, vs k-vector (T)');

```

```

    xlabel('x-axis');

```

```

    saveas(35,'Fft_all_x_T.fig')

```

```

    figure(36);clf

```

```

    plot(x,abs(fftshift(ET)), 'r');grid

```

```

    axis([-medium/2 medium/2 0 1]);

```

```

    title('The sum of transmitted fields');

```

```

    xlabel('x axis (m)');

```

```

    ylabel('E-field amplitude');

```

```

    saveas(36,'Sum_TFields.fig')

```

```

    ETabs=abs(Ef1)+abs(Ef2)+abs(Ef3);

```

```

    figure(37);clf

```

```

    ETabsfft=fft(ETabs);

```

```

    plot(fftshift(k),fftshift(abs(ETabsfft)), 'r')

```

```

    title('FFT of the sum of abs(transmitted fields)');

```

```

    xlabel('k_x (1/m)');

```

```

    ylabel('FFT sum abs(T_field)');

```

```

    saveas(37,'Fft_sum_abs_TF.fig')

```

```

figure(38);clf
plot(x,fftshift(abs(ETabs)), 'r')
axis([-medium/2 medium/2 0 1]);
title('The sum of abs transmitted fields');
xlabel('x axis (m)');
ylabel('E-field amplitude');
saveas(38,'Sum_abs_TF.fig')
%pause;
close all
end
if rearpattern==1
    ErT=E11+E12+E13;
    figure(51);clf
    ErTfft=fft(ErT);
    % Exploiting the fact that fft is same as far field profile
    plot(fftshift(k),fftshift(abs(ErTfft)), 'r');grid
    title('Fft of Reflected sum vs k-vector');
    xlabel('k_x (1/m)');
    ylabel('FFT after multiple pass');
    saveas(51,'Fft_RSum.fig')

    figure(52);clf
    plot(x,abs(fftshift(ErT)), 'r');grid
    axis([-medium/2 medium/2 0 1]);
    title('The sum of reflected fields');
    xlabel('x axis (m)');
    ylabel('E-field amplitude');
    saveas(52,'Sum_RFields.fig')

    ErTabs=abs(E11)+abs(E12)+abs(E13);
    figure(53);clf
    ErTabsfft=fft(ErTabs);
    plot(fftshift(k),fftshift(abs(ErTabsfft)), 'r')
    title('FFT of the sum of abs(reflected fields)');
    xlabel('k_x (1/m)');
    ylabel('FFT sum abs(R_field)');
    saveas(53,'Fft_sum_abs_RF.fig')

    figure(54);clf
    plot(x,fftshift(abs(ErTabs)), 'r')
    axis([-medium/2 medium/2 0 1]);
    title('The sum of abs reflected fields');
    xlabel('x axis (m)');
    ylabel('E-field amplitude');
    saveas(54,'Sum_abs_RF.fig')
    close all
end

```

```
w0,z0,dim,medium,totaldistance,dz  
Real_time=fix(clock)-t0 % tells time elapsed  
CPU_time=cputime-cpu0  
diary off
```

Bibliography

- [1] R. W. Boyd, *Nonlinear Optics*, Ch 10. Academic Press, 1992.
- [2] N. V. Kukhtarev, V. B. Markov, and S. G. Odulov, "Transient energy transfer during hologram formation in LiNbO_3 in external electric field," *Opt. Commun.*, vol. 23, pp. 338-43, 1977.
- [3] N. V. Kukhtarev, V. B. Markov, S. G. Odulov, M. S. Soskin, and V. L. Vinetskii, "Holographic storage in electro-optic crystals. I. Steady State," *Ferroelectrics*, vol. 22, pp. 949-60, 1979.
- [4] P. Yeh, "Contra-directional two-wave mixing in photorefractive media," *Opt. Commun.*, vol. 45, pp. 323-26, 1983.
- [5] K. R. MacDonald, J. Feinberg, Z. Z. Ming, and P. Gunter, "Asymmetric transmission through a photorefractive crystal of barium titanate," *Opt. Commun.*, vol. 50, pp. 146-50, 1984.
- [6] G. Cook, D. C. Jones, C. J. Finnan, L. L. Taylor, and T.W. Vere, "Optical limiting with lithium niobate," *Proc. SPIE*, vol. 3798, pp. 2-16, 1999.
- [7] N. V. Kukhtarev, T. Kukhtareva, H. J. Caulfield, P. Banerjee, H.-L. Yu, and L. Hesselink, "Broadband dynamic, holographically self recorded, and static hexagonal scattering patterns in photorefractive $\text{KNbO}_3\text{:Fe}$," *Opt. Eng.*, vol. 34, pp. 2261-2268, 1995.

- [8] M. A. Saleh, P. P. Banerjee, J. Carns, G. Cook, and D. R. Evans, "Stimulated photorefractive backscatter leading to six-wave mixing and phase conjugation in iron doped lithium niobate," *Appl. Opt.*, vol. 46, 2007. (to appear on 8/10/07)
- [9] N. Kukhtarev, T. Kukhtareva, R. Jones, J. Wang, and P. Banerjee, "Real-time holography for optical processing using photorefractive crystals," *Proc. SPIE*, vol. 3793, pp. 90-96, 1999.
- [10] G. Cook, C. J. Finnan, and D. C. Jones, "Photovoltaic contribution to counter-propagating two-beam coupling in photorefractive lithium niobate," *Opt. Commun.*, vol. 192, pp. 393-398, 2001.
- [11] P. Yeh, *Introduction to Photorefractive Nonlinear Optics*, Ch 3, 4. Wiley, New York, 1993.
- [12] J. J. Liu and P. P. Banerjee, "Role of diffusive, photovoltaic, and thermal effects in beam fanning in LiNbO_3 ," *J. Opt. Soc. Am. B*, vol. 11, pp. 1688-1693, 1994.
- [13] G. Cook, C. J. Finnan, and D. C. Jones, "High optical gain using counter-propagating beams in iron and terbium doped photorefractive lithium niobate," *Appl. Phys.*, vol. 68, pp. 911-916, 1999.
- [14] Y. H. Ja, "Energy transfer between two beams in writing a reflection volume hologram in a dynamic medium," *Optical and Quantum Electronics*, vol. 15, pp. 547-556, 1995.
- [15] D. R. Evans, M. A. Saleh, T. J. Bunning, L. Lu, R. S. Meltzer, W. M. Yen, and S. Guha, "Contra-directional two-beam coupling by use of a single input beam in an iron-doped lithium niobate multimode fiber," *Appl. Opt.*, vol. 41, pp. 6890-6893, 2002.

- [16] G. Cook, D. C. Jones, C. J. Finnan, L. L. Taylor, and T.W. Vere, "Developing photorefractive fibres for optical limiting," *Proc. SPIE*, vol. 4106, pp. 230-245, 1999.
- [17] D. R. Evans, T. Pottenger, M. A. Saleh, L. K. Patton, G. Cook, T. J. Bunning, and S. Guha, "Dependence of contra-directional two-wave mixing on diffraction and doping level in Fe:LiNbO₃," *CLEO*, Baltimore, MD, 2001. (Oral presentation)
- [18] P. A. Augustov and K. K. Shvarts, "Surface recombination and photorefraction in LiNbO₃-Fe crystals," *Appl. Phys.*, vol. 18, pp. 399-401, 1979.
- [19] A. Krumins, Z. Chen, and T. Shiosaki, "Photorefractive reflection gratings and coupling gain in LiNbO₃," *Opt. Commun.*, vol. 117, pp. 147-50, 1995.
- [20] D. R. Evans, S. A. Basun, M. A. Saleh, A. S. Allen, T. P. Pottenger, G. Cook, T. J. Bunning, and S. Guha, "Elimination of photorefractive grating writing instabilities in iron-doped lithium niobate," *IEEE J. Quantum Electron.*, vol. 38, 2002.
- [21] D. R. Evans, T. P. Pottenger, M. A. Saleh, S. A. Holmstrom, T. J. Bunning, and S. Guha, "Spatially limited optical erasure of photorefractive gratings in Fe doped LiNbO₃," Annual Meeting OSA., Long Beach, CA, 2001.
- [22] A.V. Mamaev and V.V. Shkunov, "Transient phase self-conjugation in a lithium niobate crystal," *Sov. J. Quant. Elec.*, vol. 18, pp. 829-830, 1988.
- [23] S.A. Korolkov, A.V. Mamaev, and V.V. Shkunov, "Stimulated diffusion backscattering with phase conjugation," *Int. J. Nonlinear Opt. Phys.*, vol. 2, pp. 157-169, 1993, and references therein.
- [24] I. F. Kanaev, V. K. Malinovski, and B. I. Sturman, "Induced reflection and bleaching effects in electro-optic crystals," *Sov. Phys. JETP*, vol. 47, pp. 834-837, 1978.

- [25] G. Valley, "Evolution of phase-conjugate waves in stimulated photorefractive backscattering," *J. Opt. Soc. Am. A*, vol. 9, pp. 440-1448, 1992.
- [26] H. Qiao, Y. Tomita, J. Xu, Q. Wu, G. Zhang, and G. Zhang, "Observation of strong stimulated photorefractive scattering and self-pumped phase conjugation in $\text{LiNbO}_3\text{:Mg}$ in the ultraviolet," *Opt. Express*, vol. 13, pp. 7666-7671, 2005.
- [27] E. Shamonina, B. I. Sturman, S. G. Odoulov, and K. H. Ringhofer, "Investigation of stochastic photorefractive backscattering," *J. Opt. Soc. Amer. B*, vol. 13, pp. 2242-2251, 1996.
- [28] J. Feinberg, "Self-pumped, continuous-wave phase conjugator using internal reflection," *Opt. Lett.*, vol. 7, pp. 486-488, 1982.
- [29] P. Buranasiri, P. P. Banerjee, V. Polejaev, and C. C. Sun, "Image correlation using isotropic and anisotropic higher-order generation and mutually pumped phase conjugation in photorefractive barium titanate," *Proc. SPIE*, vol. 5206, pp. 215-222, 2003.
- [30] P. Suni and J. Falk, "Measurements of stimulated Brillouin scattering phase-conjugate fidelity," *Opt. Lett.*, vol. 12, pp. 838-840, 1987.
- [31] M.D. Ewbank, "Mechanism for photorefractive phase conjugation using incoherent beams," *Opt. Lett.*, vol. 13, pp. 47-49, 1988.
- [32] D. R. Evans, J. L. Gibson, S. A. Basun, M. A. Saleh, and G. Cook, "Understanding and eliminating photovoltaic induced instabilities during contra-directional two-beam coupling in photorefractive $\text{LiNbO}_3\text{:Fe}$," *Opt. Mat.*, vol. 27, pp. 1730-1732, 2005.

R 70 2033739

- [33] S. Odoulov, B. Sturman and E. Kratzig, "Seeded and spontaneous light hexagons in $\text{LiNbO}_3\text{:Fe}$," *Appl. Phys. B*, vol. 70, pp. 645-647, 2000.
- [34] E. Hecht, *Optics*. Addison-Wesley, New York, 1987.
- [35] G. Cook, D. C. Jones, C. J. Finnan, L. L. Taylor, and T. W. Vere, "Optical limiting with lithium niobate," *Proc. SPIE*, vol. 3798, pp. 2-16, 1999.
- [36] M. Luennemann, K. Buse, and B. Sturman, "Coupling effects for counter-propagating light beams in lithium niobate crystals studied by grating translation technique for extremely high electric fields," *J. Appl. Phys.*, vol. 94, pp. 6274-6279, 2003.
- [37] C. Pollock, *Fundamentals of Optoelectronics*, Ch 9. Irwin, 1995.
- [38] T. C. Poon and P. P. Banerjee, *Contemporary Optical Image Processing with MATLAB*. Elsevier Science, 2001.
- [39] P. K. Milsom, DSTL, MOD, UK, private communication.
- [40] S. Guha, "Validity of the paraxial approximation in the focal region of a small f -number lens," *Opt. Lett.* vol. 26, pp. 1598-1600, 2001.
- [41] J. W. Goodman, *Introduction to Fourier Optics*, Ch 6. McGraw-Hill, 1996.
- [42] F. Yu, S. Yin, *Photorefractive Optics*, Ch 3. Academic Press, 2000.
- [43] P. P. Banerjee and T. C. Poon, *Principles of Applied Optics*, Ch 3, Irwin, 1991.